

US DOT National University Transportation Center for Safety

# Carnegie Mellon University















# Improve Highway Safety by Reducing the Risks of Landslides (Phase 2)

Zhuping Sheng, Ph.D. (https://orcid.org/0000-0001-8533-527x)
Oludare Owolabi, D.Sc. (https://orcid.org/0000-0002-1958-6430)
Yi Liu, D. Eng. (https://orcid.org/0000-0002-6861-2914)

Final Report – July 31, 2025

#### **DISCLAIMER**

The contents of this report reflect the views of the authors, who are responsible for the facts and the accuracy of the information presented herein. This document is disseminated in the interest of information exchange. The report is funded, partially or entirely, under [grant number 69A3552344811 / 69A3552348316] from the U.S. Department of Transportation's University Transportation Centers Program. The U.S. Government assumes no liability for the contents or use thereof.

## **Technical Report Documentation Page**

1. Report No.	2. Government Accession No.	3. Recipient's Catalog No.
Enter the report number assigned		
by the sponsoring agency.		
4. Title and Subtitle	5. Report Date	
Improve Highway Safety by Reducing	g the Risks of Landslides (Phase 2)	July 31, 2025
		6. Performing Organization Code
		Enter any/all unique numbers
		assigned to the performing
		organization, if applicable.
7. Author(s)		8. Performing Organization Report
Zhuping Sheng, Ph.D. (https://orcid.o	org/0000-0001-8533-527x)	No.
Oludare Owolabi, D,Sc. (https://orcid	d.org/0000-0002-1958-6430)	No.
Yi Liu, D. Eng. (https://orcid.org/0000	0-0002-6861-2914)	
9. Performing Organization Name a	nd Address	10. Work Unit No.
Department of Civil and Environmen University, 1700 E. Cold Spring Ln, Ba		
oniversity, 1700 L. Cold Spring Lif, Ba	sitinore, MD 21231	11. Contract or Grant No.
		Federal Grant # 69A3552344811 /
		69A3552348316
12. Sponsoring Agency Name and A	ddress	13. Type of Report and Period
Safety21 University Transportation C	enter	Covered
Carnegie Mellon University	Final Papart / Luly 1, 2024 June	
5000 Forbes Avenue	Final Report (July 1, 2024 – June	
Pittsburgh, PA 15213		30, 2025)
		14. Sponsoring Agency Code
	USDOT	
15. Supplementary Notes		1

# 15. Supplementary Notes

Conducted in cooperation with the U.S. Department of Transportation, Federal Highway Administration.

#### 16. Abstract

This report summaries research findings of Phase 2 of the project titled Improve Highway Safety by Reducing the Risks of Landslides, sponsored by National UTC – Safety 21 program. To prevent landslides hazards, multiple approaches were integrated to develop a framework for detecting and monitoring slope instability and assessing landslides risks along the state highways, railroads, and roads. In Phase 2, we reviewed geotechnical asset management (GAM) framework, current status and recommendations for implementation in Maryland. Field and lab investigations was continued with geotechnical test results. LiDAR data was utilized in detection and characterization of landslides in Prince George's County. Soil moisture mapping procedures was tested using Sentinel I data with ML approaches with a case study in Prince George's County Maryland. Numerical model development for quantitative landslide risk assessment was initiated aiming at establishing a robust, interpretable, and quantitatively grounded framework for Landslide Risk Assessment (LRA) by integrating physics-based numerical modeling with machine learning approaches. Integrating GIS-based susceptibility mapping and machine learning framework was initiated for landslide prediction and early warning with a case study in in in Baltimore County, Maryland.

17. Key Words		18. Distribution S	Statement	
Landslides, Precipitation, Slope Stability, Geotechnical Engineering, Soil Tests, Light Detection and Ranging (LiDAR), Geotechnical Asset Management, Risk Assessment, Numerical Modeling, Soil Moisture		No restrictions.		
		y Classif. (of this	21. No. of	22. Price
NONE page)			Pages	
	NONE		125	

Form DOT F 1700.7 (8-72)

Reproduction of completed page authorized



US DOT National University Transportation Center for Safety

# Carnegie Mellon University















# Improve Highway Safety by Reducing the Risks of Landslides (Phase 2)

**Zhuping Sheng**, **Ph.D.** (<u>https://orcid.org/0000-0001-8533-527x</u>)

Oludare Owolabi, D.Sc. (<a href="https://orcid.org/0000-0002-1958-6430">https://orcid.org/0000-0002-1958-6430</a>)

Yi Liu, D. Eng. (https://orcid.org/0000-0002-6861-2914)

FINAL RESEARCH REPORT – July 31, 2025

#### **DISCLAIMER**

The contents of this report reflect the views of the authors, who are responsible for the facts and the accuracy of the information presented herein. This document is disseminated in the interest of information exchange. The report is funded, partially or entirely, under [grant number 69A3552344811 / 69A3552348316] from the U.S. Department of Transportation's University Transportation Centers Program. The U.S. Government assumes no liability for the contents or use thereof.

# Contents

1	Introduction	1 -
	1.1 Geological hazards	2 -
	1.2 Updates on landslides detection and warning smart system framework	2-
	1.3 Objectives of the project (Phases 1 and 2)	3 -
	1.4 Alignment with the USDOT strategic plan	3 -
2	Review of Geotechnical Asset Management Frameworks for Highw	
	System	
	2.1 Introduction	_
	2.2 Summary of geohazards prevalent in Maryland	
	2.3 Geotechnical Assets in Transportation Systems	
	2.4 Geotechnical Asset Taxonomy	
	2.5 Review of existing GAM frameworks in the U.S	
	2.5.1 Alaska DOT&PF (Geotechnical Asset Management Program)	
	2.5.2 Washington State DOT	
	2.5.4 Alberta, Canada	
	2.6 Predictive Modeling in GAM	
	2.6.1 Statistical & Probabilistic Techniques	_
	2.6.2 ML & Predictive Modeling in GAM	
	2.6.3 Implications for Maryland	
	2.7 Investment Analysis in GAM	
	2.7.1 Theoretical Foundations & Business Case	
	2.7.2 Lifecycle Cost-Benefit Approaches	
	2.7.3 Cross-Asset Integrative Investment Planning	
	2.7.4 Challenges & Data Needs	- 19 -
	2.7.5 Implications for Maryland	
	2.8 Summary and Future Work	
	·	
3	Laboratory Investigation of Soil Properties for Landslide Risk	
	Assessment in Montgomery County	
	3.1 Introduction	
	3.2 Materials and Methodology	
	3.2.1 Materials	
	3.2.2 Field Survey and Data Collection	
	3.2.3 Laboratory Procedure	
	3.2.4 Mohr-Coulomb Failure Criteria	
	3.3 Test Results and Analysis	
	3.3.1 Sieve Size Analysis	
	3.3.3 Moisture content	
	3.3.4 CU Triaxial Test	_
	3.3.5 Summary of the Results	
	3.4 Conclusions and Future Research	
	0.4 Conclusions and I acute rescared	33 <sup>-</sup>

4 Detection and Mapping of Landslides with Remote Sensing LiDAR

	data in Prince George's County, Maryland	36 -
	4.1 Introduction	36 -
	4.1.1. Problem Statement	
	4.1.2. Research Aim and Objectives	
	4.2 Study Area	37 -
	4.3. Literature Review	
	4.3.1. Remote Sensing and LiDAR for Landslide Mapping	39 -
	4.3.2. Geomorphometric and Hydrologic Factors	
	4.3.3. Landslide Susceptibility Modeling	
	4.3.4. Risk Zonation and Validation Challenges	
	4.4. Materials and Methodology	
	4.4.1. LiDAR DEM Acquisition and Preprocessing	
	4.4.2 Resolutions of the Digital Elevation Models	
	4.4.3 Geomorphometric factor generation, classification, landslide de and mapping	
	4.4.4 Buffering and Overlay Operations (Area of Interest)	
	4.5 Results	
	4.6 Summary and Future Work	
	410 2 a y aa 2 a.a	40
5	Surface soil moisture mapping for slope instability analysis in	
	Maryland using machine learning model	_
	5.1 Introduction	
	5.2 Related Works	
	5.2.1 Reviewed Papers on Remote Sensing Models	
	5.2.2 Reviewed Papers on Machine Learning for Soil Moisture Estima	tion
	52 -	
	5.2.3 Reviewed Papers on ML Models for Soil Moisture in Geoscience	
	5.3 Materials and Methods	
	5.3.1 Study Area	
	5.3.2 Data Preparation	
	5.3.3 Methodology	
	5.4 Preliminary Results	
	5.5. Conclusion and Future Works	67 -
6	Numerical model development for quantitative landslide risk	
	assessment	69 -
	6.1 Introduction	69 -
	6.2 Objectives	71 -
	6.2.1 Overall Research Objectives	71 -
	6.2.2 Objectives of the Current Stage (Stage 2)	72 -
	6.3 Methodology	72 -
	6.3.1 Overview of Methodology	72 -
	6.3.2 Modeling details for each methodology	
	6.3.3 Groundwater Modeling and Pore Pressure Simulation	75 -
	6.3.4 Parametric Case Design	77 -
	6.4 Preliminary Results and Discussion	78 -
	6.4.1 Slope Failure Surface	
	6.4.2 Parametric analysis for FoS Calculation	

6.5 (	6.4.3 Effect of Groundwater Table Distribution	
7 Integ	rating GIS-Based Susceptibility Mapping and Machine Lo Landslide Prediction and Early Warning in in Baltimore	earning County,
	yland	
7.1 I	ntroduction	•
_	7.1.1 Research goals and objectives	
-	Related Works	
7.3 I	Materials and Methods	
	7.3.1 Study Area	-
	7.3.2 Data sources	
	7.3.3 Methodology	
	Preliminary Results	
7.5	Conclusions	103 -
7.6 I	Future Work	104 -
8 Sum	maries	105 -
8.1 (	Conclusions	105 -
8.2 1	Future Work	105 -
9. App	endices	106 -
A: Res	earch Products for this Project	106 -
	Conference Publications	
	Datasets	
	A.2.1 Appendices for Chapter 4	
	A.2.2 GIS coverages for Historical Landslides	
A.3	Research Symposium	
Bibliog	eraphy	111 -

#### Chapter 1

# 1 Introduction

Geologic hazards including slope failures, landslides, mudflows, debris flows, etc. and hydrological hazards related to floods and stormwater surge can be destructive to transportation infrastructure and threaten property and human life along the highway, railroads and roads. Landslides alone cause thousands of deaths and many billions of dollars in damage every year. Therefore, there is a great need in advancing our knowledge in slope instability and failure risks and developing technologies in detecting and monitoring, and preventing landslides, in turn sustaining the safety of transportation infrastructure and system operations in a changing environment [1]

As a member of the USDOT National University Transportation Center (UTC) – Safety 21 program led by Carnegie Mellon University, Morgan State University team proposes a multi-phase interdisciplinary project focusing on the safety of transportation infrastructure systems by preventing geohazards, specifically slope failure and landslides and minimizing impacts of geohazard along the highway, railroads, and roads. This project will employ an integrated approach of geotechnical and AI/Machine Learning methods for assessing conditions of geotechnical assets, such as cut slopes and embankment of the DOT/SHA and delineating landslides and high-risk areas [1].

This report summaries research findings of Phase 2 of the project titled Improve Highway Safety by Reducing the Risks of Landslides, sponsored by National UTC – Safety 21 program. The report is organized in the following order. In the introduction section we will provide a brief background about geological hazards and objectives of the research project. We follow with geotechnical asset management and current status (Chapter 2). The updates on field and lab investigation were provided in Chapter 3. Applications of LiDAR data in detection and characterization of landslides in Prince George's County were discussed in Chapter 4. To better understanding the roles of precipitation in triggering landslides soil moisture mapping procedures using Sentinel I data with ML approaches were proposed and tested with a case study in Prince George's County Maryland (Chapter 5). The numerical model development for quantitative landslide risk assessment was discussed in Chapter 6, aiming at establishing a robust, interpretable, and quantitatively grounded framework for Landslide Risk Assessment (LRA) by integrating physics-based numerical modeling with machine learning approaches. At the last integrating GIS-Based susceptibility mapping and machine learning framework for landslide prediction and early warning in in Baltimore County, Maryland was introduced.

#### 1.1 Geological hazards

Geologic hazards, such as landslides, land subsidence and earth fissures, and earthquakes, etc. and hydrological hazards, such as floods and stormwater surge owing to extreme weather events (tropical storms, hurricanes, tornadoes, etc.), compounding with sea-level rising due to global warming and climate change, have caused great impacts on transportation infrastructure and traffic, in turn resulting in great economic damages. Landslides are among the most devastating and costly natural disasters, causing thousands of deaths and many billions of dollars in damages annually [2–4].

The majority of landslides are precipitation-triggered [5] even though they occur over a broad range of lithological, climatological, and hydrological conditions, and land use types [6]. However, for most precipitation-triggered landslides, other complex atmospheric, surface, and subsurface conditions also play a role in slope failure by increasing the effects of downgradient forces and/or reducing the strength of the underlying slope soils/rocks [7, 8]. The effect of precipitation from these confounding factors is thus essential both for enhancing fundamental understanding of landslides and for evaluating the impact of climate change on slope failure.

# 1.2 Updates on landslides detection and warning smart system framework

We noted that it is common practice in many regions around the world to create an inventory of landslide, debris flow and/or slope failure occurrences. In addition, many studies have attempted to quantify the likelihood of the occurrence of landslides or identify areas that are susceptible to slope failures or instability, e.g., landsides susceptibility (LS) analysis based on GIS models and machine learning models [9]. MDOT/SHA manages an extensive portfolio of geotechnical assets, including slopes, embankments, and ground modifications, along the State of Maryland's roadway infrastructure. Its geotechnical asset management (GAM) plan establishes MDOT SHA's asset class strategy with a robust plan to guide infrastructure decisions; optimize the total cost of ownership; and meet performance, reliability, and risk objectives [10]. With MDOT/SHA sponsorship, MSU and Carnegie Mellon University initiated a project for incorporating precipitation data into the geotechnical asset management.

With additional support from the National UTC Safety 21 program, Morgan State University team carried out a multi-phase (multi-year) project focusing on the safety of transportation infrastructure systems by preventing geohazards, specifically slope failure and landslides and minimizing impacts of geohazards. This project employed an integrated approach of geotechnical and AI/Machine Learning methods for assessing conditions of geotechnical assets, such as cut slopes and embankment of the DOT/SHA and delineating landslides and high-risk areas. Figure 1.1 shows a framework for landslides detection and monitoring smart system built on a GIS platform.

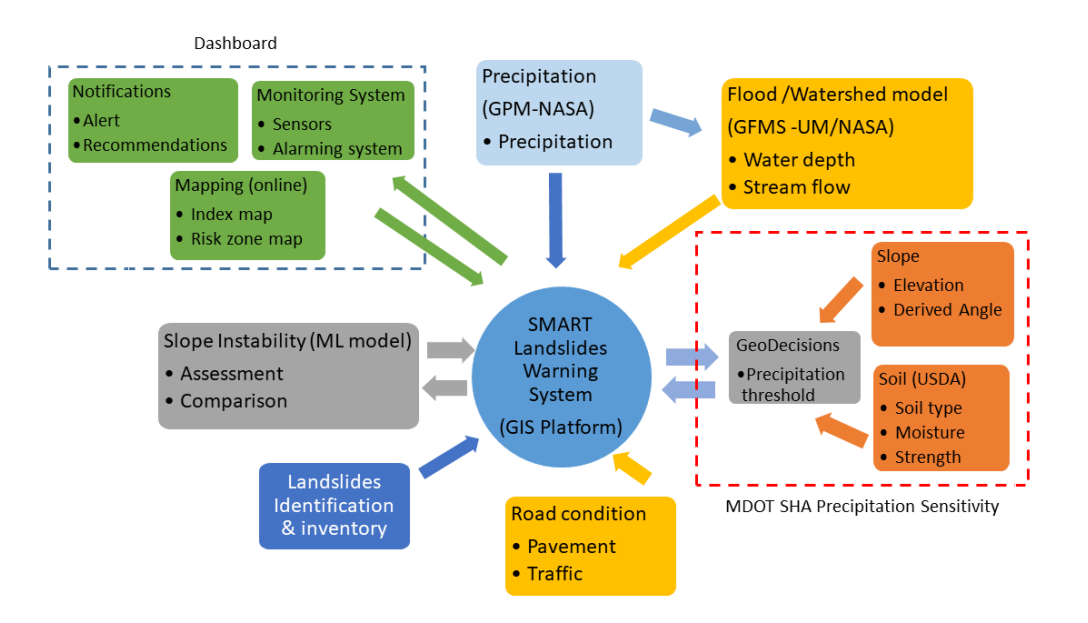


Figure 1.1: Framework for landslide risk assessment and monitoring smart system (modified from [1]).

### 1.3 Objectives of the project (Phases 1 and 2)

This project is unique by integrating geotechnical and machine learning approaches in assessing slope instability and risk of landslides and mapping high-risk areas along highway, railroad and roadways. This project is built upon an ongoing project sponsored by Maryland Department of Transportation/State Highway Administration (MDOT/SHA).

The objectives (tasks) of the project include: (1) with AI/Machine Learning approaches assess the risks of landslides based on soil/rock types, weather conditions, mechanical properties of slope materials, and the status of existing retaining structures along the selected highway sections, using Maryland as case studies, (2) identify and map the high-risk areas based on controlling factors such as geometry and mechanical properties of soil or rock, and triggering factors, including gravitational and hydraulic forces, using available survey data, remote sensing and LIDAR data and other factors like transportation modes, (3) design and test protocols for real time monitoring at selected sites in consultation with DOT SHA staff, and (4) recommend strategies for reducing the risks of landslides with real-time monitoring for the high-risk areas, and improving the safety of the transportation infrastructure. All the methods and strategies can be transferred to other states or regions with similar geological conditions and engineering configurations [1]. Phase 1 of this project covered task 1 and part of task 2. Phase 2 of this project continued to cover part of Task 1 and Task 2.

## 1.4 Alignment with the USDOT strategic plan

The proposed project will address transportation safety, especially physical infrastructure systems and roadway design, covering the following US DOT goals [1,

11]:

- Update roadway design standards to protect vulnerable road users and vehicle occupants.
- Use regulatory and policy tools to advance roadway safety to reduce fatalities and injuries across modes.
- Support the adoption and maturation of safety management systems across modes.
- Use data and data analytics to take proactive actions to address emerging safety risks and support compliance.

The project will provide technical assistance to better identify, assess, and address critical physical vulnerabilities.

- Incorporate physical protections in the standards for design of emerging automated and connected systems and technologies, such as real-time sensing and monitoring systems.
- Strengthen system response and recovery plans and protocols to minimize the effects of system disruptions and hasten system recovery from the natural disasters.
- Promote guidelines on vulnerability assessments with enhancement of AI/ML approaches.

The project will assess and mitigate the vulnerability of transportation infrastructure to extreme weather conditions and natural disasters:

- Assess the vulnerability of assets and identify novel hazards mitigation strategies.
- Enhance resilience throughout transportation planning and project development processes by updating guidance and regulations.
- Conduct case studies and pilot projects to develop and evaluate new and innovative adaptation and resiliency technologies, tools, and opportunities, such as motion sensors and early warning systems.

This project will build research capacity in the critical area of designing resilient infrastructure for geohazards and extreme weather conditions. It will also provide educational opportunities for graduate and undergraduate students to gain knowledge and experience in this important new area for resilient engineering. Thus, the project will also build human capacity to address the challenge of geohazard adaptation and mitigation related to transportation systems [1].

### **Chapter 2**

# 2 Review of Geotechnical Asset Management Frameworks for Highway System

John Tanimola, Joshua Nash, Yi Liu, Zhuping Sheng, Oludare Owolabi

#### 2.1 Introduction

Geotechnical Asset Management (GAM) applies strategic asset management principles such as lifecycle planning, risk evaluation, and data-driven decision-making to geotechnical assets including slopes, embankments, retaining walls, rockfall mitigation systems, and subgrades [1]. National Cooperative Highway Research Program (NCHRP) Report 903 defines GAM as a risk-based approach designed to extend traditional asset management frameworks, incorporating tools like GAM Planner and lifecycle-cost templates to support decision-making on geotechnical infrastructure [12]. Urban resilience hinges not only on structures like roads and bridges but critically on the stability of geotechnical assets. These earthworks often lie hidden beneath developed areas and can cause severe service disruptions and safety hazards upon failure [12]. As climate change amplifies the frequency and intensity of weather extreme events such as heavy rainfall and flooding, the stress on slopes and embankments increases, underscoring the essential role of GAM in ensuring urban infrastructure remains robust and adaptable [13].

Urban regions like Maryland, face growing vulnerability to geohazards including landslides, embankment failures, soil erosion, and slope instability driven by aging infrastructure, changing climate patterns, and increasing human activities. While transportation agencies have advanced in managing roads and bridges through data-driven asset management, geotechnical assets such as retaining walls, cut slopes, embankments, and subgrade systems have often been overlooked, treated largely as unpredictable risk sites with high liability potential. The consequences of geotechnical asset failures can include service disruptions, collateral damage to adjacent infrastructure, and public safety threats [12].

The Maryland Department of Transportation's Strategic Asset Management Plan (SAMP) outlines a proactive, risk-based lifecycle approach for its multimodal infrastructure, targeting long service lives and system reliability [14]. However, the SAMP is missing targeted strategies for managing geotechnical components even as these assets play a critical role in supporting pavements, bridges, culverts, and other highway infrastructures [14]. This omission signifies a substantial gap in Maryland's ability to anticipate, assess, and mitigate geohazard risks effectively. To close this gap,

this study seeks to review established GAM frameworks adopted by different state Departments of Transportation, assessing their applicability for Maryland's infrastructure management strategy.

#### 2.2 Summary of geohazards prevalent in Maryland

Over the past two decades, Maryland has experienced numerous geohazard events including landslides, sinkholes, slope failures, and major erosion that have directly impacted highways, roads, and related transportation infrastructure. These events, often triggered by extreme weather conditions or long-term geological instability, have led to substantial repair costs, prolonged road closures, and safety risks for commuters and freight movement. A review of documented incidents reveals that responses to such geohazards have historically been reactive rather than preventive. For example, landslides like the 2014 collapse on East 26th Street in Baltimore (Figure 2.1) or the recurring slope failures in Allegany and Washington Counties were addressed only after catastrophic events occurred, often resulting in emergency repairs and costly detours. Similarly, sinkholes in Montgomery, Frederick, and Harford Counties have emerged without structured risk prediction or targeted monitoring of vulnerable corridors. These underscore the importance of ongoing geotechnical monitoring and infrastructure resilience efforts in the state.



Figure 2.1: Retaining Wall failure leading to a Collapsed One Lane of East 26<sup>th</sup> Street in Baltimore after heavy rain on April 30, 2014. (Berlin, 2014 <a href="mailto:nationalgeographic.com">nationalgeographic.com</a>; washingtonpost.com).

## 2.3 Geotechnical Assets in Transportation Systems

Geotechnical assets including cut slopes, embankments, retaining walls, subgrades, and other earthworks play vital roles in sustaining highway systems. These assets

support pavements and roadway alignments, control drainage, and prevent slope failures and erosion that can interrupt travel and risk safety [1]. Unlike bridges or pavements, geotechnical features have not always received structured assetmanagement attention, even as failures cost agencies millions and pose liability and operational risks [12].

Recent studies have advocated integrating geotechnical assets into formal Asset Management Systems (AMS), using data-driven methods such as GIS-based inventories, hazard scoring, risk-based prioritization, and predictive modeling to address potential failures before they result in emergencies [1]. These tools provide necessary visibility into hidden infrastructure vulnerabilities and align with modern resilience objectives in transportation [1]. Effective management of geotechnical assets requires a strategic, systematic approach encompassing operation, maintenance, upgrades, and expansion throughout the asset lifecycle. This approach emphasizes both business and engineering practices for resource allocation and utilization, with the objective of better decision making based upon quality information and well-defined objectives. According to the Alaska DoT and PF technical report, geotechnical asset management processes can be summarized as illustrated in Figure 2.2.

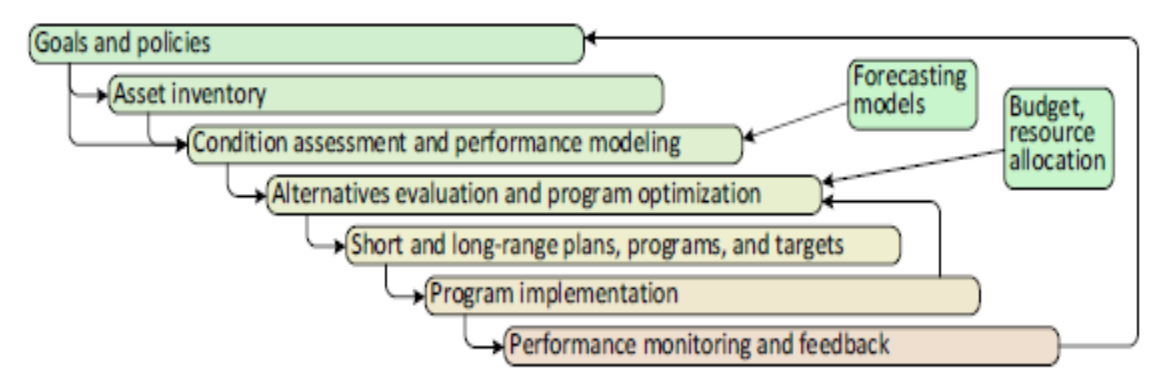


Figure 2.2: Geotechnical Asset Management Processes [15].

#### 2.4 Geotechnical Asset Taxonomy

The asset taxonomy illustrated in Figure 2.3 is adapted from Alberta Transportation's GAM framework, which emphasizes structured classification by asset type, construction origin (natural or constructed), material composition (e.g., soil, rock, concrete), and controlling behavior (e.g., erosion, slope instability, settlement). This classification system allows for consistent inventory development and enables the application of tailored deterioration models for each asset class. While Alberta's framework focuses heavily on slopes, embankments, and retaining walls, this taxonomy has been expanded for Maryland's context to include unique features such as subsidence-prone subgrades, tunnel sections, and geologically sensitive formations like Cretaceous Outcrops and the Marlboro Clay Layer (Paleocene). These additions reflect the localized geotechnical risks and support the development of a more inclusive and responsive asset register in Maryland's highway infrastructure.

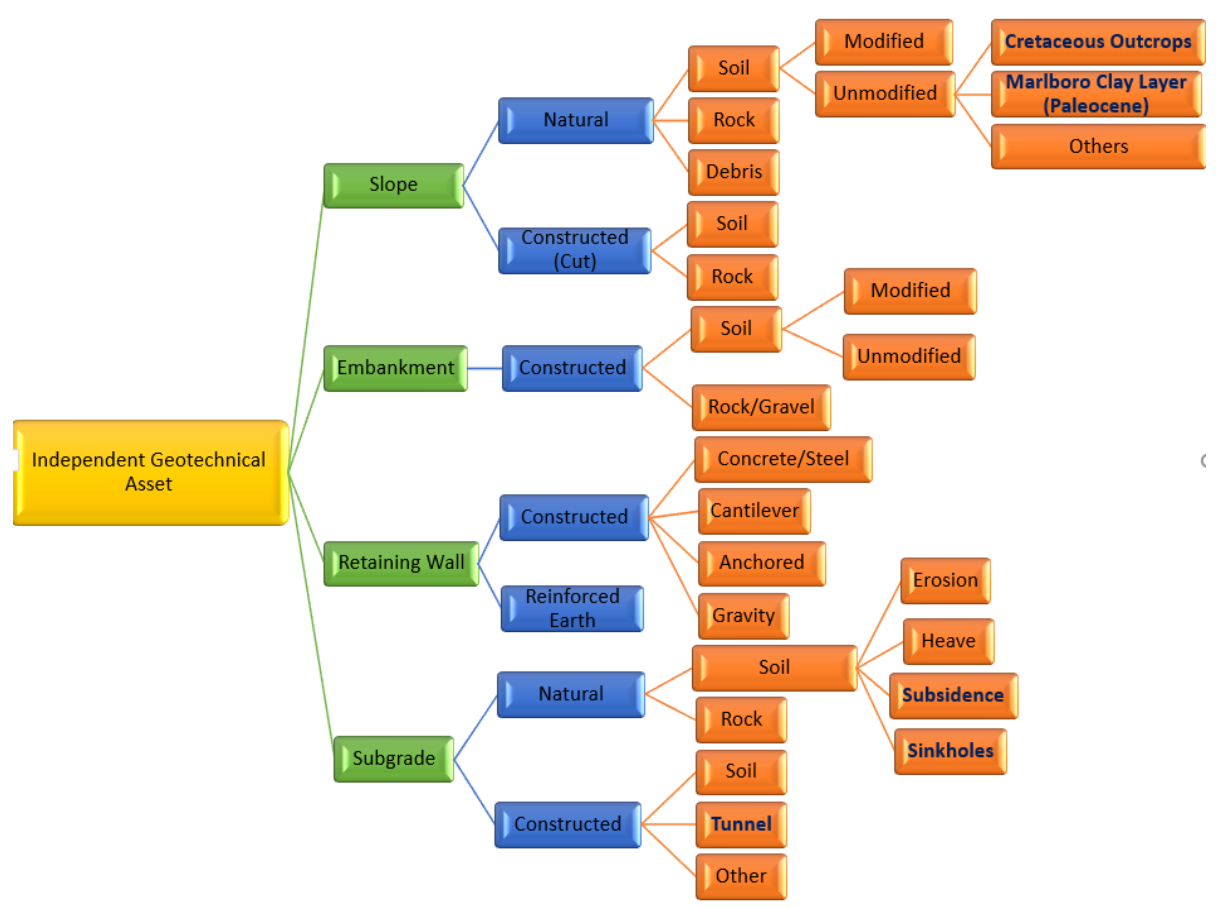


Figure 2.3: Geotechnical Asset Taxonomy (Adapted from Alberta's (Canada) GAM Framework [16].

# 2.5 Review of existing GAM frameworks in the U.S.

Tables 2.1 and 2.2 below summarize the state of practice in GAM for ten U.S. states, covering both formal DOT programs and pilot/research initiatives. Key dimensions include asset covered, system/GIS integration, strengths, gaps, implementation status, and sources of information.

Table 2.1: Overview of Geotechnical Asset Management Program in the United States

State	Type of Asset Covered	System / GIS Integration	Ref.
Alaska	<ul> <li>Rock Slopes</li> <li>Unstable Soil Slopes</li> <li>Embankments</li> <li>Retaining Walls</li> <li>Material Sites (borrow pits/quarries)</li> </ul>	<ul> <li>ArcGIS-based system for inventory and visualization. Data is stored in a GIS geodatabase;</li> <li>ArcGIS Online "Story Map" provides an interactive GAM overview. Asset Inventory Interface and Event Tracker are</li> </ul>	[15]

		accessible via GIS web	
		maps.	
Missouri	<ul> <li>Slopes (Rock &amp; Soil),</li> <li>Engineered             Embankments</li> <li>Retaining Walls</li> <li>Subgrades &amp;</li> <li>Subsidence</li> </ul>	<ul> <li>Data is integrated into MoDOT's enterprise systems.</li> <li>The field data (via Survey123) feeds into MoDOT's TMS and GIS databases.</li> <li>Asset locations are GPS-tagged and viewable on maps (KMZ layers were produced for inventoried assets).</li> </ul>	[17]
Ohio	<ul> <li>Rock slopes (rock cuts)</li> <li>Landslide-prone soil slopes along highways.</li> <li>Retaining Walls</li> <li>Abandoned Underground</li> <li>Sinkholes &amp;</li> <li>Culverts in separate programs</li> </ul>	<ul> <li>Geotechnical data integrated in enterprise GIS (TIMS – Transportation Information Mapping System, Figure 2.4).</li> <li>GIS is used for planning and to communicate hazard locations to district offices and maintenance.</li> </ul>	[18]
California	<ul> <li>Cut Slopes and</li> <li>Embankments –         particularly those         prone to landslides         or erosion along</li> <li>Retaining Structures</li> </ul>	• No public geotechnical asset GIS map statewide.	[12]
Oregon	<ul> <li>Rockfall sites (rock cut slopes prone to rockfall</li> <li>Landslides / Unstable Soil Slopes,</li> <li>Debris flow prone sites</li> <li>Retaining walls and material sources are handled separately</li> </ul>	<ul> <li>ODOT's Unstable Slopes data is stored in a database with a GIS interface. Internal users can view slope locations, ratings, and details via a map-based application.</li> <li>Oregon has not published the map due to data infancy as noted, but internally GIS is integral.</li> </ul>	[19]
Washingto n	• Unstable Slopes (soils and rocks)	WSDOT Geospatial Open Data Portal,	[12][20]

	<ul><li>retaining wall</li><li>Foundations</li><li>Embankments</li></ul>	• Online Map Center, GeoPortal	
Colorado	<ul> <li>Culverts,</li> <li>Embankments</li> <li>Geo-hazards</li> <li>Slopes</li> <li>Retaining wall</li> <li>Subgrades</li> <li>Tunnels</li> </ul>	<ul> <li>OTIS: Online transportation information system</li> <li>C-Plan: interactive online mapping platform</li> <li>GeoHub: Internal ArcGis for portal site</li> </ul>	[21][22]
Vermont	<ul><li>Retaining walls</li><li>Unstable slopes</li></ul>	<ul> <li>Planned – The Vermont         Asset Management         Information System         (VAMIS)</li> <li>integration is not         complete – essentially         no geotechnical layer         exists in their public         asset maps yet.</li> </ul>	[23]
Georgia	<ul><li>Retaining walls</li><li>Slopes</li><li>Embankments</li></ul>	• In development – The envisioned G-GAMS will be an information system to manage these assets, presumably with a GIS interface.	[24]
Louisiana	<ul><li>Embankments</li><li>Retaining walls,</li><li>Slopes,</li><li>Soil borings,</li><li>Tunnels</li></ul>	<ul> <li>ArcGIS database and a mobile ArcGIS Field Maps app for use with the GAM guide. (La DOTD ArcGIS Online)</li> </ul>	[25]

Table 2.2: Implementation Status of Geotechnical Asset Management Program in the United States

State	Implementation Status	Strengths & Weaknesses Summary Ref.	
Alaska	Transitioning to practice	Nation-leading GAM effort using NCHRP 903 guidance and GIS; incomplete inventory, not yet institutionalized	[15]
Missouri	Pilot completed (2023)	Strong GIS integration and user-friendly tools; only 2 districts piloted, lacks risk history data	[17]
Ohio	Operational (partial)	Long-standing inventories;	[26][18]

		fragmented systems hinder integration; reactive for lower-priority assets	
California	Ad-hoc	Extensive disaster response experience; lacks formal GAM program or statewide inventory	
Oregon	Emerging program; risk- based ranking to guide proactive slope fixes (shifting from reactive).	Robust BCR-based prioritization; limited funding, excludes walls	[19][12]
Washingto n	Fully implemented (slopes)	Pioneer GAM model for slopes with dedicated funds; other geotech assets excluded	[12]
Colorado	Mature & evolving	Integrated into TAMP with strong risk modeling; scale of risk challenges full coverage	[21]
Vermont	Conceptual stage	Acknowledges need for GAM; lacks data and funding to move beyond reactive posture	[23]
Georgia	Initiation phase (2024)	Structured plan with academic backing; no existing inventory yet	[24]
Louisiana	Early implementation	Focus on MSE walls with GIS support; broader geohazards not yet covered	[25]

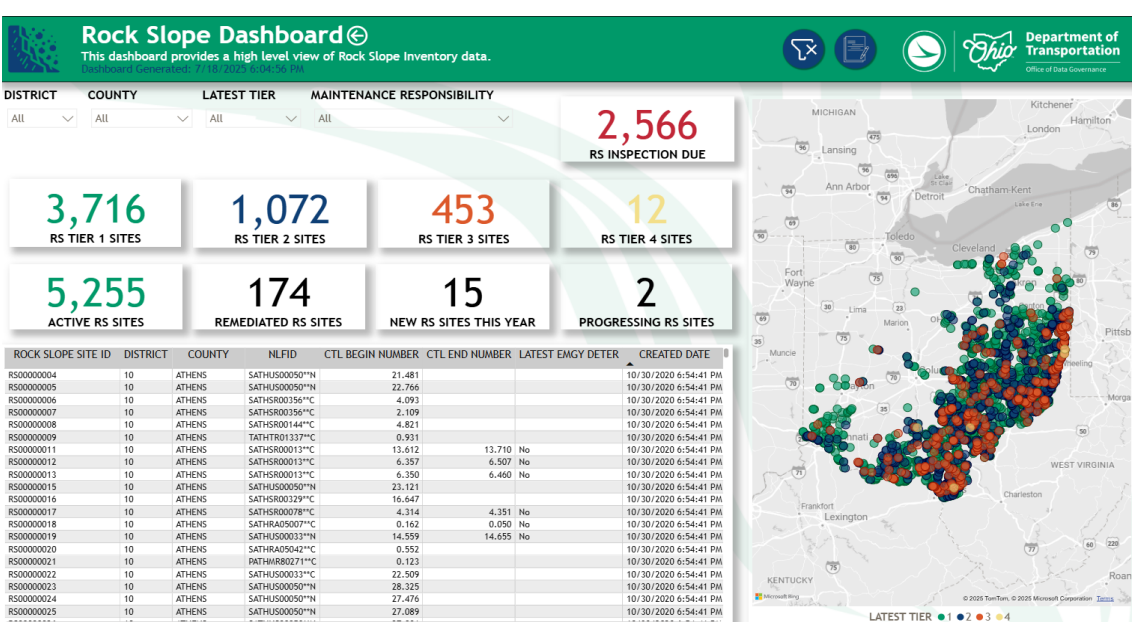


Figure 2.4: Ohio Department of Transportation (2025). Rock Slope Dashboard [Data visualization]. Retrieved July 20, 2025 from [26].

The bar chart in Figure 2.5 illustrates the frequency of geotechnical asset types managed across various U.S. state DOTs based on documented frameworks. Slopes (10 states), retaining walls (10), and embankments (7) are the most commonly

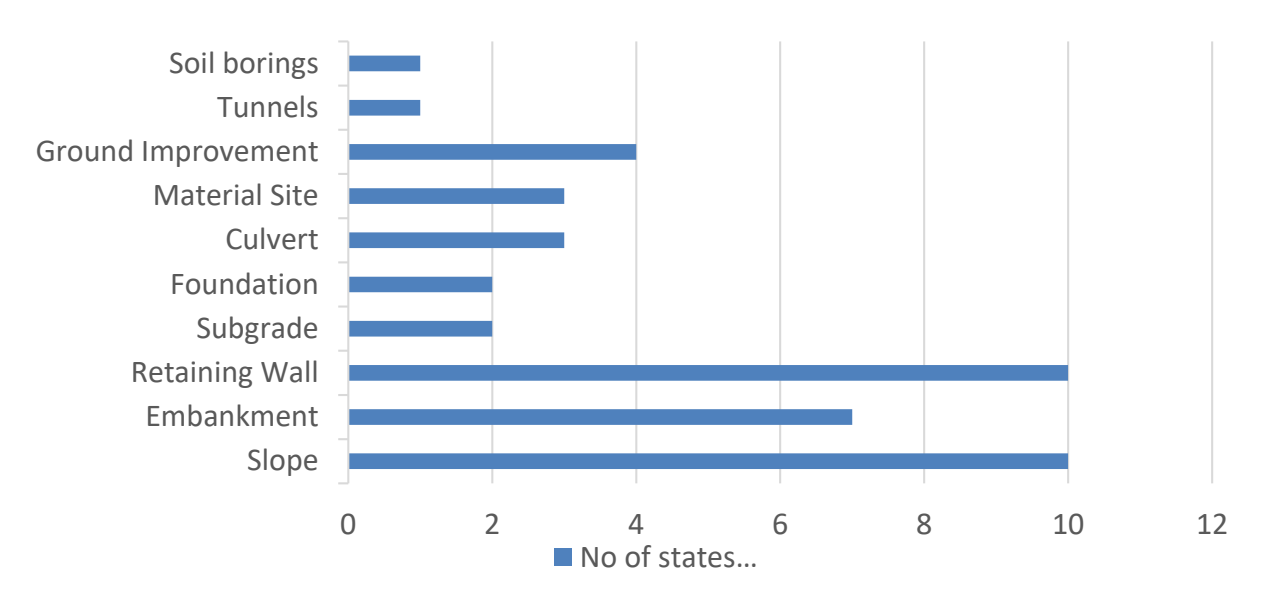


Figure 2.5: Summary of geotechnical assets covered across ten US states.

included assets, reflecting their critical role in highway stability. Less frequently managed assets include material sites, tunnels, foundations, subgrades, etc., suggesting gaps in comprehensive inventory practices across states. This underscores the need for standardized inclusion of all key geotechnical assets in asset management systems.

#### 2.5.1 Alaska DOT&PF (Geotechnical Asset Management Program)

Alaska was a pioneer state in geotechnical asset management, developing one of the nation's first comprehensive programs. The Alaska DOT&PF's program focuses on four asset classes critical to highway performance. They are rock slopes, unstable soil slopes and embankments, material sites (borrow pits), and retaining walls. Statewide inventory and condition surveys have been conducted on these assets (e.g., all rock/soil slopes along National Highway System routes), and a standardized condition state evaluation was established as part of the program. The department also developed tools to track geotechnical incidents (e.g. landslides, rockfalls); over a decade's worth of maintenance records (7,000+ geotechnical events) were mapped to identify risk "hot spots". Alaska's research-driven plan quantified the overall condition and value of geotech assets finding an estimated \$19 billion in replacement costs for slopes and walls (roughly three times the value of Alaska's bridges). Although formal performance targets (e.g., % of slopes in good condition) were not yet in place, Alaska used risk and financial impact as key performance considerations. The program employs risk-based deterioration modeling and scenario analysis at a network level. Fiscal modeling showed clear benefits to proactive maintenance: extending the service life of slopes and walls yields cost savings over time; "every dollar

invested in preservation pays for itself and saves an additional \$1.06 in long-term costs" by averting expensive failures. In essence, Alaska's models predict that early interventions on geotechnical assets have a positive lifecycle ROI. The Alaska DOT&PF integrates geotechnical assets into its Transportation Asset Management approach, using a corridor-level risk analysis to prioritize investments. High-risk sites (those whose failure would significantly impact mobility or safety) are addressed first, and the program's cost-benefit findings support allocating funds to preservation of slopes and walls as a statewide strategy. This risk-informed, performance-based approach helps Alaska justify geotechnical mitigation projects alongside traditional assets like bridges and pavements [15].

#### 2.5.2 Washington State DOT

Washington State DOT (WSDOT) manages geotechnical assets, particularly slopes, through its Unstable Slope Management System (USMS). The USMS covers all known unstable slopes, including chronic rockfall areas in the Cascades, coastal bluffs, and landslide-prone slopes statewide. WSDOT uses a quantitative rating system to evaluate slope condition and hazard, assigning numerical scores based on factors like slope geometry, observed instability, traffic exposure, and potential consequences. This system allows for consistent comparison of hundreds of slopes. WSDOT's Geotechnical Office maintains a GIS-enabled database for these assets, with district maintenance personnel able to input observations via a web interface. Performance measures focus on risk reduction, with a key metric being the number of high-risk slopes mitigated over time. Washington allocates about \$30 million per biennium for slope stabilization, aiming to keep highways open and safe from slope failures. The decline in overall network risk is tracked as slopes are stabilized. The USMS rating system provides a predictive outlook by identifying slopes likely to fail. WSDOT refines predictions with site-specific monitoring, using instruments and surveys for high-risk slopes. With data from the 1990s, WSDOT can calibrate predictions based on historical scores preceding failures. In 2017, WSDOT reviewed slope mitigation structures to ensure their condition feeds into future needs predictions. WSDOT's investment strategy prioritizes projects based on risk and benefit-cost, focusing on the most at-risk slopes on critical corridors. The \$30M biennial funding addresses topranked sites, integrating geotechnical fixes into the capital program. Although broader Geotechnical Asset Management Program expansion was shelved due to funding constraints, the core unstable slopes program remains effective, guided by data and asset management principles [12, 27].

#### 2.5.3 Colorado DOT (Retaining Wall and Geohazard Management)

Colorado DOT (CDOT) has integrated geotechnical assets into their asset management plans, focusing on retaining walls and geohazards. As of 2021, CDOT monitored approximately 2,928 retaining walls, totaling about 14 million square feet of wall face area. These include Mechanically Stabilized Earth (MSE) walls, gabion walls, and crib walls along highways. CDOT's Geohazards Program addresses natural slope hazards such as rockfalls, landslides, embankment settlements, and sinkholes [21]. CDOT established a Retaining Wall Inspection and Asset Management Manual to standardize wall inspections, assigning condition ratings based on signs of distress. The Geohazards Program uses field assessments and a scoring system to evaluate

slope conditions and risks. This system is maintained at the state level to log hazard locations and their status [21]. In Colorado's risk-based Transportation Asset Management Plan (TAMP), geotechnical assets are included as "Tier II" assets with performance projections over a 10-year period. CDOT sets goals for its wall program, such as maintaining a certain percentage of wall area in fair or better condition. For geohazards, performance is measured by the reduction in roadway closures or incidents due to natural hazards [21]. CDOT's predictive models for retaining walls consider factors like age and known failure modes to estimate remaining life. For geohazards, the program monitors precipitation and freeze-thaw cycles in known trouble spots to anticipate slides or rockfalls. This data informs when and where the next geotechnical failure might occur [21]. Colorado has institutionalized investment in geotechnical assets by creating specific programs and budget lines. The Geohazards Program directs funds to high-priority slope hazard mitigations and handles emergency responses for landslides and rockfalls. The retaining wall asset program justifies funding for repairs or replacements as part of asset preservation. By including walls and geohazards in the TAMP, CDOT competes for funds alongside bridges and pavements, emphasizing cost-effectiveness and proactive management [21].

#### 2.5.4 Alberta, Canada

Alberta's GAM framework, developed chiefly through collaboration between Alberta Transportation and Tetra Tech Canada, transforms its long-standing Geohazard Risk Management Program (GRMP) into a proactive, risk-based asset management system. A key innovation is the GAM Planner, an enhanced Excel-based decision-support tool adapted from NCHRP Report 903 that integrates site-specific inputs such as inspection data, traffic volume, detour lengths, monetized risk, lifecycle costs, and inventory condition to prioritize intervention timing and funding based on economic and risk criteria [28].

The framework follows a logical sequence:

- 1. Asset taxonomy and inventory data collection for slopes, embankments, retaining walls, and subgrades approximately 500 geohazard sites identified.
- 2. Risk-based rating, calculating probability and consequence factors to yield monetized risk scores, then classifying sites for action.
- 3. Site-specific deterioration modeling, which underpins targeted treatment categories (e.g., maintain, rehabilitate, reconstruct).
- 4. Lifecycle investment planning, using agency and user cost analyses to determine NPV and BCR for treatments.
- 5. Annual update cycle, aligning with capital planning and budgeting, enabling consistent, data-driven decisions [16].

Through this structured Excel-driven system, Alberta effectively combines inspection, risk assessment, predictive modeling, and economic analysis into a comprehensive GAM process delivering strategically prioritized, cost-effective interventions that substantially strengthen provincial highway resilience. Tetra Tech's overall approach for the GAM framework development and pilot-scale implementation is summarized in the process flow chart in Figure 2.6. The flow chart shows the sequence and interdependency of components in the framework.

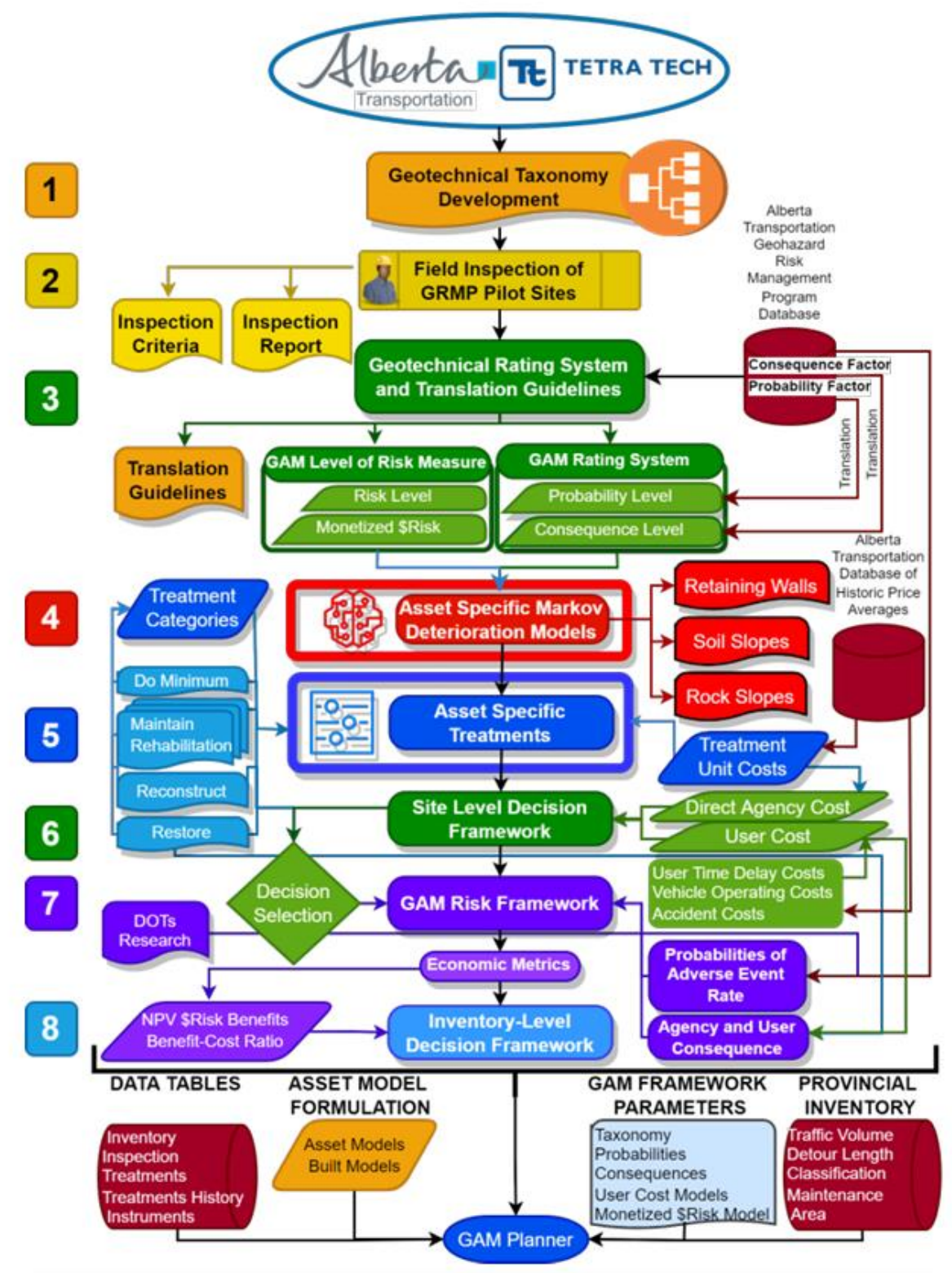


Figure 2.6: GAM Framework Development Process Flowchart [28].

# 2.6 Predictive Modeling in GAM

Predictive modeling is increasingly vital in GAM to anticipate geotechnical asset

deterioration or failure, enabling proactive management and optimized investment planning. The suite of methods ranges from traditional statistical models to advanced machine learning (ML) and probabilistic approaches.

#### 2.6.1 Statistical & Probabilistic Techniques

Markov and semi-Markov models: An essential component of effective GAM is the integration of deterioration models that forecast asset performance over time, enabling strategic budgeting and lifecycle planning. Unlike pavements or bridges, where gradual decline is common, geotechnical assets often display stepwise deterioration and sudden drops in condition due to rare but severe events. Despite this, the aggregated behavior of asset networks remains predictable by using probabilistic models. One such model is the Markov chain which depicts the likelihood of an asset transitioning between condition states annually, based on the current condition. These transitions are quantified through same-state and next-state probabilities derived from median transition times between states [12, 15]. Alaska DOT's GAM Plan provides a practical example: expert-elicited Markov models outline deterioration for soil slopes, rock slopes, retaining walls, and material sites. For instance, soil slopes exhibit a 0.9875 probability of remaining in their current state each year and a 0.0125 probability of transitioning to the next-worse state corresponding to a 55-year median time between State 1 and State 2 [15] The general probability formula used is

$$P_{jj} = (0.5)^{1/t} (2.1)$$

where j = condition state (before and after 1 year) and t = transition time in years.

Such models enable GAM systems to simulate future conditions by applying these transition probabilities year after year, guiding interventions linked to risk thresholds and cost-benefit outcomes. As GAM systems mature like Alberta's GAM Planner, these models can be further refined with real condition monitoring, strengthening predictive capabilities and investment prioritization [16].

#### 2.6.2 ML & Predictive Modeling in GAM

Recent research highlights the transformative power of machine learning (ML) in enhancing Geotechnical Asset Management, especially for slope stability forecasting. A pivotal study by Li et al. [29] reported >90% accuracy in predicting shallow slope failures through an ensemble random forest framework that couples physical models with unsaturated soil moisture dynamics under rainfall conditions. The study demonstrated similar predictive performance to traditional methods like Scoops3D while greatly reducing computational time [30]. Complementing these findings, Aminpour et al. [30] developed ML-based surrogate models (using Random Forest, SVM, and Bagging ensembles) to approximate Monte Carlo reliability analyses for heterogeneous slopes, achieving >85% accuracy in classifying slope failure and reducing computational time from several months to just hours.

These advances suggest a practical roadmap for integrating ML within GAM frameworks: ensemble models to predict near-term factor-of-safety (FoS), surrogate

ML tools for fast probabilistic failure assessments, and Bayesian-inspired models to support time-dependent life-cycle planning. Importantly, states like Alberta, Alaska, and Oregon already maintain rich geotechnical conditions and risk datasets, ideal foundations for training and refining ML models as part of predictive GAM systems [29, 30]. Embracing these tools can substantially accelerate asset risk estimation and economic evaluation, paving the way for more targeted and timely interventions.

#### 2.6.3 Implications for Maryland

Maryland SHA's pilot slope inventory with condition and risk scores provides foundational data essential for predictive modeling. The next phase could involve:

- Implementing ML classification or regression models for categorical condition and FoS prediction.
- Developing surrogate models to enable fast, parameterized risk analysis across wide geotechnical asset portfolios.
- Building time-dependent deterioration emulators to inform life-cycle cost analysis and schedule interventions.

Introducing one or multiple modeling methods ML-based classification, Bayesian degradation emulation, or surrogate probabilistic analysis would significantly enhance the adaptive and data-driven capacity of Maryland's GAM framework.

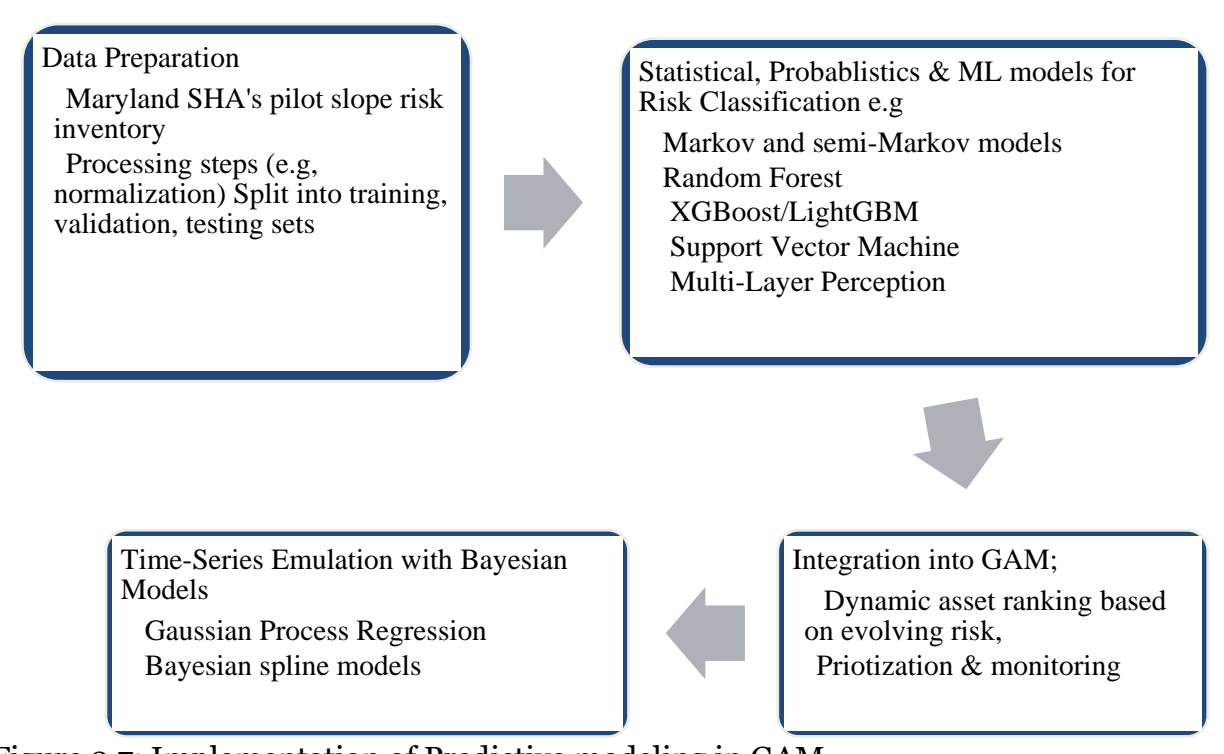


Figure 2.7: Implementation of Predictive modeling in GAM.

# 2.7 Investment Analysis in GAM

Investment analysis in Geotechnical Asset Management focuses on systematically

determining the optimal allocation of limited funds to geotechnical assets such as slopes, walls, embankments by comparing costs, risks, and benefits over their entire lifecycle [12]

#### 2.7.1 Theoretical Foundations & Business Case

GAM is underpinned by the integration of economic evaluation tools that support data-driven decision-making. One of the core theoretical models in GAM is presented in *NCHRP Report 903* [32], which offers a spreadsheet-based Net Present Value (NPV) GAM Planner and lifecycle cost templates. These tools facilitate informed treatment selection and investment timing by calculating the long-term economic consequences of failure and repair. Globally, GAM systems have shown impressive financial benefits, with reported cost savings ranging from 3% to 38% through proactive and risk-based investment strategies. Notably, the United States Army Corps of Engineers (USACE) estimates a typical return on investment (ROI) of 15–40% for projects managed under GAM principles. The efficacy of these systems lies in their ability to support risk-based business cases, where agencies can quantify asset consequences and maintenance costs, thus enabling proactive rather than reactive infrastructure investment [12].

#### 2.7.2 Lifecycle Cost-Benefit Approaches

Lifecycle cost-benefit analysis (LCCA) is an essential methodology within GAM, allowing transportation agencies to compare the long-term financial impact of preventative interventions against the potential cost of post-failure repairs. This analysis extends beyond initial construction costs to include future maintenance, user delays, and safety consequences. [31]. For example, the Alaska Department of Transportation and Public Facilities (DOT&PF) documented notable economic returns, achieving a 38% ROI for rock slope preservation, 148% for retaining wall stabilization, and an extraordinary 882% haul-cost reduction through proactive material site management [15]. Similarly, the Oregon DOT incorporates cost-benefit ranking into its Unstable Slope Management Program to ensure that projects delivering the highest risk reduction per dollar spent are prioritized. These practices demonstrate that early geotechnical intervention offers substantial financial and operational advantages compared to reactive maintenance [31].

#### 2.7.3 Cross-Asset Integrative Investment Planning

Modern GAM frameworks are expanding to support cross-asset investment planning, allowing agencies to evaluate trade-offs between geotechnical assets and other infrastructure categories such as pavements and bridges. This integrative approach leverages multi-objective decision frameworks to ensure limited resources are allocated for maximum benefit across asset types [31].

Tools like AssetManager NT (for network-level decisions) and AssetManager PT (for program-level prioritization), developed under previous NCHRP projects, exemplify this shift toward system-wide investment coordination. These tools enable transportation agencies to develop comprehensive and optimized investment portfolios, balancing geotechnical needs with broader transportation system objectives [33].

#### 2.7.4 Challenges & Data Needs

Despite these advances, the full implementation of GAM remains constrained by several challenges. A critical limitation is data scarcity; many Departments of Transportation (DOTs) do not possess sufficient long-term cost, delay, and performance data, hindering the reliability of lifecycle cost analyses. Another major hurdle is the difficulty of estimating indirect costs such as user delays, safety impacts, and environmental consequences. These estimates often rely on modeling and assumptions that introduce uncertainty and potential bias. Furthermore, the lack of integration between GAM-specific tools and broader Transportation Asset Management (TAM) systems presents logistical issues. Currently, GAM tools often operate in silos, making it cumbersome for agencies to perform cross-asset trade-offs and consolidate programmatic decision-making [31].

#### 2.7.5 Implications for Maryland

To implement effective investment analysis, Maryland could:

- Adapt the NCHRP 903 GAM Planner and cost templates for local geotechnical contexts [32]
- Collate data on incident frequency, repair and delay costs, and potential consequences (detours, safety risks)
- Integrate with MDOT SHA's existing asset management and budgeting tools (e.g., VAMIS, TMS)
- Develop a cross-asset tradeoff platform (inspired by AssetManager NT) to evaluate geotech investment against other transportation needs

This approach would enable Maryland to go beyond reactive maintenance investing strategically, reducing long-term costs, and enhancing resilience.

## 2.8 Summary and Future Work

This report presents a critical review of GAM frameworks with a focus on their applicability to highway systems in Maryland. It begins by examining Maryland's increasing vulnerability to geohazards such as landslides, sinkholes, and slope failures, while emphasizing the shortcomings of traditional reactive maintenance approaches. The study evaluates well-established GAM programs from states including Alaska, Washington, and Colorado, highlighting key tools such as GIS-based inventories, risk-scoring mechanisms, and lifecycle cost models. Notably, Alberta's Excel-based GAM Planner and the use of predictive models ranging from Markov chains to machine learning algorithms demonstrate how deterioration forecasting can guide investment planning. A cross-state comparative analysis involving ten U.S. DOTs outlines varying levels of program maturity, implementation challenges, and strategic innovations. Techniques such as Net Present Value (NPV) analysis and crossasset trade-off frameworks are explored to support cost-effective decision-making. The review recommends that Maryland adopt best practices from these models, improve data integration capabilities, and develop customized predictive tools to embed geotechnical asset management within its broader transportation asset management system.

An important future direction is the development of a Maryland-specific GAM Planner; a decision-support tool that integrates geotechnical asset inventory,

condition ratings, risk profiles, and lifecycle cost calculations. Inspired by the Alberta GAM Planner and tools documented in NCHRP Report 903, this planner would enable engineers and asset managers in Maryland to simulate treatment scenarios, compare investment strategies, and optimize maintenance schedules using Net Present Value (NPV) and Benefit-Cost Ratio (BCR) frameworks.

## Chapter 3

# 3 Laboratory Investigation of Soil Properties for Landslide Risk Assessment in Montgomery County

Shakirat Aliyu, Alpha Bah, Jalah Pryor, Joshua Narh, Seok Jun Kang, Yi Liu, Zhuping Sheng, Oludare Owolabi

#### 3.1 Introduction

Landslides represent a hazardous phenomenon that can lead to injuries, fatalities, environmental damage, and the destruction of infrastructure. The major trigger for landslides is human actions, such as deforestation, slope excavation for construction purposes, and development in precarious hillside regions driven by population expansion and urban growth. Natural slopes may suddenly collapse or become unstable due to various factors, including rugged terrain, hydrological conditions, significant elevation changes, and the properties of the underlying rocks [34]. According to [35], landslides are defined as the downward movement of rocks and earth triggered by either translational or rotational rupture inside the earth's crust. Particularly vulnerable to landslides during and after periods of intense precipitation are mountainous areas, which can cause fatalities and disruptions to the built environment. Human-caused processes such as weathering, deforestation, and slope collapses make mountain slopes more vulnerable and increase the likelihood of landslides in lowland regions. Slope geometry, relative relief, groundwater conditions, lithology and structures, and shifts in land cover and use are some of the major contributors to slope instability. Building and growing transportation networks in hilly areas may inadvertently result in natural slope shift circumstances, which would compromise the stability of excavated slopes [36]. Understanding and mitigating the risk of landslides in susceptible areas requires a thorough understanding of geotechnical assessments and slope stability evaluations. Slope stability analysis in landslide hazard zones requires the characterization of the rock and soil. This may entail determining the underlying soil characteristics, geological formations, and environmental elements that contribute to slope instability. Shear resistance (which depends on density, cohesion, plasticity, and internal friction angle), porosity, permeability, grain size, moisture content, and organic matter content are among the geotechnical soil factors that affect slope stability. Slope stability may be impacted by a number of discontinuity properties, including joint orientation, opening, continuity, filling material, and degree of weathering. The moisture content and the properties of the materials used to fill the fractures have a significant impact on the stability of fractured rocks [34]. Essential geotechnical characteristics, including permeability,

moisture content, consolidation, and shear strength, are frequently neglected. This lack of data obstructs accurate landslide forecasting and diminishes emergency response effectiveness. In the absence of thorough soil assessments, efforts for mitigation and adaptation will continue to be inadequate. Consequently, soil testing is crucial for comprehending slope dynamics and aiding in hazard mapping. The objective of this project is to produce critical geotechnical information that promotes long-term risk mitigation and enhances infrastructure resilience planning. The objectives of this study are to conduct a thorough soil assessment in areas of Maryland that are vulnerable to landslides and floods, evaluate geotechnical hazards, develop hazard prediction, and assist in the development of resilient infrastructure planning and efficient mitigation techniques. The following specific goals will help achieve this.

- a. Identify Flood- and Landslide-Prone Areas / Sample Collection.
- b. Perform soil classification and consistency evaluation using sieve analysis techniques, including Grain size distribution, moisture content determination, and Atterberg Limits testing.
- c. Conduct UC Triaxial Tests to evaluate key soil strength parameters, including shear strength, consolidation behaviour, and saturation levels.

# 3.2 Materials and Methodology

#### 3.2.1 Materials

Labelled sample bags; trowels, augers, and scoops for collection; drying trays; moisture cans; a precision weighing balance (±0.01 g); an oven maintained at 105–110°C; a Standard Proctor mold (1/30 ft³ volume, 4-inch diameter) with a 5.5 lb rammer and 12-inch drop; a straightedge and extruder; a large mixing bowl and scoop; and a Consolidated Undrained (CU) triaxial testing system, including a test cell, sample holder, manual load frame, pressure gauge and back-pressure system, dial gauges, rubber membranes, O-rings, filter papers, and de-aired water

#### 3.2.2 Field Survey and Data Collection

A couple of days were dedicated to a preliminary field survey to collect general information about the various sites. For this survey, sites were visually examined to collect information about slope stability and landslip threats. To identify and locate critical slope portions, a thorough field survey was carried out. The fieldwork included a variety of measurements, including joint spacing, discontinuity orientation assessment, and geometric variables (height and distance) measurement

The sites examined include the Montgomery US 29 SWM Retrofit site, as shown in Figure 3.1 (latitude 39.05301, longitude -76.97719), where disturbed soil samples labelled as Site 1A and Site 1B were collected and tested to assess their properties influencing landslide susceptibility. Soil samples for Site 1A, representing topsoil, were taken at depths of 1–2 ft, while samples for Site 1B were taken at depths of 1–3 ft with an auger (Figure 3.2).



Figure 3.1: Montgomery US 29 SWM Retrofit site.

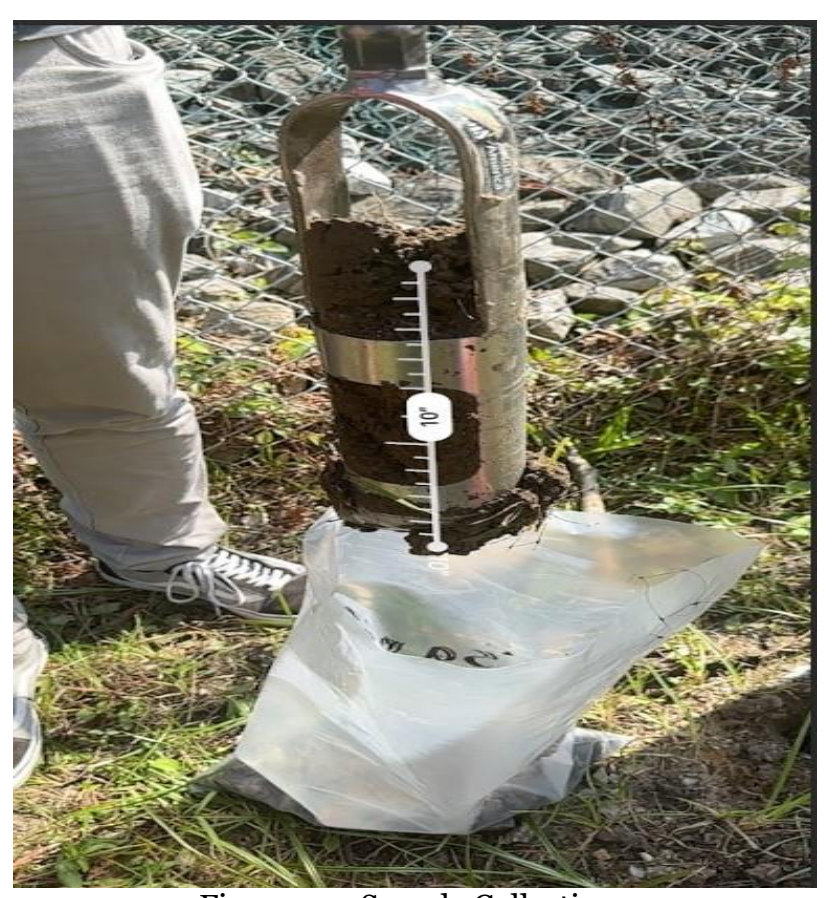


Figure 3.2: Sample Collection.

#### 3.2.3 Laboratory Procedure

The soil samples were analyzed in a lab after completing the field investigation. The soil's geotechnical characteristics, including its natural moisture content, specific gravity, unit weight, shear strength, Atterberg limits, and grain size distribution using both sieve and hydrometer methods, were evaluated following ASTM guidelines. Figures 3.3, and 3.4 below illustrate the steps involved in analyzing the steps used in the laboratory testing. Therefore, the procedure involves. Sampling and preparation for sieve size analysis, as shown in Figure 2, where disturbed soil samples were collected from Sites 1A, 1B, and 15 using trowels, augers, and scoops. The samples were

placed in labelled sample bags for proper field identification and transported to the laboratory. Moisture content was determined by using moisture cans to measure wet and dry weights, a precision balance (±0.01 g), and an oven maintained at 105–110°C to dry the samples to a constant weight. Grain size distribution was assessed through sieve analysis with a mechanical sieve shaker, complete sets of ASTM standard sieves (including No. 4 [4.75 mm] and No. 200 [0.075 mm]), along with a brush and pan for cleaning and collecting fines.



Figure 3.3: Sampling and preparation for sieve size analysis.

Figure 3.4 shows the Sampling and preparation for CU triaxial Test. Disturbed soil samples were collected from Sites 1A, 1B, and 15 using trowels, augers, and scoops. Each sample was placed in a labeled bag for proper field identification and transported to the laboratory. Moisture content determination was conducted using moisture cans for wet and dry weight measurements, a precision weighing balance (±0.01 g), and an oven maintained at 105-110°C to dry the samples to a constant weight. Compaction characteristics were determined with the Standard Proctor Test, using a Proctor mold (1/30 ft<sup>3</sup> volume, 4-inch diameter), a rammer with a 12-inch drop, a straightedge, and an extruder. Soil samples were thoroughly mixed in a large mixing bowl and layered into the mold for compaction testing. Shear strength and consolidation properties were assessed through Consolidated Undrained (CU) triaxial testing on the disturbed soil samples. The CU triaxial setup included a test cell, sample holder, and manual loading frame for axial loading. A pressure gauge and back-pressure system were used for saturation, while dial gauges measured deformation during loading. Rubber membranes, O-rings, and filter papers sealed the specimens, and de-aired water was used for saturation and back-pressure to ensure accurate strength and deformation measurements.

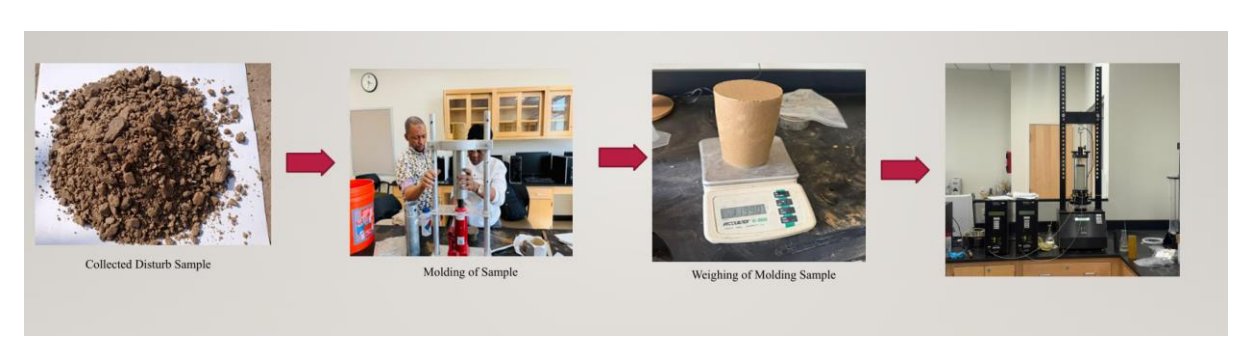


Figure 3.4: Sampling and preparation for CU triaxial Test.

#### 3.2.4 Mohr-Coulomb Failure Criteria

This study examines soil's shear strength based on the Mohr-Coulomb Failure Criteria, which is a geotechnical model describing the conditions under which soil or rock undergoes shear failure. It states that shear strength depends on cohesion c, normal stress  $\sigma$ , and the angle of internal friction  $\phi$ . The Mohr-Coulomb failure envelope is expressed as:

$$\tau_f = C + \sigma \tan \tan \phi \tag{3.1}$$

where  $\tau$  = shear strength C= cohesion,  $\sigma$  = normal stress,  $\phi$  = angle of internal friction

#### 3.3 Test Results and Analysis

#### 3.3.1 Sieve Size Analysis

Analysis of particle size is a crucial method for describing the mechanical properties of materials. A widely used method for separating particles by size is sieve analysis, which uses a stack of sieves with varying mesh sizes. Tables 3.1, 3.2, and 3.3 present the comprehensive sieve analysis of the cumulative retained and passing percentages, respectively. Figures 3.5, 3.6, and 3.7. illustrate a semi-logarithmic graph depicting the grain size distribution derived from the sieve study. A logarithmic scale is employed to represent grain size, while the natural scale is used to plot the percentage of finer grains. The coefficient of uniformity and the coefficient of curvature were determined from Figures 3.5, 3.6, and 3.7, respectively.

Tables 3.1, 3.2, and 3.3 present the grain size distribution data for Site 1A, Site 1B, and Site 15(M). These tables include sieve sizes, individual weights retained, cumulative weights, percentages of mass retained, and percentages passing. The total sample masses for Site 1A, Site 1B, and Site 15(M) are 403.6 g, 358.5 g, and 575.2 g, respectively, after washing and oven drying. The percentages of coarse-grained soils retained on the No. 4 sieve (4.75 mm) for Site 1A, Site 1B, and Site 15(M) are 20.12%, 17.71%, and 7.88%, respectively. The sample from Site 1A shows a broad distribution across fine and coarse particles, with approximately 32.66% passing the 0.2489 mm sieve, while the sample from Site 1B shows about 43.65% passing, and the sample from Site 15(M) shows 34.79% passing.

The mass retained and percentage passing are calculated using the following equation

$$\% \ \textit{Mass Retained} = \frac{\textit{Cumm Weight}}{\textit{Total Mass of Soil Sample}} * 100$$
 
$$\% \ \textit{Mass Passing} = 100 - \textit{Mass Retained}$$

Table 3.1: Particle Size Distribution (Site 1A)

Sieve Opening (mm)	Individual Weight (g)	Cum Weight (g)	% Mass Retained	Percent Passing
4.75	81.2	81.22	20.119	79.881
2	21.7	102.9	25.496	74.504
0.841	26.8	129.7	32.136	67.864
0.4191	54.7	184.4	45.689	54.311
0.2489	87.4	271.8	67.344	32.656
0.1499	71.5	343.3	85.059	14.940
0.1041	30.1	373.4	92.517	7.482
0.0737	22.3	395.7	98.043	1.957
PAN	7.9	403.6		
Total	403.6			

Table 3.2: Particle Size Distribution (Site 1B)

<b>Sieve Opening</b>	Individual	<b>Cum Weight</b>	% Mass	Percent
(mm)	Weight (g)	<b>(g)</b>	Retained	Passing
4.75	63.5	63.5	17.713	82.287
2	20	83.5	23.291	76.708
0.841	25.9	109.4	30.516	69.484
0.4191	38.1	147.5	41.144	58.856
0.2489	54.5	202	56.346	43.654
0.1499	60.9	262.9	73.333	26.667
0.1041	40.5	303.4	84.630	15.369
0.0737	37.7	341.1	95.146	4.854
PAN	17.4	358.5		
Total	358.5			

Table 3.3: Particle Size Distribution (Site 15M)

Sieve				
Opening	Individual	<b>Cum Weight</b>	% Mass	Percent
(mm)	Weight (g)	(g)	Retained	Passing
4.75	45.3	45.3	7.8756	92.124
2	14.9	60.2	10.466	89.534
0.841	15.9	76.1	13.230	86.770
0.4191	121.3	197.4	34.318	65.682
0.2489	177.7	375.1	65.212	34.788
0.1499	95.4	470.5	81.798	18.202
0.1041	42.6	513.1	89.204	10.710
0.0737	35.8	548.9	95.428	4.572
PAN	26.3	575.2		
Total	575.2			

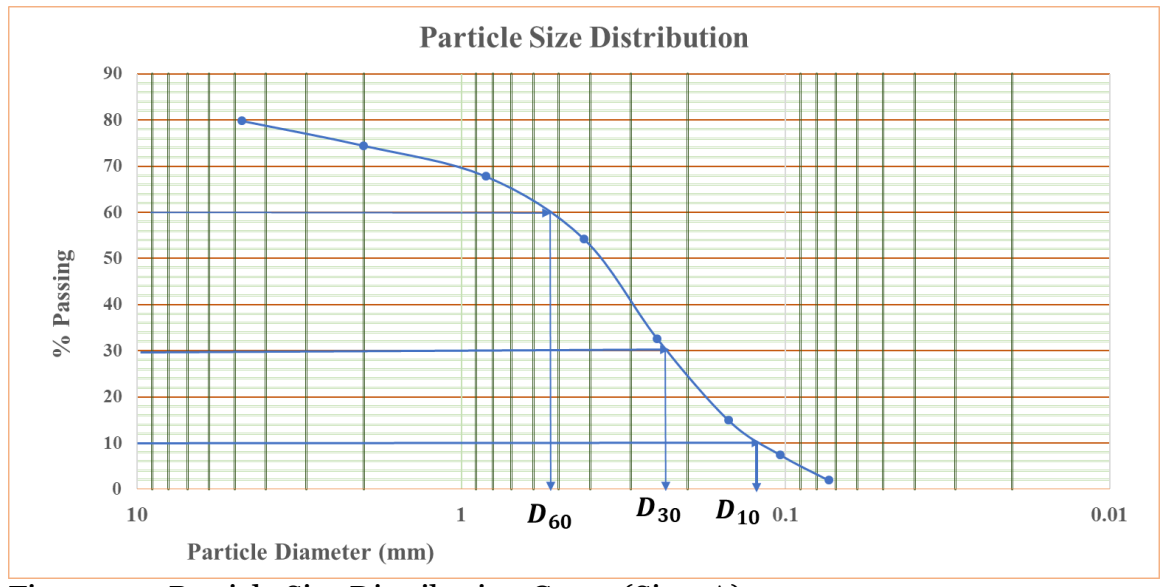


Figure 3.5: Particle Size Distribution Curve (Site 1A).

$$C_u = \frac{D_{60}}{D_{10}} = \frac{0.52}{0 \cdot 14} = 3.71$$

$$C_C = \frac{D_{30}^2}{D_{60}D_{10}} = \frac{(0.23)^2}{(0 \cdot 52)(0 \cdot 14)} = 3.71$$

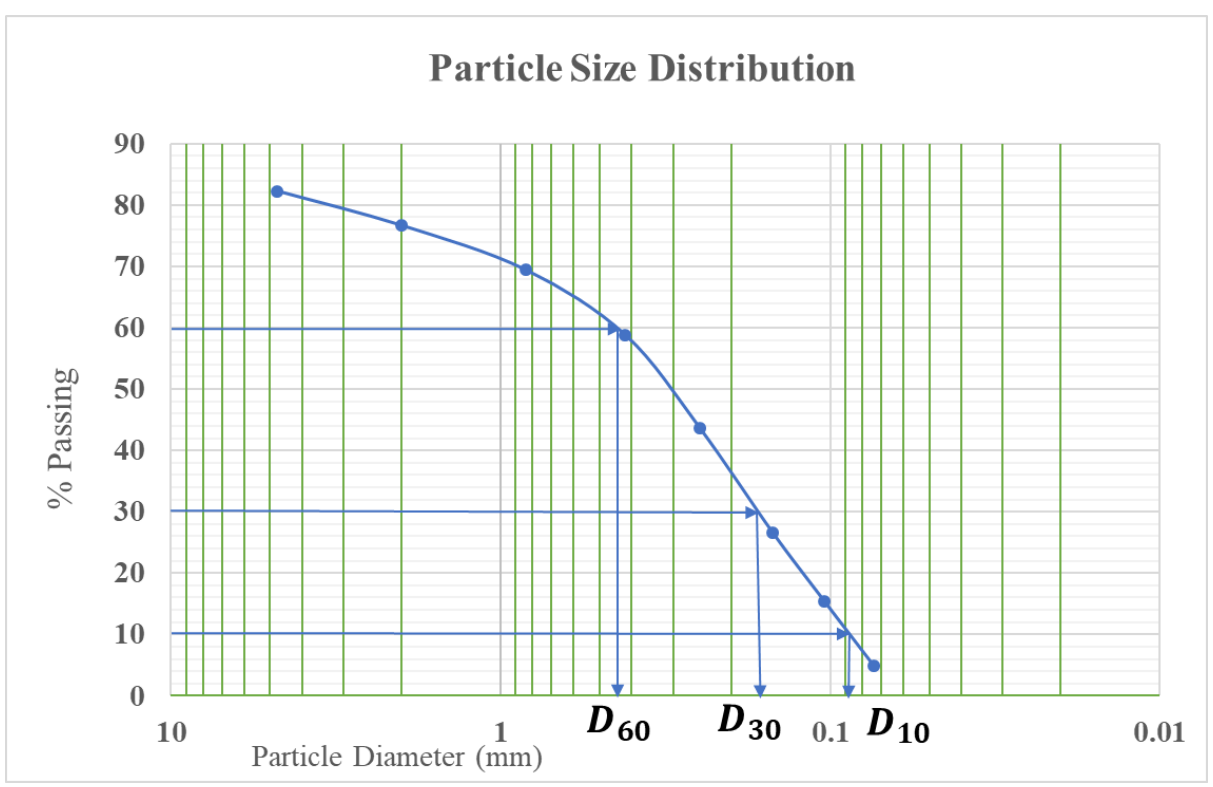


Figure 3.6: Particle Size Distribution Curve (Site 1B).

$$C_u = \frac{D_{60}}{D_{10}} = \frac{0 \cdot 45}{0.09} = 5$$

$$C_C = \frac{D_{30}^2}{D_{60}D_{10}} = \frac{(0.18)^2}{(0 \cdot 45)(0 \cdot 09)} = 5$$

## 3.3.2 Classification

The classification for sites 1A and 1B is done by using the Unified Soil Classification Chart (After ASTM 2011).

## Site 1A

- The percentage of mass retained in No 200 sieve is 98.04%, hence it is coarse—grained soil.
- The percentage of fines passing in No 4 sieve is 79 .88%, hence it is considered as sand.
- The percentage of fines passing No. 4 sieve is 1.9% which is less than 5%, hence, it is classified as clean. Since  $C_u = 3.71$  less than 6, and  $C_c = 0.73$ , it is poorly graded sand (SP)

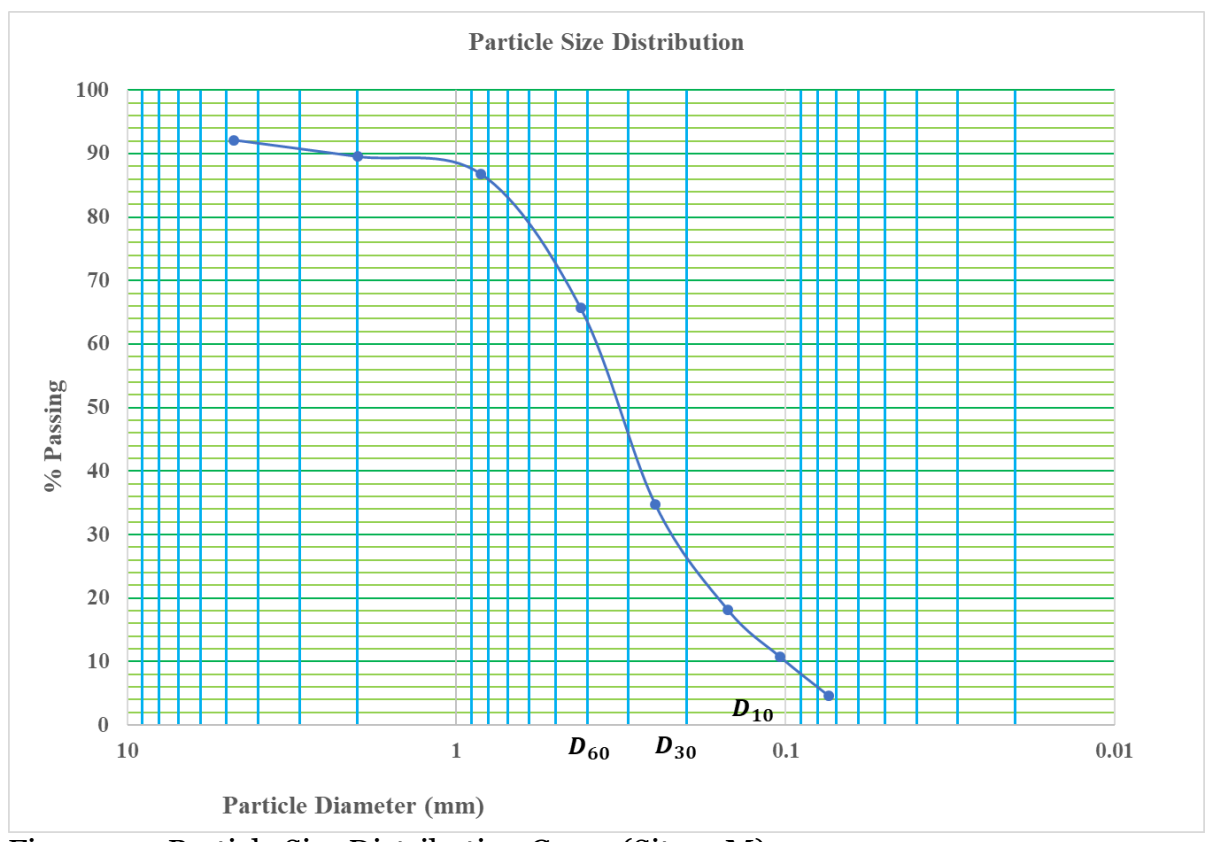


Figure 3.7: Particle Size Distribution Curve (Site 15M).

$$C_u = \frac{D_{60}}{D_{10}} = \frac{0 \cdot 38}{0.10} = 3.8$$

$$C_C = \frac{D_{30}^2}{D_{60}D_{10}} = \frac{(0.22)^2}{(0 \cdot 38)(0 \cdot 10)} = 1.27$$

## Site 1B

- The percentage of mass retained in the No. 200 sieve is 95.146%, hence it is coarse—grained soil.
- The percentage of fines passing in No. 4 sieve is 82.28%, hence, it is considered as sand.
- The percentage of fines passing No. 4 sieve is 4.854% which is less than 5%, hence, it is classified as clean sands and. Since  $C_u = 5.0$ , greater than 6, and  $C_c = 0.8$ , it is well-graded sand (SW).

## Site 15M

- The percentage of mass retained in No. 200 sieve is 95.43%, hence it is coarse—grained soil.
- The percentage of fines passing in No. 4 sieve is 92.12%; hence, it is considered as sand.
- The percentage of fines passing No. 200 sieve is 4.6% which is less than 5%; hence, it is classified as clean sands. Since  $C_u = 3.8$  and  $C_c = 1.27$ , it is well–graded sand (SW).

## 3.3.3 Moisture content

Moisture content is an important geotechnical characteristic that indicates the volume of water in a sample of rock or soil. Engineering behavior, such as strength, compressibility, and permeability, is significantly impacted. Valid geotechnical data requires precise measurements of moisture content [34]. The study examined soil samples taken from the top (disturbed and undisturbed) and bottom of landslides at site 21 and site 27 (10-inch and 10- to 17-inch landslides. In contrast, the landslide soil at site 21 (top) had moisture contents of 31.32% and 32.50%, and site 21 (bottom) had moisture contents of 37.20% and 24.68%, respectively, according to the data. The soil at site 27 had a moisture content of 26.10% and 20.39%. Since excessive moisture content can increase soil weight and decrease shear strength, increasing the risk of landslides, these comparatively low moisture levels indicate that the soils are generally stable. The sample was weighed again, and the results are presented in Table 3.4.

Table 3.4: Moisture content for the various landslide soil samples.

S/No.	Site 27 (10 inch)	Site 27 (10 – 17 inch)	Site 21 (Sample #2 Top, D)	Site 21 (Sample #2 Top, UD	Site 21 (Sample #3, Btm, Disturbed)	Site 21 (Sample #3, Btm, UD)
Weight of can/tare, g	22.7	22.6	22.7	20.6	22.6	22.8
Weight of can + Sample (wet), g	112.7	166.1	125.0	184.1	103.0	191.0
Weight of can + sample (dry), g	94.1	141.8	100.6	144.0	81.2	157.7
Moisture content (%)	26.10	20.39	31.32	32.50	37.20	24.68

## 3.3.4 CU Triaxial Test

This is a fundamental geotechnical technique used to determine the shear strength parameters of a soil sample. Critical properties, including shear strength, cohesion, and the angle of internal friction, are measured by shearing a specimen positioned between two plates along a predetermined plane. These parameters are essential for engineering designs involving slopes, retaining walls, and foundations. Results from CU as shown in Figure 3.8 through 3.13 indicate that Site 1A has an effective stress friction angle of 33.5° and cohesion of 0.606 psi, Site 1B has an effective stress friction angle of 29.2° and cohesion of 1.12 psi, and Site 15 has an effective stress friction angle of 29.6° and cohesion of 2.62 psi. Under total stress conditions, Site 1A exhibited a friction angle of 20.6° and cohesion of 1.74 psi, Site 1B showed a friction angle of 17.9° and cohesion of 2.74 psi, and Site 15 showed a friction angle of 17.2° and cohesion of

1.33 psi. All values were determined under confining pressures of 5, 10, and 20 psi.

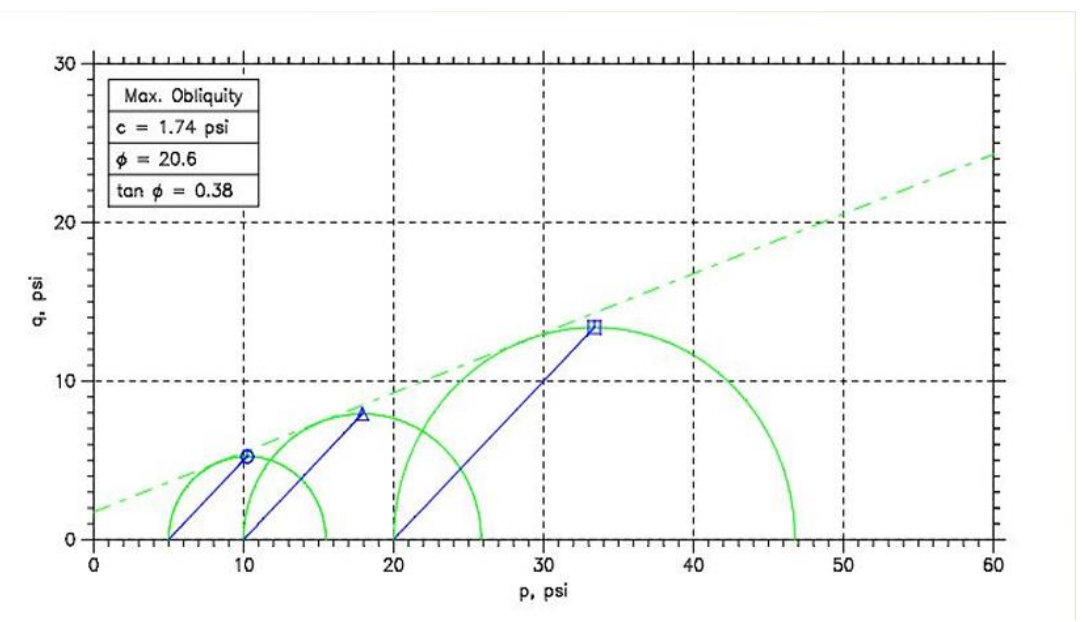
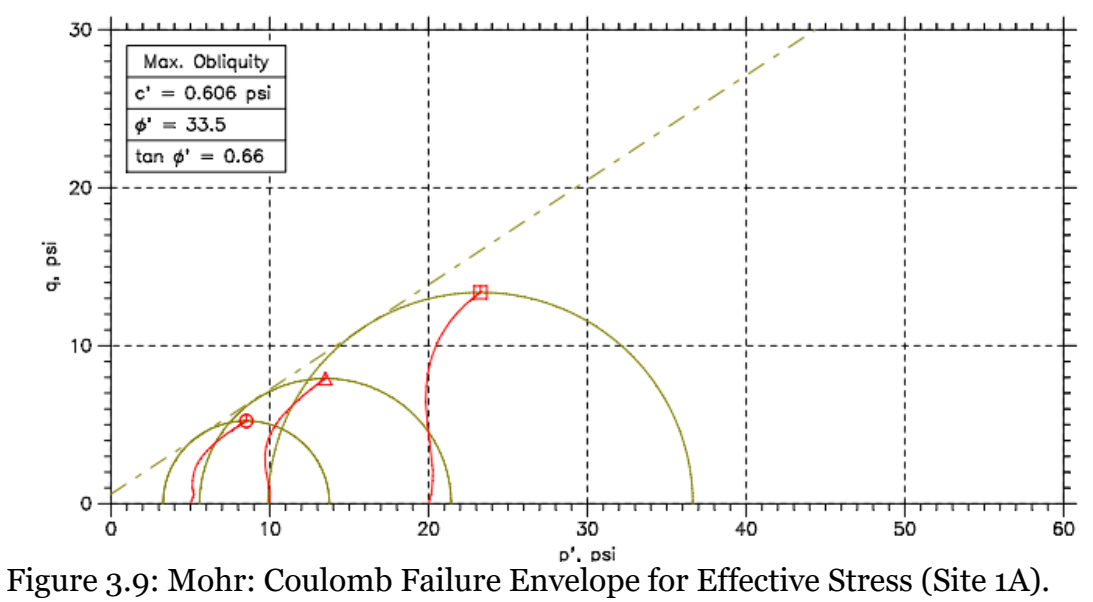


Figure 3.8: Mohr: Coulomb Failure Envelope for Total Stress (Site 1A).



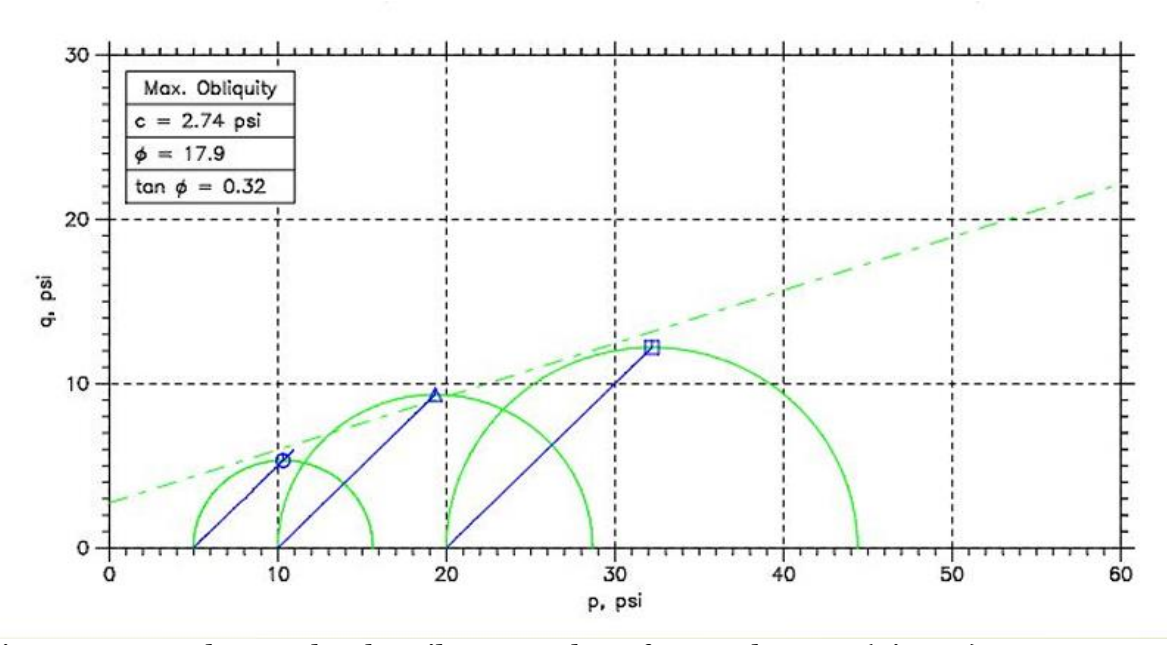


Figure 3.10: Mohr: Coulomb Failure Envelope for Total Stress (Site 1B).

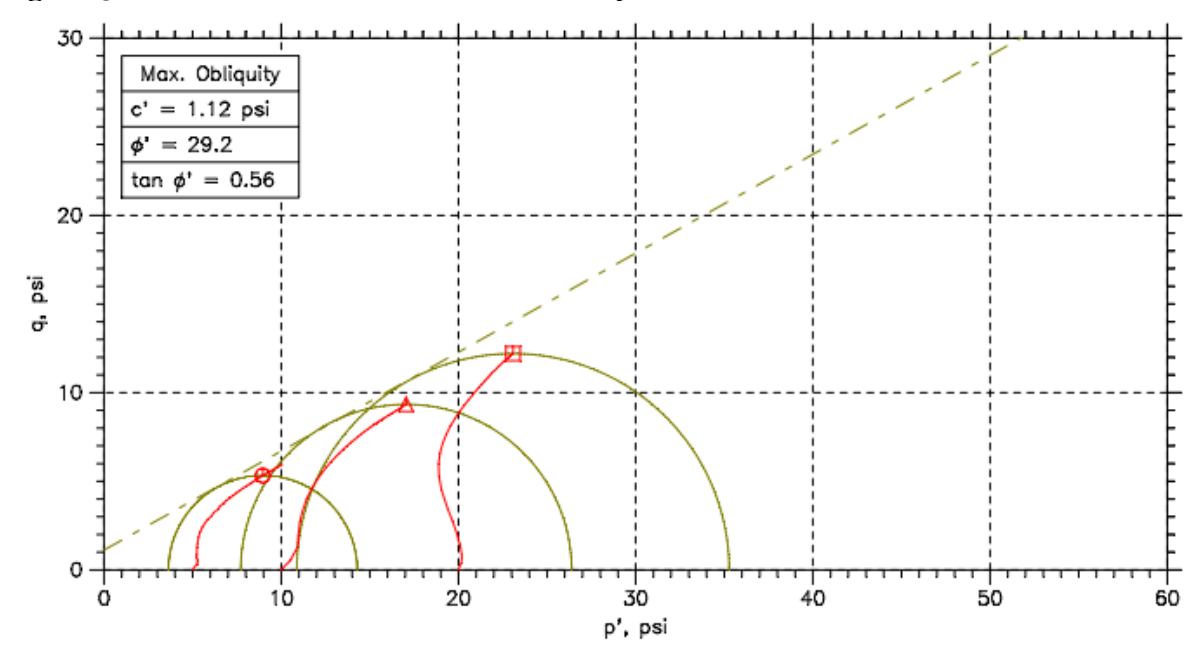


Figure 3.11: Mohr: Coulomb Failure Envelope for Effective Stress (Site 1B).

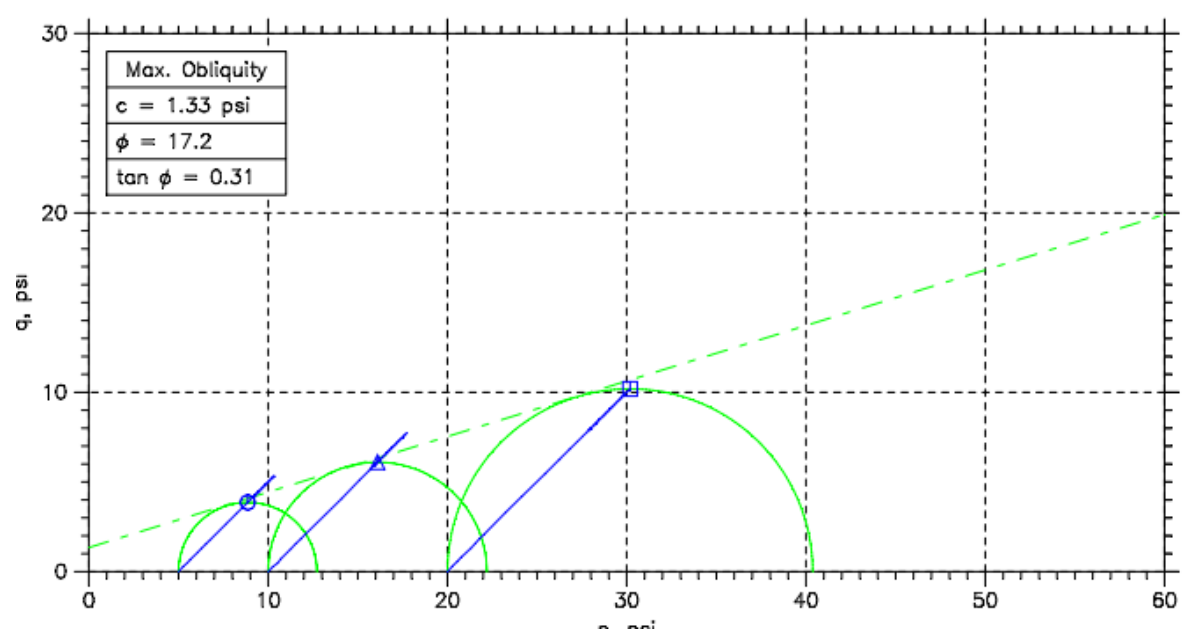


Figure 3.12: Mohr: Coulomb Failure Envelope for Total Stress (Site 15M).

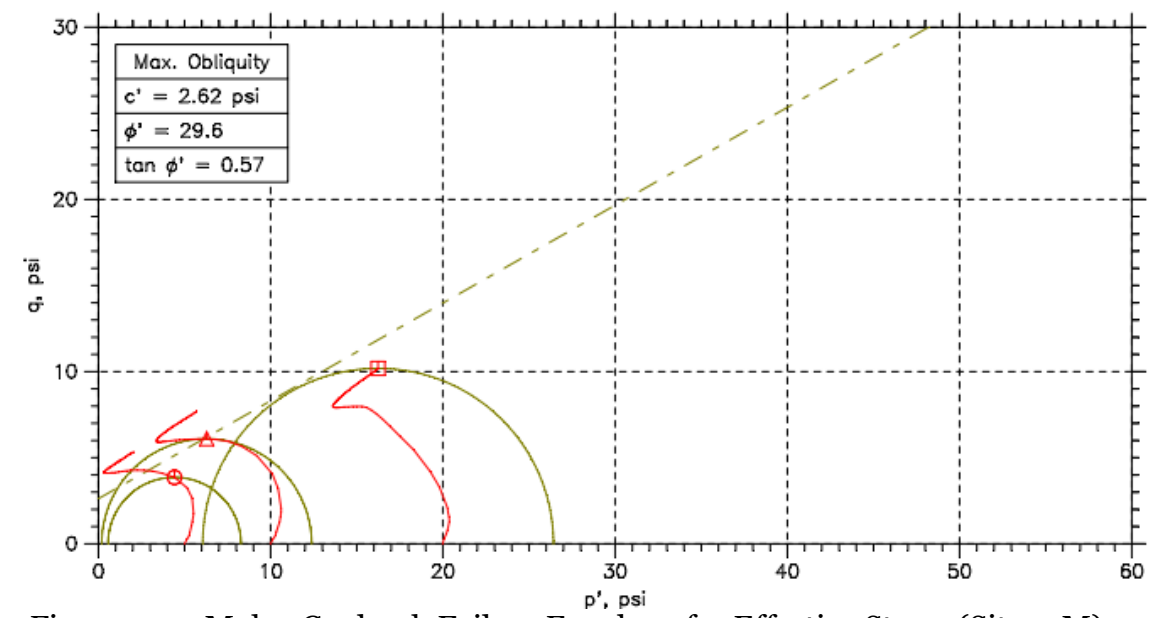


Figure 3.13: Mohr: Coulomb Failure Envelope for Effective Stress (Site 15M).

Three series of consolidated undrained (CU) triaxial tests were conducted on soil specimens from Sites 1A, 1B, and 15M, each representing slightly different depths and compaction characteristics. In Site 1A, samples molded with 5.875 in height, 2.8 in diameter, underwent a stage CU triaxial test, and a dry density of 101.7 pcf was tested at vertical effective consolidation stresses of 5.049 psi, 9.999 psi, and 19.98 psi. With a moisture content of 12.2% and full saturation confirmed by a B-value of 0.95, shear strength increased from 5.237 psi to 13.38 psi with increasing consolidation. Deviator stress and effective major principal stress followed this trend, confirming that higher

effective stress enhances shear resistance in saturated conditions.

In Site 1B, samples of similar dimensions, 5.79 in height and 2.8 in diameter, underwent a stage CU triaxial test but with higher moisture content (25.6%) and lower dry density (97.2 pcf) were tested. Void ratios ranged from 0.706 to 0.734, and full saturation was again achieved (B = 0.95). The applied vertical effective consolidation stresses were 4.982 psi, 9.998 psi, and 19.98 psi. Correspondingly, shear strength increased from 5.933 psi to 12.2 psi, and the deviator stress peaked at 26.4 psi, with the major principal stress at 35.28 psi. These results reaffirm the direct relationship between increased effective consolidation and improved shear strength under saturated conditions.

For Site 15M, it underwent three series of consolidated undrained (CU) triaxial tests and had a uniform moisture content of 25.7%. The heights are 5.909, 5.912, and 5.88 in with the diameters of 2.796, 2.784, and 2.783, respectively. The dry density ranged from 100.8 to 102.3 pcf, but B-values varied from 0.67 to 0.94, indicating differing saturation efficiency. The vertical effective consolidation stresses applied were 4.982 psi, 9.977 psi, and 19.95 psi. Shear strength correspondingly increased from 5.332 psi to 10.18 psi, with the highest deviator and major principal stresses observed in the most saturated sample. Notably, the variation in saturation levels (B-value) influenced the minor principal stress, highlighting the importance of full saturation in strength development.

## 3.3.5 Summary of the Results

CU test results are summarized in Table 3.5.

Table 3.5: Results of CU Triaxial Tests.

Site	Soil Type	Total Stress Frictional angle (Ø)	Total Stress Cohesion (psi)	Effective stress Frictional angle (Ø')	Effective stress Cohesion C' (psi)
Site 1A	Poorly graded sand (SP)	20.6	1.74	33.5	0.606
Site 1B	Well– graded sand (SW)	17.9	2.74	29.2	1.12
Site 15 (Middle)	Poorly graded sand (SP)	17.2	1.33	29.6	2.62

# 3.4 Conclusions and Future Research

This study demonstrates that rigorous geotechnical investigation is essential for accurately assessing and mitigating landslide risks in Maryland and surrounding regions, where climate-driven environmental pressures continue to intensify. By analyzing soil samples from the Montgomery US 29 SWM Retrofit site (latitude 39.05301, longitude -76.97719) and additional sites, this research establishes how fundamental soil properties moisture content, shear strength, and particle size distribution, govern slope stability and failure potential.

The laboratory findings reveal distinct behaviors across sites, underscoring the variability in soil response under stress. Site 1A, classified as poorly graded sand (SP) from 1-2 ft depths, displayed a high friction angle (33.5°) but low cohesion (0.606 psi) under effective stress, characteristics that make it more prone to movement when saturated or destabilized. Site 1B, a well-graded sand (SW) from 1-3 ft, exhibited higher cohesion (1.12 psi) but a lower friction angle (29.2°), while Site 15, also poorly graded sand (SP), demonstrated the highest cohesion (2.62 psi) with a moderate friction angle (29.6°), suggesting greater stability under loading or saturated conditions. Total stress analyses under confining pressures of 5, 10, and 20 psi further confirmed the variability in soil strength, with cohesion reaching up to 2.74 psi in Site 1B despite reduced friction angles.

These results not only clarify the engineering behavior of soils in a landslide-prone corridor but also provide critical design parameters for slope stability analyses, physical modelling, and predictive risk assessments. By integrating standardized laboratory testing with field observations, this study enhances the reliability of hazard mapping and informs the development of proactive, science-driven strategies for infrastructure planning and climate resilience in Maryland.

Future research should broaden the geographic scope of sample collection to encompass a wider variety of geological conditions and soil types throughout Maryland and other study areas. Additionally, monitoring ground movement, pore water pressure, and moisture variation over an extended period of time might improve landslip risk prediction modelling. Finally, incorporating forecasts of climate data would enable evaluations of the potential effects of shifting weather patterns on soil behavior and slope stability in the future.

# **Chapter 4**

# 4 Detection and Mapping of Landslides with Remote Sensing LiDAR data in Prince George's County, Maryland

Micheal Oketunde Okegbola, Caleb Mincey, Oludare Owolabi, Zhuping Sheng. Yi Liu

## 4.1 Introduction

Landslides can be defined as the downslope movement of a mass of soil and/or bedrock materials [37]. Landslides are among the most destructive and widespread natural hazards, often triggered by intense or prolonged rainfall, seismic activity, or anthropogenic disturbances. Globally, landslides result in considerable socio-economic losses, environmental degradation, and human casualties. According to the World Health Organization (WHO) [38], landslides affected approximately 4.8 million people and caused more than 18,000 deaths worldwide between 1998 and 2017. These impacts are expected to increase in frequency and severity because of ongoing climate change and the intensification of extreme weather events [39].

Landslides vary in type, magnitude, and spatial extent, and their occurrence is closely related to terrain morphology, geological structure, soil type, and land cover. Accurate and timely detection and mapping of landslides are essential for hazard assessment, risk reduction, and sustainable land-use planning among other mitigating strategies. Conventional field-based mapping techniques, although effective, are time-consuming, labor-intensive, and often limited in spatial coverage [40]. To address these limitations, recent advancements in remote sensing technologies, particularly the use of Light Detection and Ranging (LiDAR), have significantly improved landslide detection, mapping, and susceptibility modelling by enabling the capture of high-resolution elevation data over large areas [41, 42].

LiDAR-derived Digital Elevation Models (DEMs) provide sub-meter resolution elevation data that can reveal subtle topographic changes associated with landslide processes, including surface displacement, scarps, and accumulation zones (Pradhan, 2010). When acquired for multiple time periods, LiDAR DEMs allow for the computation of DEM of Difference (DoD) layers, facilitating the identification of terrain elevation changes indicative of slope instability [43]. These DEMs can also be used to extract geomorphometric parameters such as slope, aspect, curvature, Stream Power Index, and Topographic Wetness Index (TWI), which are fundamental in understanding the factors influencing landslide initiation and movement [44].

Several studies have integrated remote sensing with spatial modeling techniques to generate landslide susceptibility maps. Approaches such as logistic regression [45, 46],

frequency ratio, and multi-criteria decision analysis [47] have demonstrated robust results in various terrains. These models, when combined with historical landslide inventories and field validation, enhance the reliability and predictive power of susceptibility assessments [48].

In Maryland, particularly in Prince George's County, the combination of diverse terrain, weather variability, and land-use changes creates a predisposition to landslides. Despite this, comprehensive, high-resolution landslide mapping and susceptibility modeling are limited. This study addresses this gap by leveraging high-resolution LiDAR data from multiple years (2014, 2018, 2020) and GIS-based analytical methods to detect and map landslide-prone areas in Prince George's County. Through the extraction of geomorphometric parameters and the comparison of DEMs over time, the study aims to identify zones of significant elevation change that may correspond to landslide activity. The results will support proactive hazard mitigation, spatial planning, and contribute to the growing body of knowledge on remote sensing-based geohazard analysis.

## 4.1.1. Problem Statement

Prince George's County, Maryland, faces increasing susceptibility to landslides due to its varied topography, intense precipitation patterns, and urban expansion. This is evident in the fact that the county has the highest records of landslide occurrences (39 landslide inventories) in Maryland, yet it lacks high-resolution, spatially detailed landslide detection and susceptibility mapping based on advanced remote sensing techniques such as LiDAR.

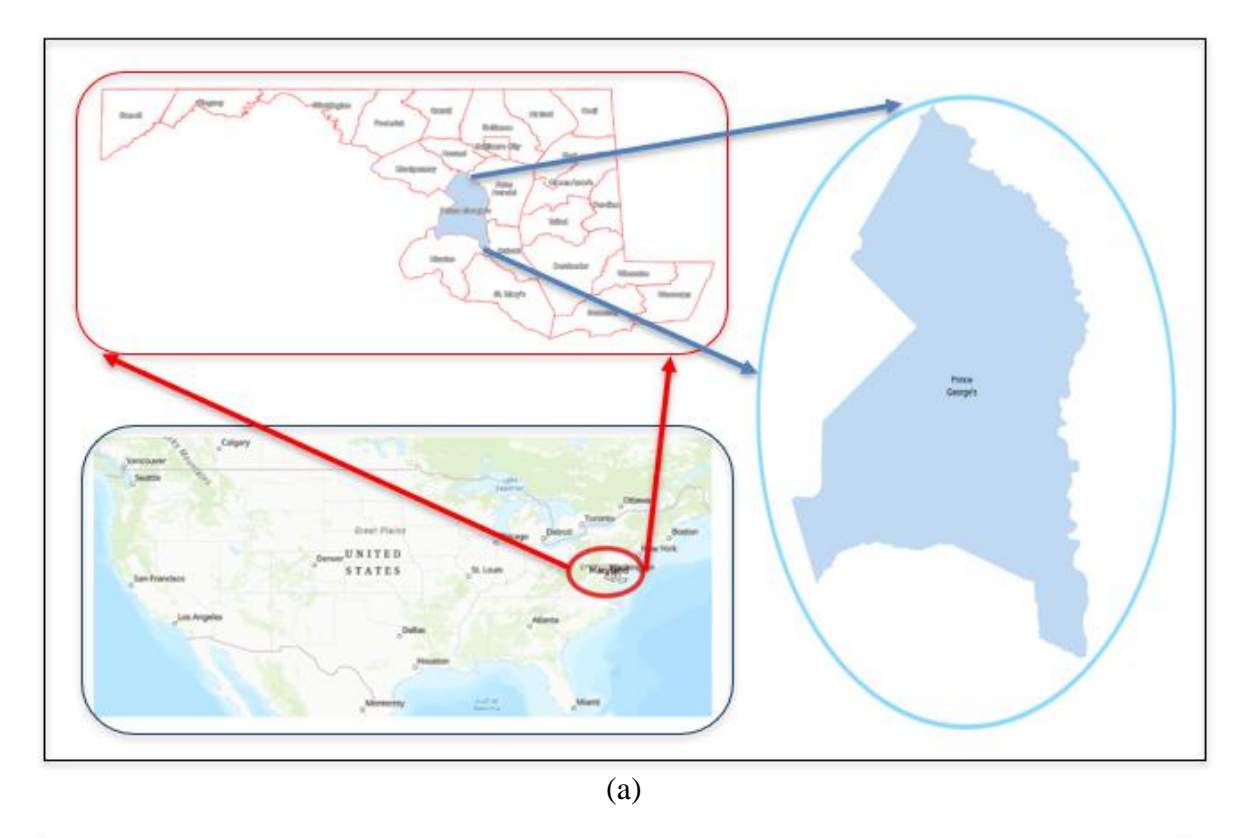
## 4.1.2. Research Aim and Objectives

The research ais is to detect and map landslide-prone areas in Prince George's County using multi-temporal LiDAR data and GIS-based remote sensing techniques. Following are research objectives:

- a. To preprocess high-resolution LiDAR DEMs for selected years covering Prince George's County.
- b. To derive geomorphometric parameters such as slope, aspect, curvature, TWI, and DoD.
- c. To detect and map potential landslide zones based on terrain deformation and susceptibility indicators.
- d. To validate identified landslide zones using historical inventories and spatial analysis.

# 4.2 Study Area

The study focuses on Prince George's County (Fig. 4.1a), located in the central region of the state of Maryland, United States, within the Mid-Atlantic coastal plain and Piedmont Plateau physiographic provinces. The county lies approximately from 38.5°N and 39.1°N



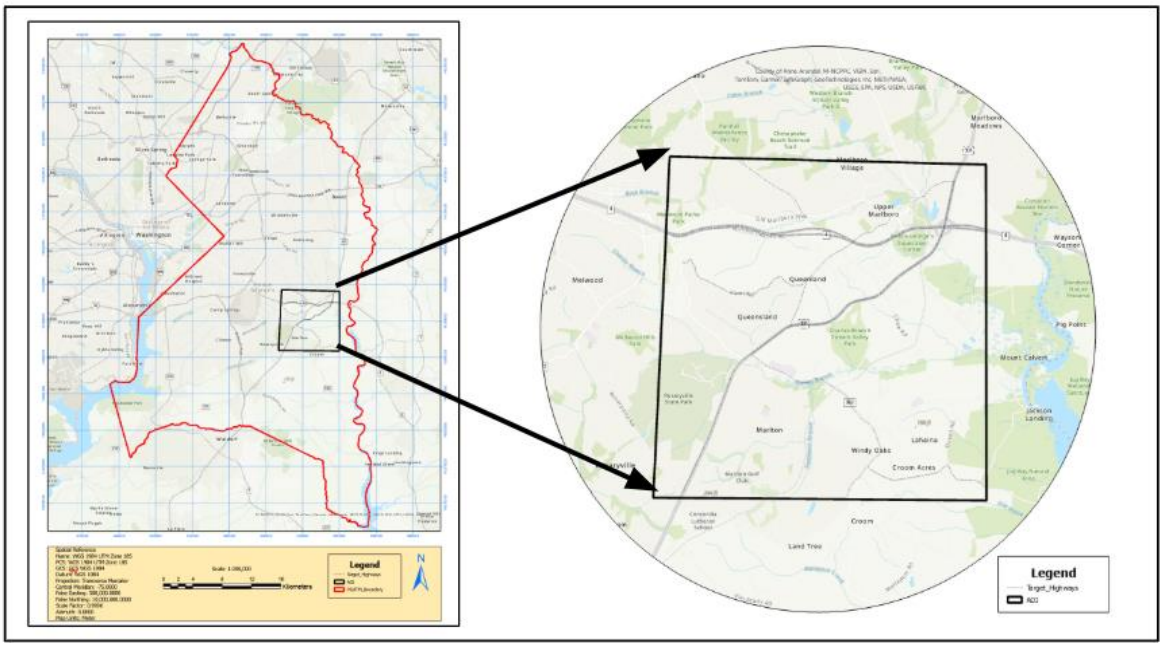


**Figure 4.1:** (a) Study Area (Prince George's County) and (b) Area of Interest within PG County

latitude, and 76.6°W and 77.1°W longitude, encompassing diverse topographic conditions, urban development, and critical transportation corridors (Fig. 4.1b focused more on selected

(b)

highways as the area of interest within the PG County). Its complex terrain and proximity to the Potomac River make it a suitable region for assessing landslide susceptibility using high-resolution LiDAR elevation data.

# 4.3. Literature Review

Landslide susceptibility mapping and detection have evolved significantly over the past two decades, largely driven by advances in remote sensing, geospatial analysis, and modeling techniques. As a geohazard, landslides are complex events influenced by multiple environmental and anthropogenic factors, including slope angle, geological structure, land use, soil moisture, and rainfall intensity [4]. Understanding these factors and their spatial interaction is critical for hazard assessment and risk management.

## 4.3.1. Remote Sensing and LiDAR for Landslide Mapping

The spatial accuracy of landslide mapping has greatly increased with the introduction of high-resolution remote sensing data. LiDAR has gained recognition for producing high-resolution Digital Elevation Models (DEMs) that can uncover micro-topographic features hidden beneath vegetation cover. For recognizing and categorizing landslide events, these characteristics, such as accumulation zones, displaced debris, and scarps, are essential indicators [41, 42]. DoD, a technique for identifying elevation changes over time, can be computed using multi-temporal LiDAR datasets. This makes it easier to identify terrain deformation that is consistent with landslide movement [43].

Landslide-prone areas have made extensive use of LiDAR's ability to penetrate canopy and provide precise terrain data. The usefulness of LiDAR in probabilistic landslide hazard assessments at the basin size was shown by [41]. Similarly, Scudero and De Guidi [42] created comprehensive landslide susceptibility maps in northeastern Sicily, Italy, using LiDAR-derived topographic parameters.

## 4.3.2. Geomorphometric and Hydrologic Factors

When modeling terrain instability, geomorphometric factors like slope, aspect, curvature, and drainage patterns that are obtained from DEMs are crucial. Since steeper slopes are frequently associated with greater vulnerability, slope gradient is a key element. While curvature aids in identifying concave (depositional) or convex (erosional) terrain features that may suggest movement zones, aspect affects moisture retention and vegetation growth [12]. Furthermore, DEM-derived hydrological indices like the Stream Power Index (SPI) and Topographic Wetness Index (TWI) are crucial for comprehending surface runoff and possible erosion zones [43].

# 4.3.3. Landslide Susceptibility Modeling

There are several methods for mapping landslide vulnerability. These consist of expert-based approaches like the Analytical Hierarchy Process (AHP), statistical models (such as logistic

regression and frequency ratio), and hybrid approaches. Akgun [45] conducted a comparison of multi-criteria decision analysis (MCDA), logistic regression, and likelihood ratio approaches for susceptibility mapping in İzmir, Turkey, and concluded that hybrid approaches perform better. Similarly, Pourghasemi, Pradhan, and Gokceoglu [47] combined Analytical Hierarchy Process (AHP) with fuzzy logic to map landslides in Iran's Haraz watershed, producing accurate findings in settings with little data.

In Malaysia, Lee and Pradhan [46] created hazard maps with high predictive performance by combining logistic regression and frequency ratio models. The usefulness of combining statistical modeling with parameters generated from remote sensing was highlighted by Pradhan [49], who also investigated multivariate techniques for landslide mapping. Using topographic and lithologic data, Ayalew and Yamagishi [44] performed a GIS-based logistic regression study for landslide susceptibility in the Kakuda-Yahiko Mountains, Japan. Their findings demonstrate how reliable logistic regression is when paired with high-quality spatial datasets.

## 4.3.4. Risk Zonation and Validation Challenges

Despite methodological advancements, landslide hazard and risk zonation remain challenging. According to Van Western et al., [40], discrepancies often arise from variations in data quality, spatial resolution, and subjective expert judgements in factor weighting. Moreover, the absence of reliable or sufficient landslide inventories complicates model calibration and validation while using Machine Learning (ML) in Landslide modeling. Petrucci [50] emphasized the importance of systematic reviews and structured inventories to improve fatality risk assessments and support global monitoring frameworks.

Zezere et al. [48] advocated for the integration of spatial and temporal data in hazard modeling, allowing for the definition of different risk scenarios over time. Their work in the Lisbon region of Portugal underscored the importance of combining terrain factors with historical landslide events for a more comprehensive susceptibility analysis.

# 4.4. Materials and Methodology

This study employed a remote sensing and Geographic Information System (GIS-based) analytical approach using multi-temporal high-resolution LiDAR-derived DEM datasets (2014, 2018, and 2020) covering Prince George's County, Maryland. LiDAR DEM processing and analysis were conducted using ArcGIS Pro 3.1.0, with the Spatial Analyst and 3D Analyst among other extensions enabled. Historical landslide inventories were also used for the study.

The Methodology involved a structured workflow (Fig. 4.2) beginning with preprocessing of the LiDAR DEM, including projection, sink filling, and clipping to the Area of Interest (AOI). Geomorphometric parameters such as slope, aspect, curvature, Topographic Wetness Index (TWI), Contour, and DoD were derived to highlight terrain dynamics associated with landslides. To identify spatial correlation with infrastructure, buffering and overlay operations were performed along highways within the AOI.

Detected landslide zones, derived through raster classifications, were converted to polygons for spatial filtering and zonal analysis. These results were validated using available

historical landslide inventories and expert interpretation. The final outputs were landslide susceptibility maps delineating **Downward displacement**, **Stable**, and **Upward Displacement Zones** including a point map of detected landslides.

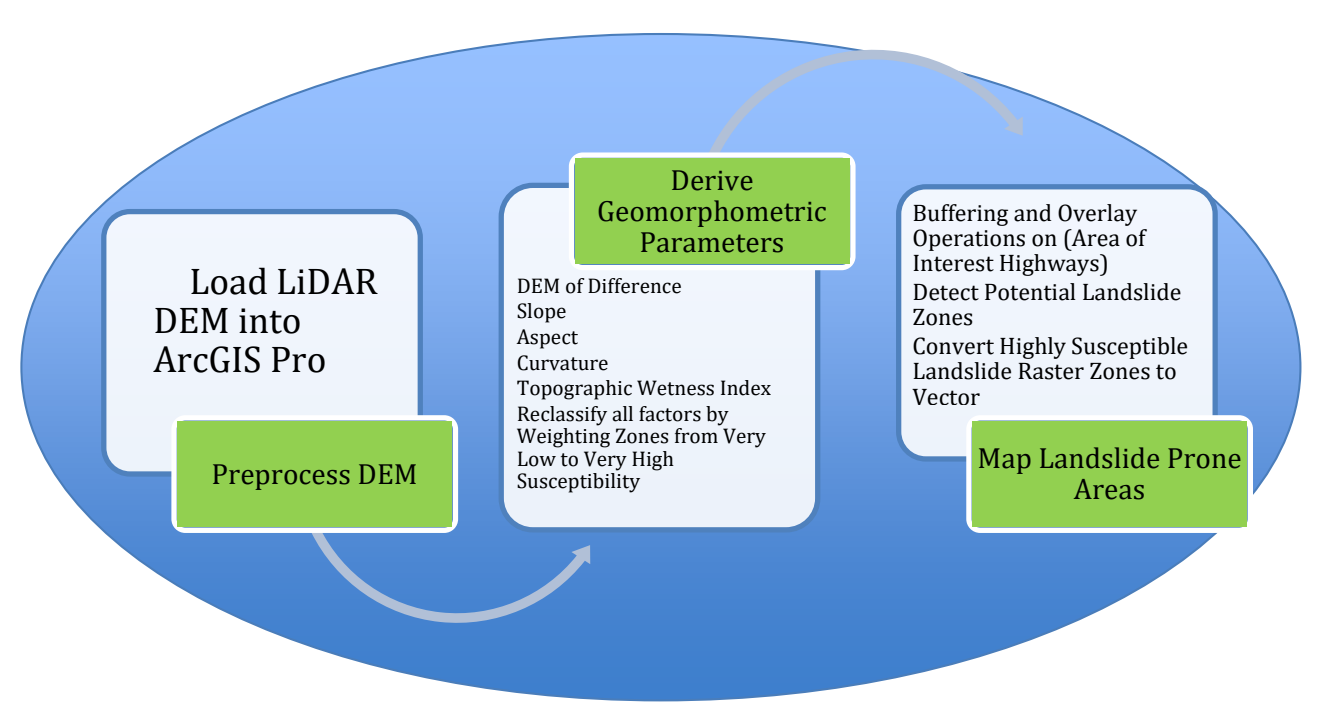


Figure 4.2: Methodology Flowchart for Landslide Detection and Susceptibility Mapping

## 4.4.1. LiDAR DEM Acquisition and Preprocessing

The LiDAR DEM data were readily available through the Maryland Department of Transportation (MDOT) data services website (<a href="https://doitdataservices.maryland.gov/s/N9xGBYPKq4QSZNq">https://doitdataservices.maryland.gov/s/N9xGBYPKq4QSZNq</a>). Figure 4.3 shows the downloaded DEMs of Prince George's County for the years 2014, 2018, and 2020. All other processed DEM for the three (3) years is included in the appendices section. The DEMs were projected to the same coordinate reference system (WGS 84 UTM Zone 18S), fill all sinks for any holes, clipped to the Area of Interest (AOI), and resampled to the same pixel dimension for proper and further spatial comparison and analysis (see Fig. 4.4 for DEM's preprocessing workflow).

Through the raster calculator tool in ArcGIS Pro, the DoD) between 2014 and 2018, 2018 and 2020, and 2014 and 2020 were determined to obtain the terrain variations within these epochs. Other terrain factors (such as slope, aspect, curvature, contour etc.) were also generated through the ArcGIS Pro spatial analysis tool; these factors were then classified based on an expert model and weighting classifications (previous relevant studies) to detect areas that highly suggest susceptibility to landslides. Results of the analysis and maps are attached to the appendices.

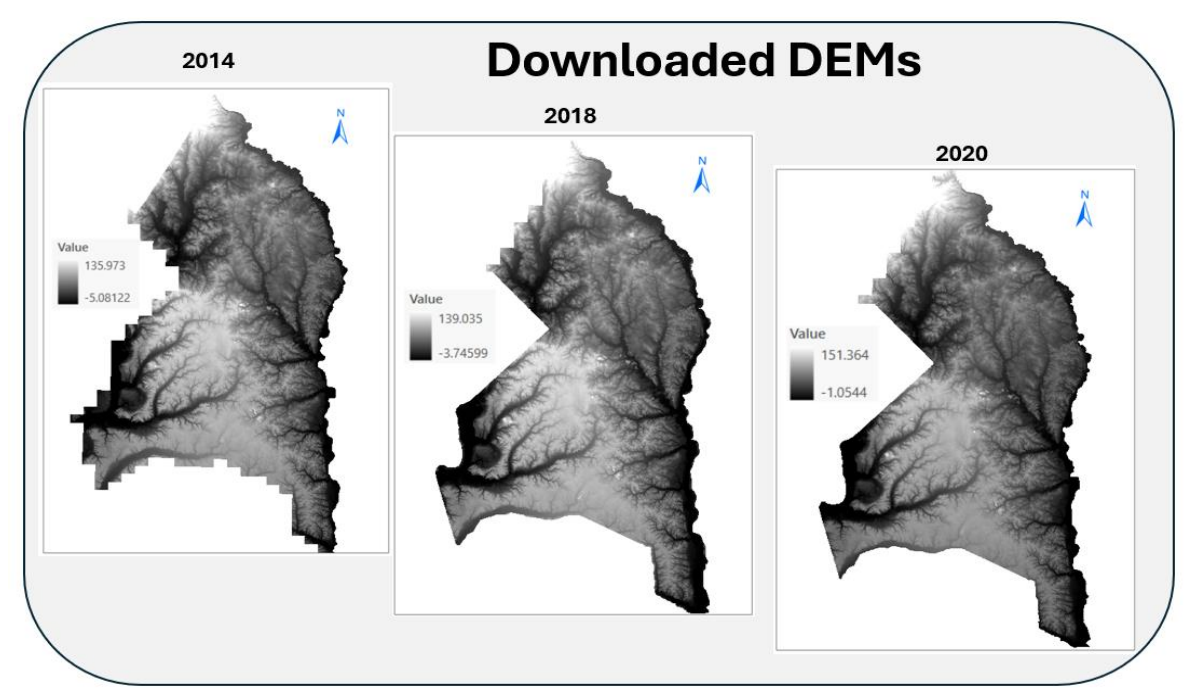


Figure 4.3: LiDAR DEMs of Prince George's County

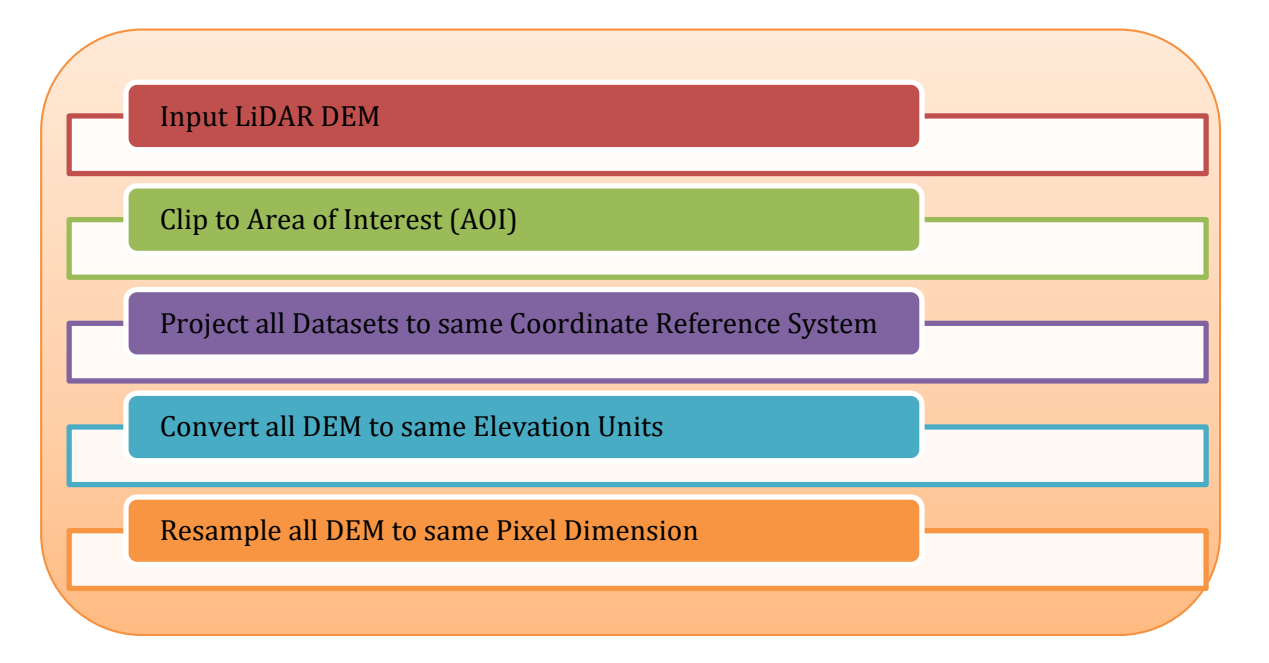


Figure 4.4: Preprocessing workflow for the LiDAR DEM.

## 4.4.2 Resolutions of the Digital Elevation Models

The study utilized high-resolution LiDAR-derived Digital Elevation Models (DEMs) acquired for Prince George's County, Maryland, across three time periods: 2014, 2018, and 2020, (Table 4.1). The spatial resolution of the DEMs progressively improved over the years, with the 2014 DEM captured at a 0.9 meters (3 feet) resolution, the 2018 DEM at 0.6 meters (2 feet), and the

2020 DEM at 0.3 meters (1 foot). These increasingly finer resolutions enabled the detection of subtle topographic variations critical for accurate landslide identification, especially when performing DoD analysis and extracting terrain attributes such as slope, curvature, and surface deformation.

Table 4.1: LiDAR DEMs (Raw Data Metadata)

S/No.	County	Year	DEM Hz. Resolution	Required Vz. Accuracy by ASPRS	RMSE (z)	DEM Vz. Accuracy RMSE(z) x 1.9600	Horizontal Coordinate Reference System
1	Prince George	2014	0.9m / 3 feet	0.643 ft	0.059m	0.11564m / 0.37940ft	NAD 83 HARN State Plane
2	Prince George	2018	0.6m / 2 feet	0.643 ft	0.298ft	0.58408ft / 0.17803m	NAD 83 HARN State Plane
2	Prince George	2020	1 foot / 0.3m	0.643 ft	0.051m	0.10000m / 0.32808ft	NAD 83 HARN State Plane

# 4.4.3 Geomorphometric factor generation, classification, landslide detection and mapping

High-resolution LiDAR-derived DEMs were utilized to extract key geomorphometric parameters including slope, aspect, curvature, contour (Fig. 4.5), and Topographic Wetness Index (Fig. 4.6) which are critical in understanding terrain instability and hydrological response. Fig. 4.7 shows a DoD which was generated by subtracting elevation surfaces across temporal datasets (2014, 2018, and 2020), to detect areas of significant vertical displacement, indicative of slope failures. These derived factors were reclassified into susceptibility classes using classification schemes with thresholds calibrated based on previous studies and terrain analysis (Fig. 4.5).

Landslide-prone areas were identified and mapped by integrating these geomorphometric layers with spatial overlays, including proximity to highways and historical landslide data. The resulting outputs delineated three distinct zones: Downward displacement, Stable, and Upward displacement zones, providing a geospatial basis for targeted risk mitigation and future monitoring. (See results in appendices).

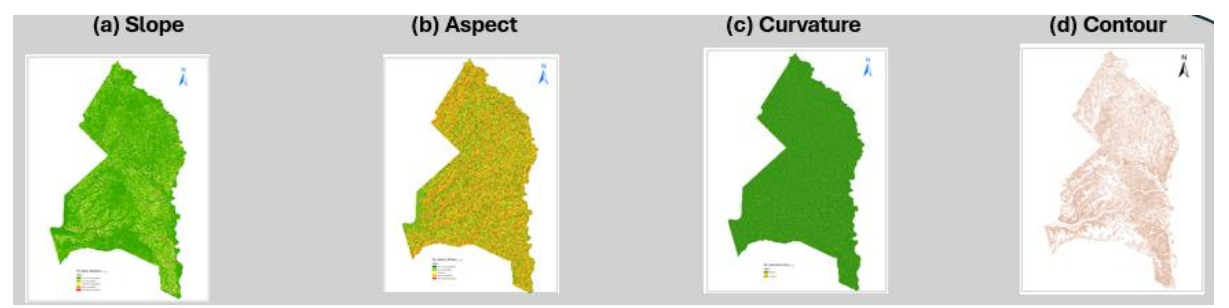


Figure 4.5: Sample generated factor maps.

Topographic Wetness Index (TWI) was derived through the raster calculator in ArcGIS Pro using:

$$TWI = \ln\left(\frac{a}{\tan(\beta)}\right) \tag{4.1}$$

where:

a = specific catchment area (from Flow Accumulation)

 $\beta$  = slope in radians.

The Flow Direction and Flow Accumulation parameters were also obtained through the spatial analyst tools in ArcGIS Pro.

Flow Direction: Spatial Analyst Tools – Hydrology – Flow Direction

Input Surface Raster = FillSink\_DEM.tif; Output Flow Direction Raster = FlowDir.tif

Flow Accumulation: Spatial Analyst Tools – Hydrology – Flow Accumulation

Input Flow Direction Raster = FlowDir.tif; Output Accumulation Raster = FlowAcc.tif

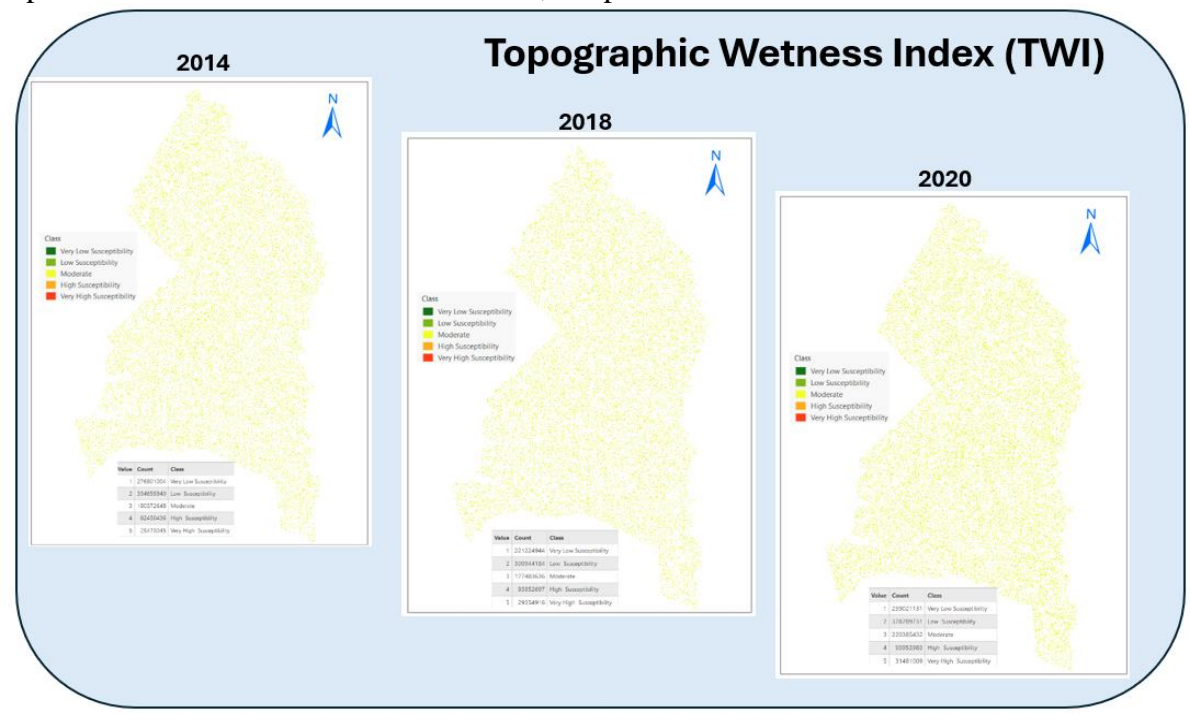


Figure 4.6: Topographic Wetness Index (TWI).

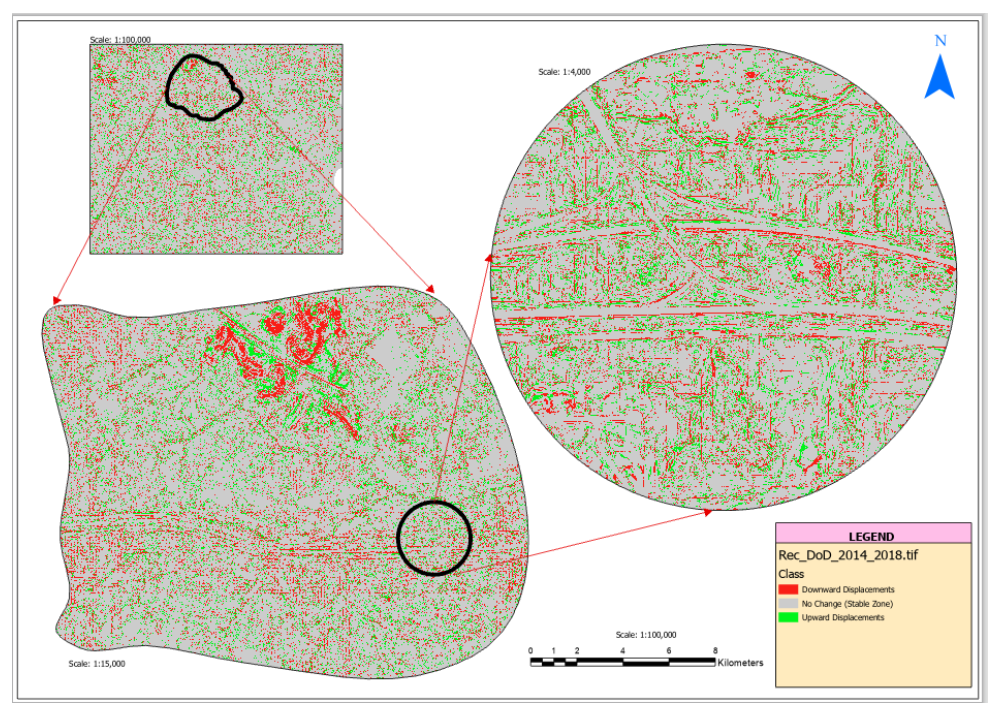


Figure 4.7: Sample Reclassified DEM of Difference (DEM 2018 minus DEM 2014). More factor maps generated are included in the appendices.

## 4.4.4 Buffering and Overlay Operations (Area of Interest)

Due to the large size of the LiDAR datasets, a specific Area of Interest (AOI) was carved out within Prince George's County, focusing on selected corridors with notable topographic variation and infrastructure relevance. Buffering and overlay operations were then performed on major highways within this AOI to analyze the spatial interaction between landslide-prone zones and transportation infrastructure. Buffer zones (100 meters from the centerline at both sides) were generated around these highways to establish impact corridors, which were overlaid with classified susceptibility maps and DoD results (see Fig. 4.8). This approach enabled the identification of critical segments (Fig. 4.9) where terrain deformation closely intersects roadways, informing risk prioritization and supporting resilient infrastructure planning.

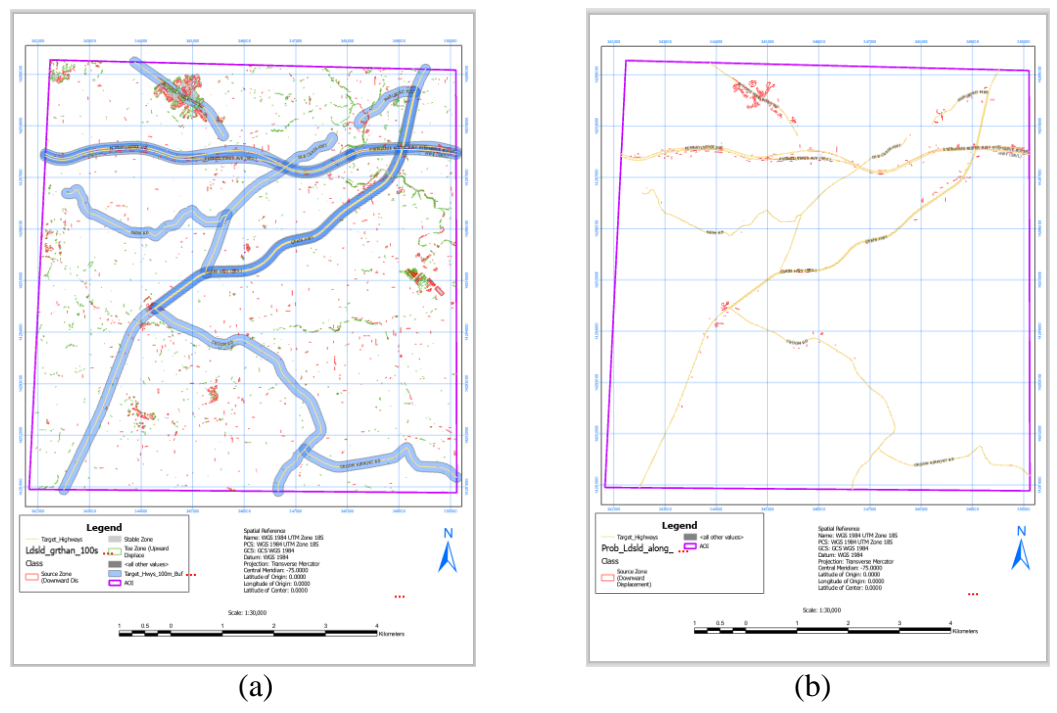


Figure 4.8: (a) Buffering (100 meters) and Overlay (b) Detected Probable Landslide Zones (Polygons).

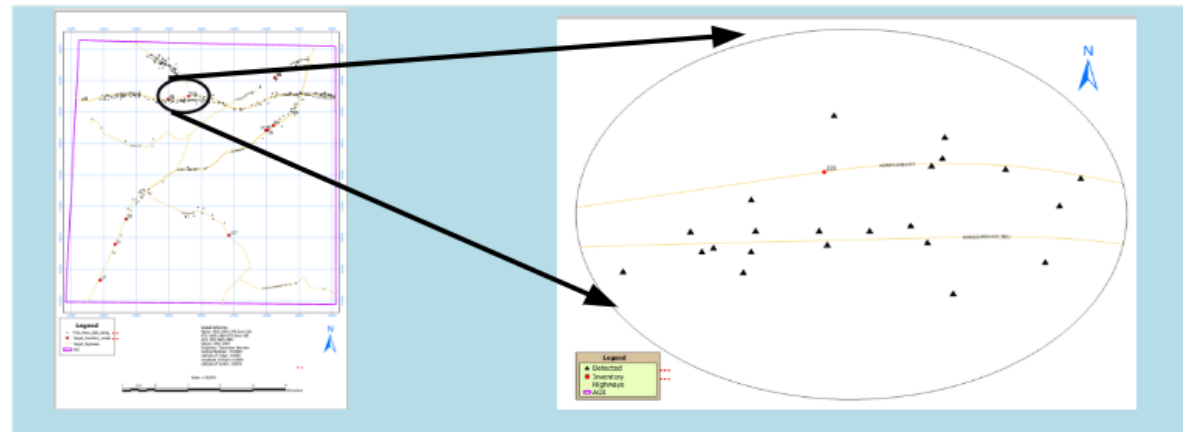


Figure 4.9: Detected (new) probable landslide risk points.

# 4.5 Results

The integration of LiDAR-derived DEMs for the years 2014, 2018, and 2020 enabled the extraction of key geomorphometric parameters essential for landslide analysis, including slope, aspect, curvature (profile and plan), contour, TWI, and DoD (Fig. 4.10). The derived slope and curvature maps revealed localized steep gradients and concave terrain segments, which corresponded closely with observed mass movement areas. Aspect analysis showed a predominance of instability on south-facing slopes, potentially linked to microclimatic influences on soil moisture dynamics.



Figure 4.10: Reclassed Factor Maps from different years.

The DoD analysis provided clear spatial differentiation of elevation changes over the selected years and focused areas, allowing for the detection of terrain displacement patterns consistent with landslide events. Notably, positive and negative DoD values indicated upward and downward displacements, respectively, while the near-zero values are stable zones. These results were overlaid through other factor maps such as slope, aspect, and others, which highlighted and corroborated areas that coincide with active or historical landslide sites (see Fig. 4.11 for sample result).

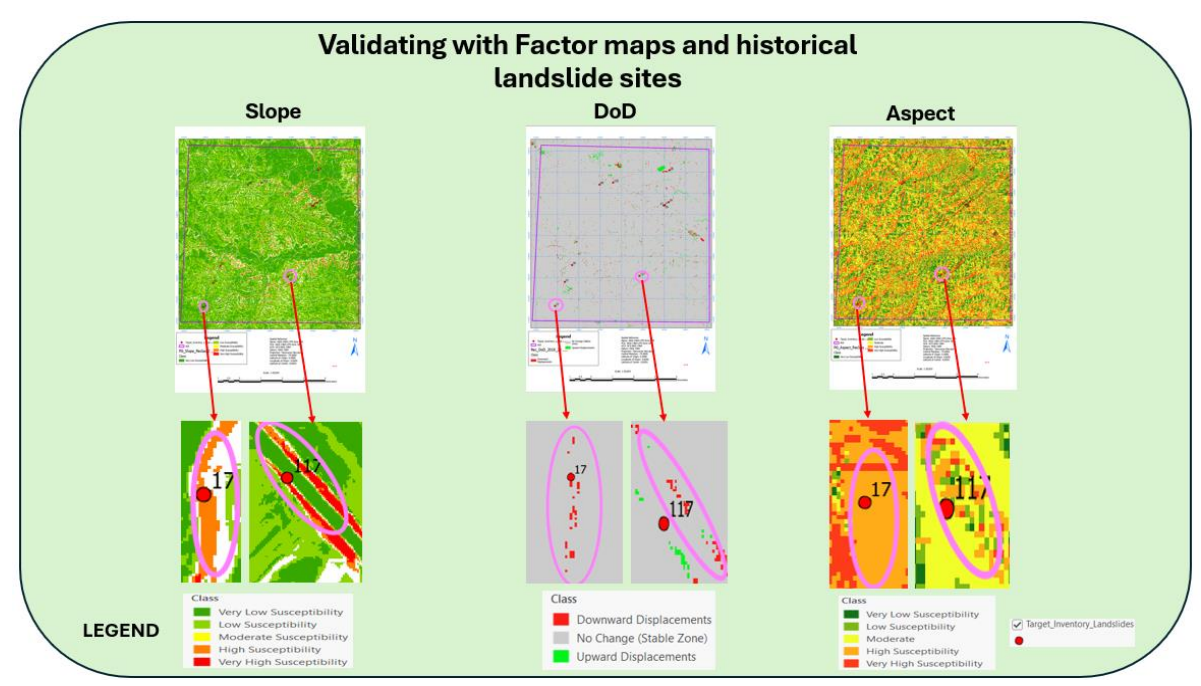


Figure 4.11: Showing correlations between factor maps overlaid with historical landslide sites.

Landslide susceptibility classification was performed using a weighted overlay of all geomorphometric factors, based on methodologies previously adopted in relevant studies and documented literature. The resulting susceptibility map was categorized into five zones: very low, low, moderate, high, and very high. High susceptibility areas were predominantly located near sharp slope transitions and concave curvature profiles.

Overlay analysis with buffered highway corridors revealed that segments of transportation infrastructure within the AOI intersected stable to downward displacement (landslide-prone) zones. These intersections represent potential risk hotspots for future slope failure, warranting geotechnical interventions and continuous monitoring. The buffering and overlay process further validated the relevance of spatial proximity between anthropogenic activities and geomorphic processes.

# 4.6 Summary and Future Work

This study effectively demonstrated the utilization of LiDAR-derived geomorphometric parameters for identifying landslide-prone zones within Prince George's County. These parameters included slope, aspect, curvature, contour, Topographic Wetness Index (TWI), and DoD. The analysis was conducted across the years 2014, 2018, and 2020. Temporal DEM analysis enabled the detection of terrain instability, while buffer and overlay operations confirmed the vulnerability of key transportation corridors to geomorphic hazards, reinforcing earlier findings by Galli et al. [51] on the importance of geospatial integration for landslide detection and infrastructure risk assessment.

In alignment with the previous studies [49, 50, 52], future work will focus on expanding the landslide inventory through field-based validation using ground truthing and the collection of soil samples from newly detected probable landslide sites. These will be compared with

existing inventory points for verification and soil classification with terrain behavior. In addition, InSAR time-series deformation data will be integrated with LiDAR-based outputs to enhance temporal sensitivity [54]. Quantitative modeling using statistical and machine learning techniques such as logistic regression and random forest by Corominas et al., [55], Yilmaz, [56]; Chen et al., [57] will be pursued to improve landslide susceptibility mapping and prediction accuracy. These efforts aim to strengthen disaster preparedness and inform resilient transportation planning.

# Chapter 5

# 5 Surface soil moisture mapping for slope instability analysis in Maryland using machine learning model

Atieh Hosseinizadeh\*, Kayla Collymore, Zhuping Sheng, Yi Liu, Oludare Owolabi

(\*Part of material in this chapter will be submitted to a journal for consideration of publication)

# 5.1 Introduction

Soil moisture is a critical component of the land surface system, influencing water and energy exchanges that affect hydrological processes and slope stability. It plays a vital role not only in agriculture and drought monitoring but also in geohazard modeling, especially for landslide prediction. Accurate soil moisture data are essential for developing prediction models used in early warning systems and risk mitigation in landslide-prone areas [58]. However, soil moisture varies significantly across time and space due to complex climate-soil interactions, making precise measurement and modeling challenging [59]. Recent research has demonstrated that including realistic soil moisture conditions substantially improves landslide forecasting accuracy, emphasizing that rainfall alone is insufficient for reliable predictions [67].

Advances in remote sensing and machine learning have enhanced soil moisture estimation for landslide forecasting. Satellite missions such as Sentinel-1, Sentinel-2, and SMAP, combined with in-situ and model data, provide soil moisture information at various depths and resolutions [60, 61]. Deep learning models like attention-based LSTM, CNN-LSTM, and GAN LSTM have shown strong performance in capturing temporal moisture dynamics relevant to slope failure [62, 63, 64]. These models integrate meteorological variables, vegetation indices, and terrain features to better represent environmental factors affecting subsurface water movement and slope stability [65, 66]. Interpretability methods such as SHAP further help clarify the role of input variables, facilitating operational use in landslide monitoring [63].

Despite these advances, significant research gaps remain. Many models are developed for specific regions or land uses, limiting their transferability. For example, some focus only on unirrigated wheat systems or single locations without remote sensing inputs [64, 65]. Others face challenges related to limited explainability or uncertain performance across different climates [60]. Most studies also emphasize long-term seasonal dynamics without thoroughly addressing spatial resolution or terrain complexity [58, 59]. Traditional remote sensing

methods, including microwave retrievals and GPS bistatic radar, report limitations in sensitivity and spatial detail, particularly in rough or vegetated terrain [68-70].

One of the major obstacles in closing the existing gap is the significant computational burden involved in processing full-resolution raster datasets over hundreds of time steps and multiple input layers. Conventional machine learning pipelines, which often require loading entire rasters into memory, are not well-suited for managing datasets of this scale. To address this, the present research proposes an innovative deep learning architecture for spatiotemporal soil moisture estimation.

Meanwhile, traditional soil moisture monitoring techniques and most supervised machine learning approaches often depend on in-situ measurements or gravimetric sampling to serve as observational inputs or training labels. While these methods offer precise data at specific points, they lack broad spatial coverage and are often too costly to deploy at large scales. This spatial limitation may result in overfitting to specific locations, reducing the ability of models to generalize across diverse terrain. Satellite-based remote sensing provides a more extensive spatial reach through missions like SMAP, SMOS, and ASCAT. However, their coarse resolution typically ranges from 10 to 36 km, which makes them unsuitable for applications like landslide hazard assessments that require fine-scale soil moisture data.

To tackle these issues and close the current gaps in soil moisture mapping, this study introduces a deep learning framework designed to generate high-resolution spatiotemporal surface soil moisture (SSM) maps. The model employs a convolutional long short-term memory (ConvLSTM) network capable of learning from a blend of static features (such as DEM, slope, and soil properties), time-varying meteorological variables (including precipitation, temperature, humidity, wind, and evapotranspiration), and seasonal vegetation dynamics. By utilizing dense, high-resolution SSM labels derived from Sentinel-1 imagery through a self-calibrated change detection method, the approach eliminates reliance on sparse field observations while preserving physical consistency. This enables the continuous prediction of soil moisture at fine spatial and temporal scales, offering a critical tool for modeling infiltration, forecasting hydrological responses, and evaluating landslide susceptibility in regions with limited data and complex terrain.

# **5.2 Related Works**

# **5.2.1** Reviewed Papers on Remote Sensing Models

Li et al. [62] developed an attention-aware LSTM model (ILSTM\_Soil) for predicting soil moisture and temperature 1 to 7 days ahead using data from ten FLUXNET sites. The model integrates predictor and temporal attention mechanisms, allowing it to identify key input features and relevant time steps. ILSTM\_Soil outperformed baseline models including Random Forest, SVR, Elastic-Net, standard LSTM, and A-LSTM in terms of RMSE and R<sup>2</sup>. While the attention layers improved model interpretability, the study was limited by its geographic scope and did not address deeper soil layers or long-term seasonal forecasting.

Jiang et al. [65] enhanced an LSTM-based model for soil moisture prediction by incorporating autocorrelation between soil depths and meteorological variables. Trained on data from six unirrigated wheat-field monitoring sites in the Yellow and Huaihai regions, the model outperformed the standard LSTM in predictive accuracy and error reduction. The results

showed better alignment with observed soil conditions. However, the study is limited to seasonal wheat systems and has not been validated under irrigated conditions or with other crop types.

Wang et al. [63] conducted a comprehensive evaluation of ten deep learning models for soil moisture prediction, including standard LSTM, feature-attentive LSTM (FA LSTM), and generative adversarial network-based LSTM (GAN LSTM). These models were tested across multiple soil types and depths to assess their robustness and adaptability. Results showed that FA LSTM and GAN LSTM consistently outperformed the baseline LSTM model in terms of predictive accuracy and stability across time. The inclusion of attention mechanisms allowed the models to focus more effectively on relevant temporal and feature-level information, enhancing both performance and interpretability. SHAP analysis further contributed to transparency by identifying the relative importance of different input variables in the prediction process. Despite these strengths, the study highlights key limitations: the models demand large volumes of high-quality input data and were only validated in a few specific climate regions. This raises questions about their scalability and reliability in more diverse or data-sparse environments.

Kone et al. [64] developed hybrid models combining convolutional neural networks (CNN) with LSTM (CNN LSTM) and bidirectional LSTM (Bi LSTM) to predict next-day soil moisture using climate and soil data. These models were benchmarked against a standard LSTM, with CNN LSTM achieving the best performance, exhibiting an  $R^2$  of approximately 0.98 and RMSE near 0.37, slightly outperforming both LSTM ( $R^2 \sim 0.97$ ) and Bi LSTM. The study highlights the strength of CNN LSTM in capturing spatial-temporal features relevant to soil moisture dynamics. However, the approach was limited by its testing on specific soil types at a single location, without incorporating remote sensing data or evaluating the models across diverse terrains and moisture regimes, thus constraining its broader applicability.

# **5.2.2** Reviewed Papers on Machine Learning for Soil Moisture Estimation

Batchu et al. [60] proposed a machine learning regression network that fuses multi-source data including Sentinel-1 SAR, Sentinel-2 optical imagery, SMAP satellite data, SoilGrids, GLDAS, and ground-based measurements to estimate 5 cm soil moisture globally at a spatial resolution of 320 meters. Evaluated across approximately 1,300 monitoring stations, the model achieved an average correlation coefficient of 0.727 and an RMSE of 0.054, demonstrating promising accuracy in soil moisture retrieval. Despite these encouraging results, the study identified significant limitations related to the model's low explainability and inconsistent performance across different climatic zones and sensor data inputs. These challenges restrict its immediate application in hybrid physical AI systems where interpretability and robustness across diverse conditions are critical.

Ahmad et al. [66] applied support vector machines with kernel regression to estimate soil moisture in the top 0 to 10 cm layer using TRMM precipitation data and NDVI from AVHRR at ten sites within the Colorado River Basin. Their results demonstrated that SVM outperformed artificial neural networks and showed strong agreement with VIC model benchmarks. However, the study focused solely on surface soil moisture and was limited by sparse sampling, restricting its ability to capture moisture dynamics at greater depths and over seasonal timescales.

Liu et al. [61] compared six machine learning algorithms including artificial neural networks (ANN), Bayesian methods, classification and regression trees (CART), k-nearest neighbors (KNN), Random Forest, and support vector machines (SVM) to improve the spatial resolution of satellite-derived soil moisture data using inputs such as digital elevation model (DEM), land surface temperature (LST), normalized difference vegetation index (NDVI), and albedo across multiple climate zones. The study found that Random Forest consistently delivered the highest accuracy, achieving the strongest correlation and lowest error metrics in four different regions. Despite these strengths, some models, notably ANN, CART, and SVM, showed inconsistent performance across varying surface types and faced challenges in generalizing to diverse environmental conditions. This highlights the need for further research to enhance model robustness and adaptability.

Orth and Sungmin [59] used LSTM neural networks trained on soil moisture data from over 1,000 stations to estimate daily soil moisture at multiple depths (0 to 10, 10 to 30, and 30 to 50 centimeters) spanning from 2000 to 2019. Their results demonstrated strong temporal performance and improvements compared to satellite retrievals and traditional model outputs. However, the study noted that the spatial resolution remains relatively coarse, originally at 0.25 degrees and improved only to 0.1 degrees, and that there has been limited evaluation of error characteristics specific to each soil depth. These limitations suggest the need for further refinement in resolution and depth-specific accuracy assessment.

Senyurek et al. [71] applied machine learning techniques to estimate soil moisture from CYGNSS satellite data, incorporating ground measurements across the United States. The study demonstrated that this approach outperforms previous CYGNSS-based methods by providing more accurate soil moisture estimates that closely match in situ observations while offering broader spatial and temporal coverage. Despite these improvements, challenges remain in obtaining reliable estimates in areas with dense vegetation and complex terrain. Additionally, the model's performance outside the tested regions has not yet been validated, highlighting the need for further evaluation to ensure generalizability.

Persson and Haridy [72] estimated soil water content using electrical conductivity measurements obtained from short time-domain reflectometry (TDR) probes. Their results showed that this method provides accurate and reliable soil moisture estimates that closely match actual water content. However, the study noted that soil texture and salinity levels can influence conductivity readings, potentially introducing errors in the estimation process. This limitation points to the need for further investigation into how varying soil properties affect measurement accuracy.

Vereecken et al. [58] reviewed the role of soil moisture measurements in vadose zone hydrology, emphasizing their importance for understanding water flow and transport processes. Their findings indicate that accurate soil moisture data contribute to improved calibration of hydrological models, reduce uncertainties, and enhance the reliability of model predictions. Despite these benefits, the review identified significant limitations in current measurement techniques, particularly their insufficient spatial and temporal resolution. The authors highlighted the need for improved methods to integrate soil moisture observations with models across varying scales to advance hydrological understanding.

## 5.2.3 Reviewed Papers on ML Models for Soil Moisture in Geoscience

Jackson et al. [68] used an airborne microwave radiometer to measure soil moisture and validate AMSR-E satellite sensor data during the Soil Moisture Experiment 2002 (SMEX02). Their results showed that airborne measurements closely matched ground-based soil moisture observations, confirming the accuracy of AMSR-E soil moisture products. However, the study noted that airborne measurements are limited to relatively small areas, and additional validation is required across diverse soil types and vegetation conditions to fully assess the satellite sensor's performance.

Masters et al. [69] investigated the use of airborne GPS bistatic radar measurements to estimate soil moisture during the Soil Moisture Experiment 2002 (SMEX02). Their results demonstrated that this radar-based approach provides reliable soil moisture estimates that correspond closely with ground observations. Despite these positive findings, the study highlighted the need to improve spatial resolution and to evaluate the method across diverse terrain types and vegetation covers to better understand its broader applicability.

Paloscia et al. [70] developed a multifrequency algorithm to estimate soil moisture on a large-scale using microwave data from the SMMR and SSM/I satellites. Their results showed that this algorithm provides more accurate soil moisture estimates across different regions compared to single-frequency approaches. However, the study noted challenges in accounting for surface roughness and vegetation effects, which can reduce estimation accuracy under certain conditions. These limitations indicate a need for further improvements to address these factors.

# **5.3Materials and Methods 5.3.1 Study Area**

The study area is Prince George's County, located in central Maryland. This region was selected for its geographic diversity, varied topography, and history of extreme weather events, including heavy rainfall and landslides. Covering approximately 500 square miles, the county includes a representative mix of urban, suburban, and rural land uses, reflecting the broader environmental variability found across the Mid-Atlantic region. Due to its combination of physical and climatic characteristics, Prince George's County provides a practical setting for developing and testing the machine learning model at a localized scale, with plans to later expand the framework to the wider Maryland area and other regions.

Prince George's County lies within the transitional zone between the Atlantic Coastal Plain and the Piedmont Plateau, creating a geologically complex landscape. This setting results in varied terrain, diverse soil types, and a range of slope gradients that directly influence both hydrological processes and slope stability. The county experiences a humid subtropical climate with consistent precipitation throughout the year, offering favorable conditions for studying rainfall-driven processes such as soil moisture fluctuations and slope failures. According to the most recent landslide inventories compiled by the State Highway Administration (SHA), the United States Geological Survey (USGS), and NASA, Maryland recorded 129 landslides between 2008 and 2019, with most classified as shallow failures (Fig. 5.1).

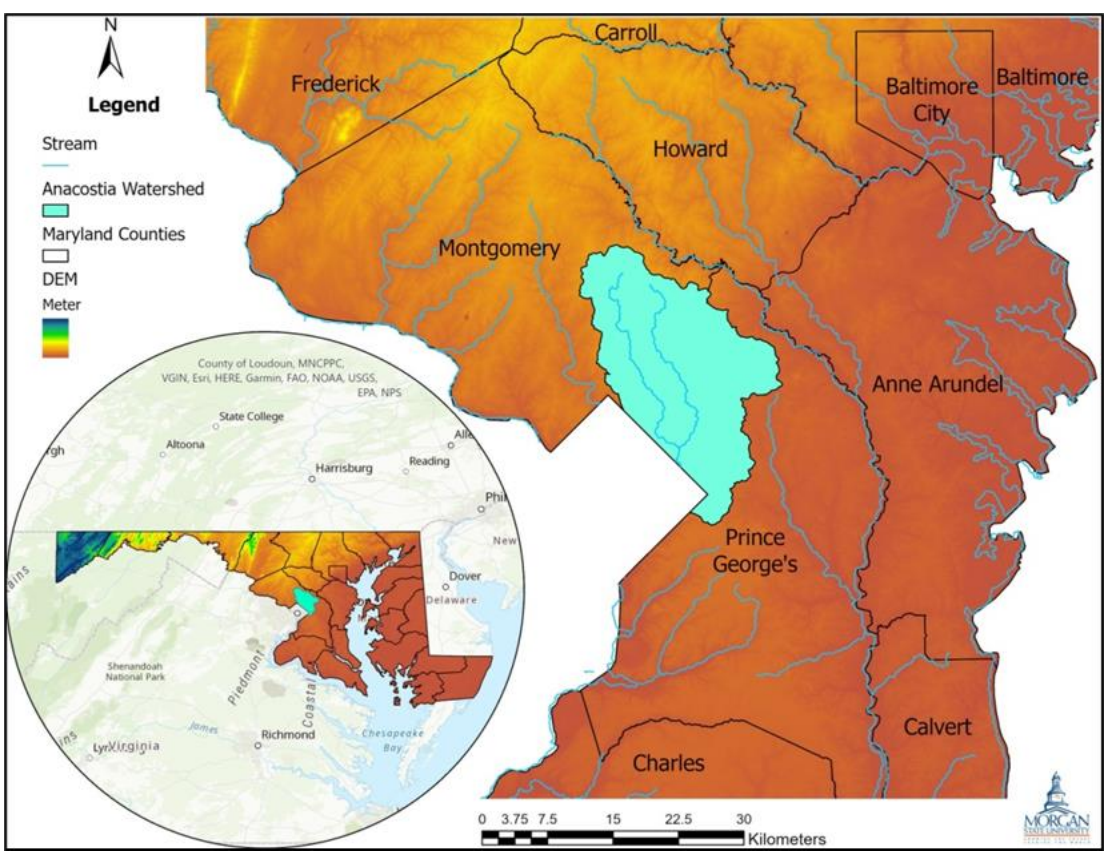


Figure 5.1: Historical landslide location in Maryland and the selected case study area, Prince George's County.

Figure 5.2(a) shows that Prince George's County has recorded the highest number of landslide events in Maryland, accounting for approximately 30 percent of the state's total occurrences. Since the county is also one of the most densely populated in the state, assessing, forecasting, and reducing landslide risk is especially important for protecting communities and infrastructure. Figure 5.2(b) shows a clear temporal pattern between rainfall and landslide frequency, with peak activity in 2011, 2014, and 2018. These years also saw the highest annual rainfall totals, emphasizing the strong role of precipitation and subsequent infiltration as key triggering factors for landslides in the region.

Figures 5.2(c) and 5.2(d) depict how the frequency of 132 landslide events relates to both rainfall intensity and soil moisture levels. The analysis shows that many landslides occurred during periods of relatively low rainfall, indicating that some vulnerable slopes in Maryland can fail even with light precipitation. In contrast, a stronger correlation is observed between landslide occurrences and elevated soil moisture, emphasizing the critical role of subsurface moisture in slope instability. This underscores the importance of incorporating soil moisture monitoring into predictive models rather than relying solely on rainfall data.

To explore these patterns more thoroughly, this study focuses on Prince George's County—a well-documented and representative area. Its susceptibility to climate-driven hazards, rapid urbanization, and stormwater challenges makes it an ideal case for advancing landslide prediction models.

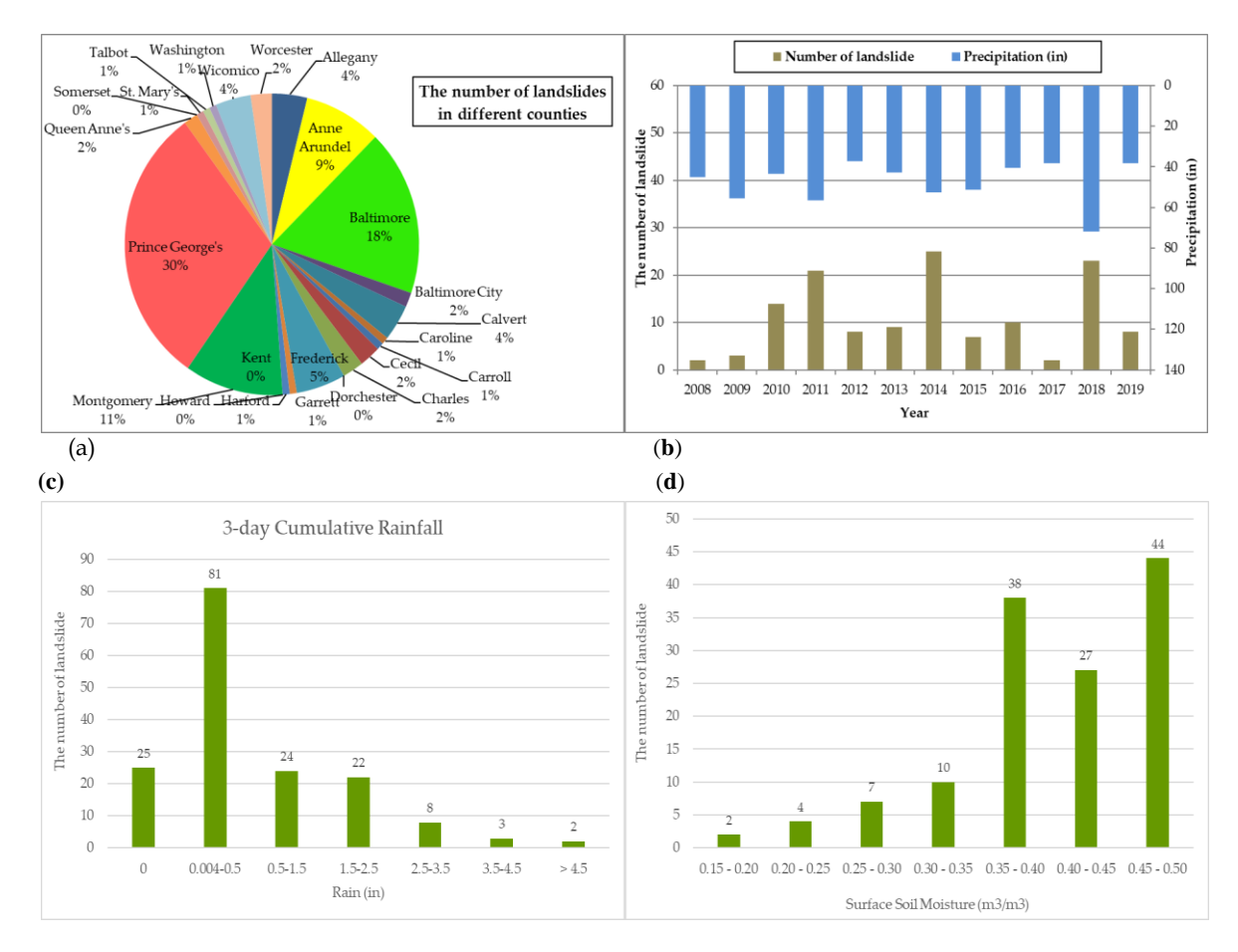


Figure 5.2: Landslide analysis in Maryland: (a) Number of landslides by county; (b) Annual precipitation vs. number of landslides; (c) Three-day cumulative rainfall vs. number of landslides; (d) Surface soil moisture (from Open-Meteo) vs. number of landslides.

## 5.3.2 Data Preparation

Figure 5.3 shows the workflow used in this study to develop a machine learning based surface soil moisture model (ML SSM) using soil moisture maps derived from Sentinel 1 satellite data. The diagram outlines the key datasets required to train the model, including the target variable (surface soil moisture), weather conditions, and geological characteristics. These inputs include both spatial and temporal data such as soil moisture maps, weather variable maps, and land use or land cover maps, as well as static spatial data such as soil type, topography, and slope.

#### 5.3.2.1 Sentinel-1 Data to Generate SSM Maps

The evaluation of the ML-SSM model utilizes surface soil moisture (SSM) maps derived from Sentinel-1 radar imagery, captured at six-day intervals. Sentinel-1 is part of the European Space Agency's Copernicus initiative and has offered high-resolution radar data since 2014. Its C-band Synthetic Aperture Radar (SAR) system ensures consistent data collection in all weather and lighting conditions [73], making it well-suited for soil moisture applications.

Sentinel-1A and Sentinel-1B, operating on alternating 12-day cycles, collectively provide imagery with a six-day revisit frequency [74]. This frequent temporal resolution supports ongoing SSM monitoring for large-scale hydrological analysis and landslide hazard evaluation. The imagery used in this research comes from the Interferometric Wide (IW) swath mode, which spans 250 km with a ground resolution of approximately 20 m by 22 m [75]. SSM values were retrieved using vertical-vertical (VV) polarization, and the final maps were resampled to a 15-meter spatial resolution.

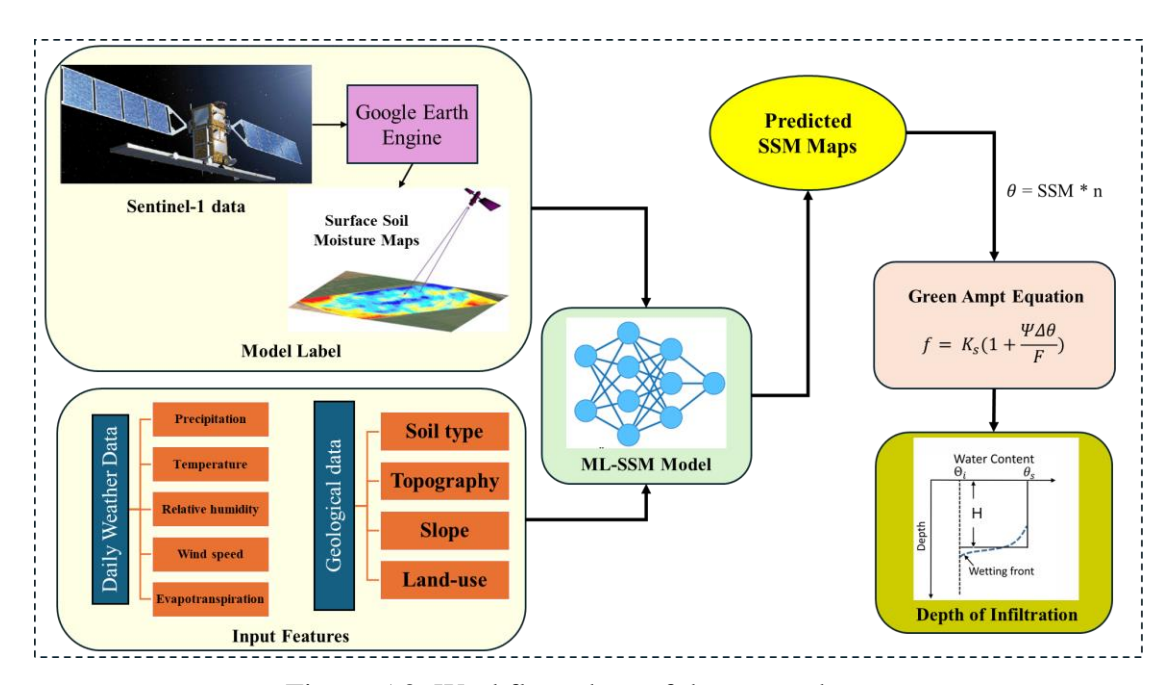


Figure 5.3: Workflow chart of the research.

#### 5.3.2.2 Weather Data

To develop the ML SSM model, a time series of daily climate variables was compiled, including precipitation, maximum and minimum temperature, relative humidity, wind speed, and evapotranspiration. These datasets were sourced from the Open Meteo database at a spatial resolution of 9 kilometers. Since this resolution is too coarse for detailed spatial modeling, the data were interpolated and resampled to create weather variable maps at a finer 15-meter resolution. In this study, the Inverse Distance Weighting (IDW) method was used to interpolate all climate variables. IDW is a widely accepted technique for estimating meteorological conditions such as precipitation and temperature, especially when measurement stations are limited and spatial variability is relatively smooth [76]. The locations of the original weather stations used in the interpolation process are shown in Figure 5.4.

### 5.3.2.3 Geological Data

A detailed soil map was acquired from the Maryland Soil Survey Geographic Database (SSURGO) for the creation of static maps. Soil polygons along highways that lacked attribute information on soil properties and materials were identified, and the percentages of clay, silt, and sand for these polygons were estimated by averaging values from neighboring polygons. At the same time, topographic features were extracted using 1/3 arc-second LiDAR-based

Digital Elevation Models (DEMs) specific to Maryland. The slope map was then derived from the DEM using ArcGIS tools. Vegetation changes over time were tracked by creating Normalized Difference Vegetation Index (NDVI) maps from Sentinel-2 satellite imagery within the Google Earth Engine (GEE) platform.

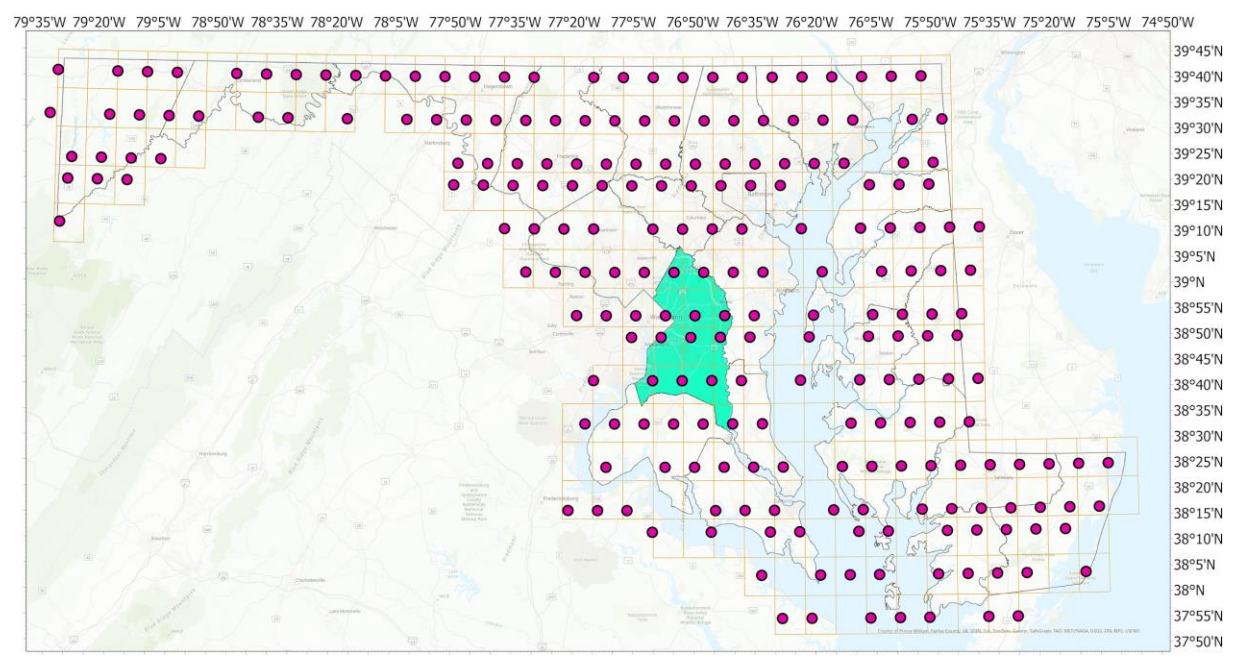


Figure 5.4: Spatial distribution of weather observation points from the Open-Meteo database used for interpolation.

Sentinel-2, part of the Copernicus program by the European Space Agency (ESA), delivers high-resolution optical imagery with a spatial resolution of up to 10 meters and a revisit time of 5 days, making it particularly suitable for vegetation analysis [77]. NDVI was calculated using the standard formula:

$$NDVI = \frac{NIR - RED}{NIR + RED} \tag{5.1}$$

where NIR and RED represent reflectance values from the near-infrared (Band 8) and red (Band 4) wavelengths, respectively. In Google Earth Engine (GEE), Sentinel-2 surface reflectance data were pre-processed to mask clouds using the QA60 band and a cloud probability threshold. NDVI was then calculated for each image and temporally aggregated to create consistent NDVI maps aligned with the acquisition dates of the SSM maps. These NDVI maps offer valuable information on vegetation cover, an important factor affecting surface soil moisture and rainfall infiltration [78]. Figure 5.5 shows the spatial distribution of all input parameters used in building the ML-SSM model for the study area, including meteorological variables, topographic features, land use, and soil properties.

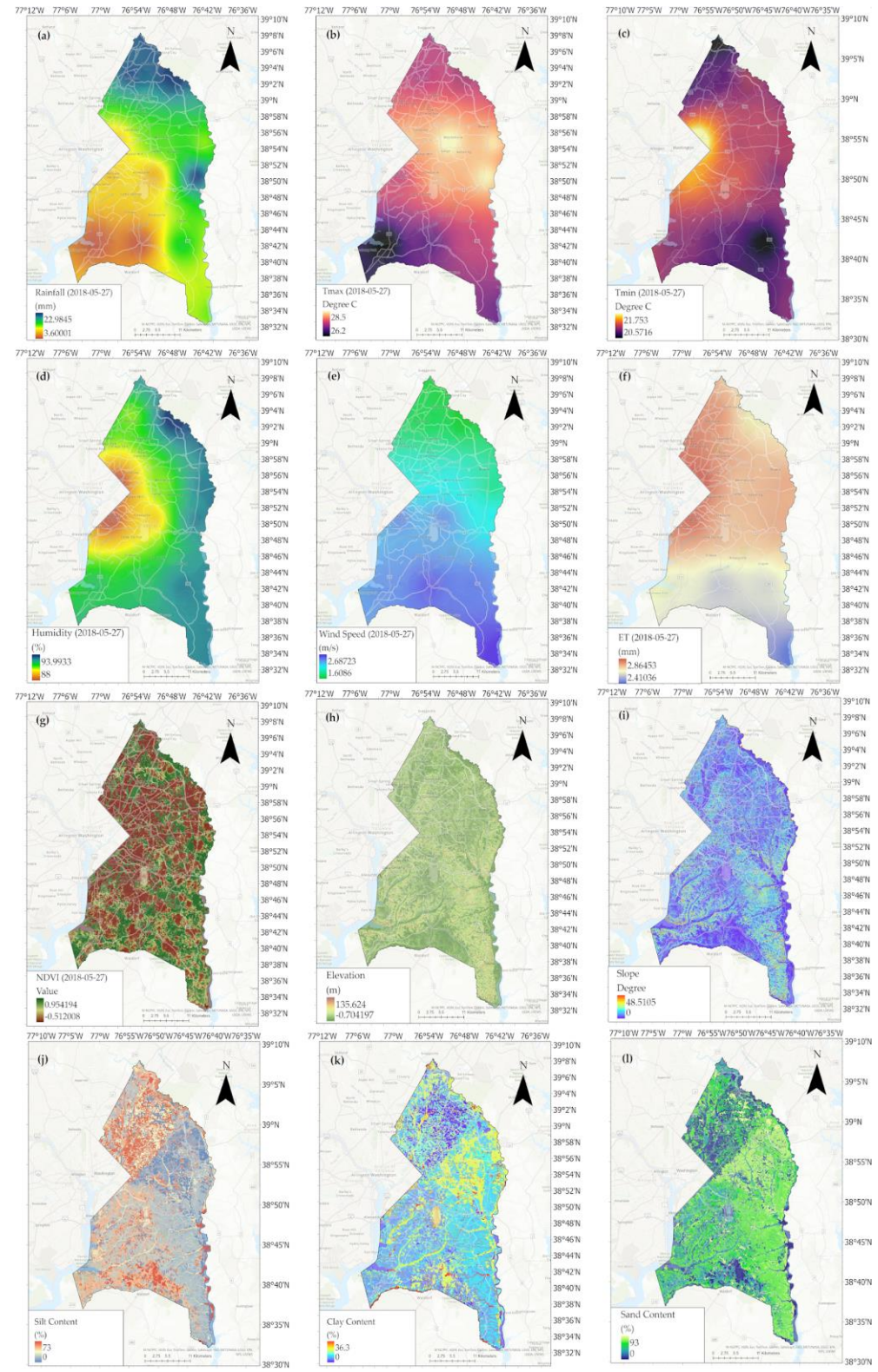


Figure 5.5: SInput data to ML-SSM model: (a) Rainfall; (b) Maximum temperature; (c) Minimum temperature; (d) Relative humidity; (e) Wind speed; (f) Evapotranspiration; (g) NDVI; (h) Elevation; (i) Slope angle; (j) Silt content; (k) Clay content; (l) Sand content.

## 5.3.3 Methodology

### 5.3.3.1 Producing SSM Maps using Sentinel-1

This study uses the SSM retrieval algorithm based on the TU Wien Change Detection Model [79] to produce SSM maps from Sentinel-1 data as target maps for the ML model. This physically based model estimates soil moisture directly from radar backscatter coefficients ( $\sigma^0$ ), which indicate surface reflectivity. It assumes that changes over time in backscatter mainly reflect variations in soil moisture, while factors like surface geometry, roughness, and vegetation structure remain constant over time.

The model operates through a self-calibrated, pixel-based approach that uses long-term backscatter time series to determine site-specific dry and wet reference values, denoted as  $\sigma^{o}_{dry}$  and  $\sigma^{o}_{wet}$ . For each acquisition at time t and local incidence angle  $\theta$ , the observed backscatter is normalized to a reference angle  $\Theta$  and scaled between the dry and wet reference values to derive the relative surface soil moisture (SSM) as a percentage, calculated by:

$$SSM(t) = \frac{\sigma^0(\Theta, t) - \sigma^0_{dry}(\Theta, t)}{\sigma^0_{wet}(\Theta, t) - \sigma^0_{dry}(\Theta, t)}$$
(5.2)

This normalization mitigates the impact of vegetation and surface roughness by focusing on temporal changes at each pixel location, enabling consistent and reliable surface soil moisture (SSM) estimates across broad regions. The SSM retrieval algorithm is implemented using the Google Earth Engine (GEE) platform to generate SSM maps at six-day intervals over the study period from 2016 to 2024. The analysis specifically uses Sentinel-1 data in vertical-vertical (VV) polarization mode. In VV mode, radar signals are both transmitted and received with vertical polarization, making the backscatter more sensitive to dielectric properties such as soil moisture and less affected by vegetation compared to vertical-horizontal (VH) polarization. VH polarization, influenced more by volume scattering from vegetation, yields weaker backscatter signals and is less suitable for detecting soil moisture. Therefore, this study uses VV polarization to ensure more accurate and robust SSM retrieval, emphasizing sensitivity to surface wetness while minimizing interference from vegetation.

In Sentinel-1 data, the orbitProperties-pass field indicates the satellite's orbit direction relative to the Earth's surface, with values of ASCENDING and DESCENDING. During an ascending orbit, the satellite travels from south to north, usually capturing data during nighttime or early morning hours. These cooler, less evaporative conditions typically correspond to higher surface soil moisture levels. In contrast, the descending orbit moves from north to south and collects images during the daytime when increased solar radiation leads to higher evapotranspiration rates, often resulting in lower apparent moisture levels.

Both ascending and descending passes provide valuable information for mapping surface soil moisture using Sentinel-1 SAR data. The ascending orbit is especially useful for estimating peak moisture conditions, while descending orbit data help analyze moisture variability during drier periods. By combining data from both orbits, the temporal resolution is improved, and the accuracy and reliability of soil moisture retrieval are enhanced by capturing different hydrological states of the surface.

### 5.3.3.2. Develop ML-SSM Model

The ML-SSM framework consists of five key steps designed to predict surface soil moisture maps based on spatial and temporal environmental inputs.

### Step 1: Data Preparation and Patch Extraction

Temporal raster maps of weather variables, including rainfall, maximum temperature, minimum temperature, relative humidity, wind speed, and evapotranspiration, were collected along with NDVI and static environmental parameters such as elevation, slope, silt, sand, and clay contents. All datasets were spatially aligned. For each available SSM date, a two-step time window of input data was created and stacked with static layers, resulting in a twelve-band spatiotemporal tensor. These tensors and corresponding SSM maps were divided into smaller patches of sixteen by sixteen pixels using a sliding window with a defined stride. Each patch represented a local spatial area with temporal context and was saved to disk because of memory limitations. Global min-max normalization was applied across each variable to reduce scale sensitivity during training.

### Step 2: Patch Dataset Management

The extracted patches were indexed and split into three non-overlapping subsets: training with eighty percent, validation with ten percent, and testing with ten percent. A custom data generator was created to load these patches in batches during model training to avoid memory overload and to enable efficient and scalable model development.

### Step 3: Patch Data Generators

Custom TensorFlow Sequence generators were implemented to load the input (X) and target (y) patches from disk in batches. This ensured smooth feeding of spatiotemporal data into the model along with random shuffling of training samples between epochs to enhance generalization and prevent overfitting.

#### Step 4: Model Architecture and Training

A Convolutional Long Short-Term Memory neural network was designed to learn both spatial and temporal patterns from the sequence of input raster patches. This model extends the standard LSTM architecture introduced by Shi et al. [80] by replacing matrix multiplications with convolutional operations in both input-to-state and state-to-state transitions. This allows the model to preserve spatial structure while capturing temporal dynamics, making it effective for spatially distributed variables evolving over time. This approach has been successful in precipitation nowcasting [80], flood mapping [81], and soil moisture prediction [82]. The final model architecture, selected after extensive testing, takes input tensors shaped (2, 16, 16, 12) representing two consecutive time steps of sixteen by sixteen patches with twelve environmental features. It begins with a ConvLSTM2D layer with 32 filters and a 3 by 3 kernel, configured to return the full temporal sequence and capture spatial and temporal dependencies. Batch normalization and dropout layers follow to improve stability and prevent overfitting. A second ConvLSTM2D layer compresses the sequence into a single spatial output, again followed by batch normalization and dropout. The output passes through a Conv2D layer with 16 filters and ReLU activation for spatial feature refinement. Finally, a Conv2D output layer with a single filter and sigmoid activation generates the predicted surface soil moisture map normalized between zero and one. The model was trained using the Adam optimizer and means absolute error loss function with early stopping based on validation loss. This architecture allows simultaneous learning of how terrain, soil type, and temporal weather dynamics influence soil moisture levels.

### Step 5: Model Evaluation

After training, the model's performance was evaluated on unseen validation and test patches using mean absolute error, root mean squared error, and the coefficient of determination (R<sup>2</sup>). Predictions were flattened and compared with actual surface soil moisture values to assess accuracy and generalization across different locations and conditions.

### 5.3.3.3. Estimating Infiltration from SSM Maps

Once the ML-SSM model is developed, it can predict SSM maps under various weather conditions, supporting real-time applications and future scenario analyses. However, for future landslide susceptibility assessments, it is important to estimate infiltration depth rather than soil moisture alone. Therefore, the next step involves converting the predicted SSM maps into infiltration maps, which represent the depth of water penetration into the soil and are more directly related to slope stability and landslide triggering. According to Wagner et al. [79], SSM can be interpreted as the degree of saturation, which allows estimation of volumetric soil moisture by multiplying SSM by soil porosity. With volumetric moisture determined, the Green-Ampt equation [83] will be applied, as previous studies have demonstrated its effectiveness for estimating infiltration from soil moisture. The equation is:

$$f = K_s (1 + \frac{\Psi \Delta \theta}{F}) \tag{5.3}$$

where f is the potential infiltration rate,  $K_s$  is the effective saturated hydraulic conductivity (permeability coefficient),  $\Psi$  is average suction across the wetting front,  $\Delta\theta = \theta_s - \theta_i$  is the moisture deficit,  $\theta_s$  is the saturated water content,  $\theta_i$  is the initial water content, and F is the cumulative infiltration. The actual depth of the wetting front is given by  $H = \frac{F}{\Delta\theta}$ .

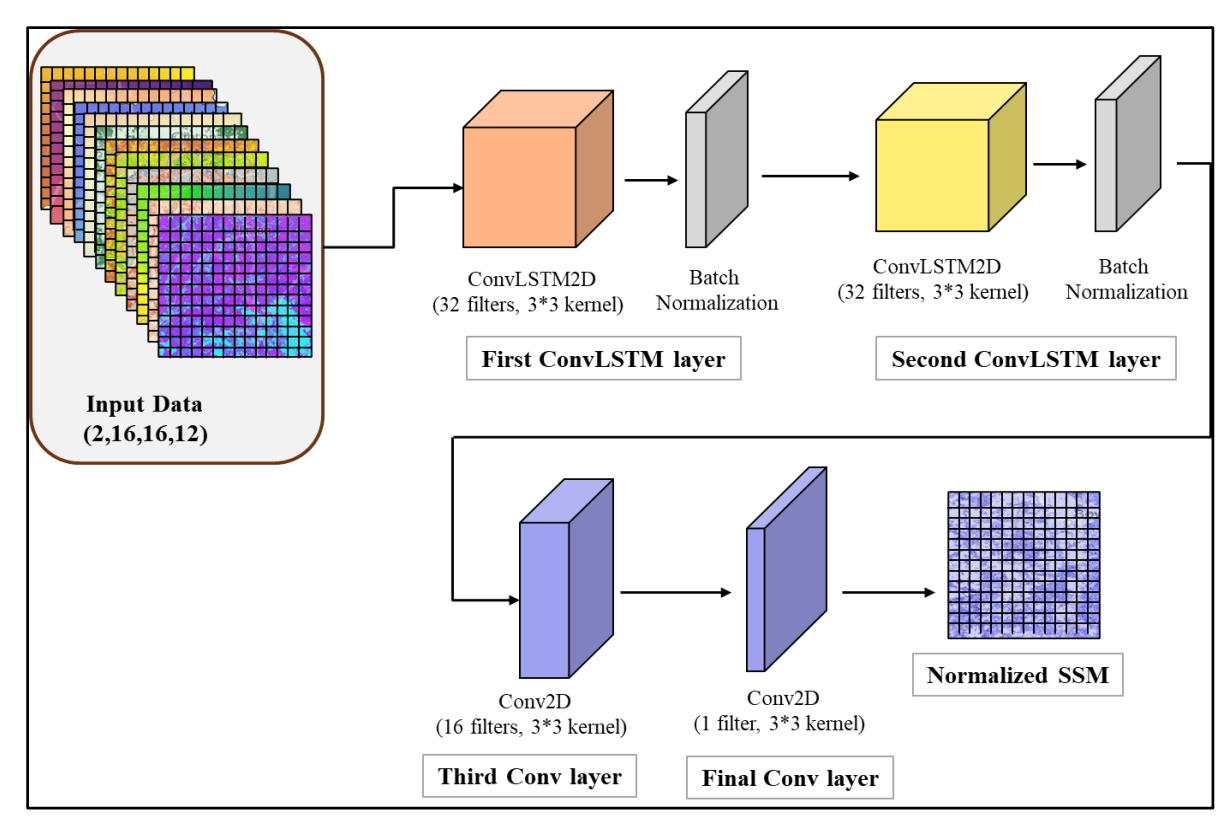


Figure 5.6: ConvLSTM model architecture used in the ML-SSM framework.

Table 5.1 shows the amount of saturated hydraulic conductivity, suction across the wetting front, and saturated water content for different soil types [84, 85].

Table 5.1: Green-Ampt parameter estimates based on soil texture.

Soil No. Water	USDA Texture	Saturated	Saturated Hydraulic Conductivity (K <sub>s</sub> ) (cm/h)	Suction at Wetting Front (Ψ) (cm)
1	Sand	0.417	23.56	9.62
2	Loamy sand	0.401	5.98	11.96
3	Sandy loam	0.412	2.18	21.53
4	Loam	0.434	1.32	17.5
5	Silt loam	0.486	0.68	32.96
6	Sandy clay loam	0.330	0.30	42.43
7	Clay loam	0.390	0.20	40.89
8	Silty clay loam	0.432	0.20	53.83
9	Sandy clay	0.321	0.12	46.65
10	Silty clay	0.423	0.10	57.77
11	Clay	0.385	0.06	62.25

# **5.4 Preliminary Results**

In this study, various model configurations were tested to determine the optimal architecture for accurate SSM prediction. Initially, a 2-layer ConvLSTM model was implemented, but due to its limited performance, the model depth was increased to four layers. Figure 5.7 presents the training and validation loss graphs for the 1-day configuration, in which weather data for the same date as the SSM observations were used as input features. In this configuration, the model was trained for 40 epochs with 16 filters to assess how filter size affects performance.

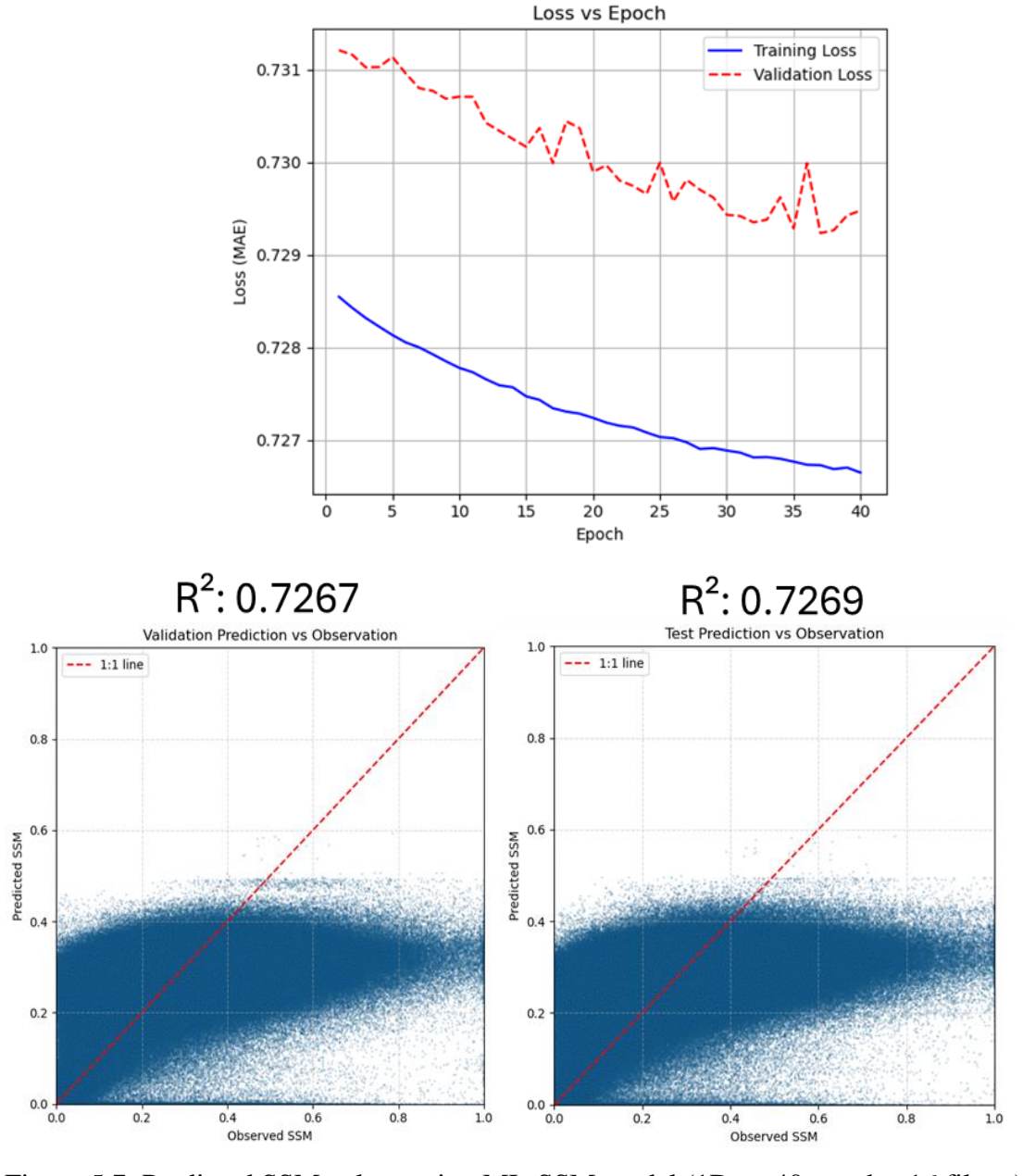


Figure 5.7: Predicted SSM values using ML-SSM model (1Day, 40 epochs, 16 filters) versus observed SSM.

Figure 5.8 illustrates the results for a 2-day configuration, where rainfall and ET were

accumulated over two days, and other variables were averaged. This model used 32 filters and was trained for 20 epochs. As shown, increasing the number of filters significantly improved the model's performance, even with fewer training epochs.

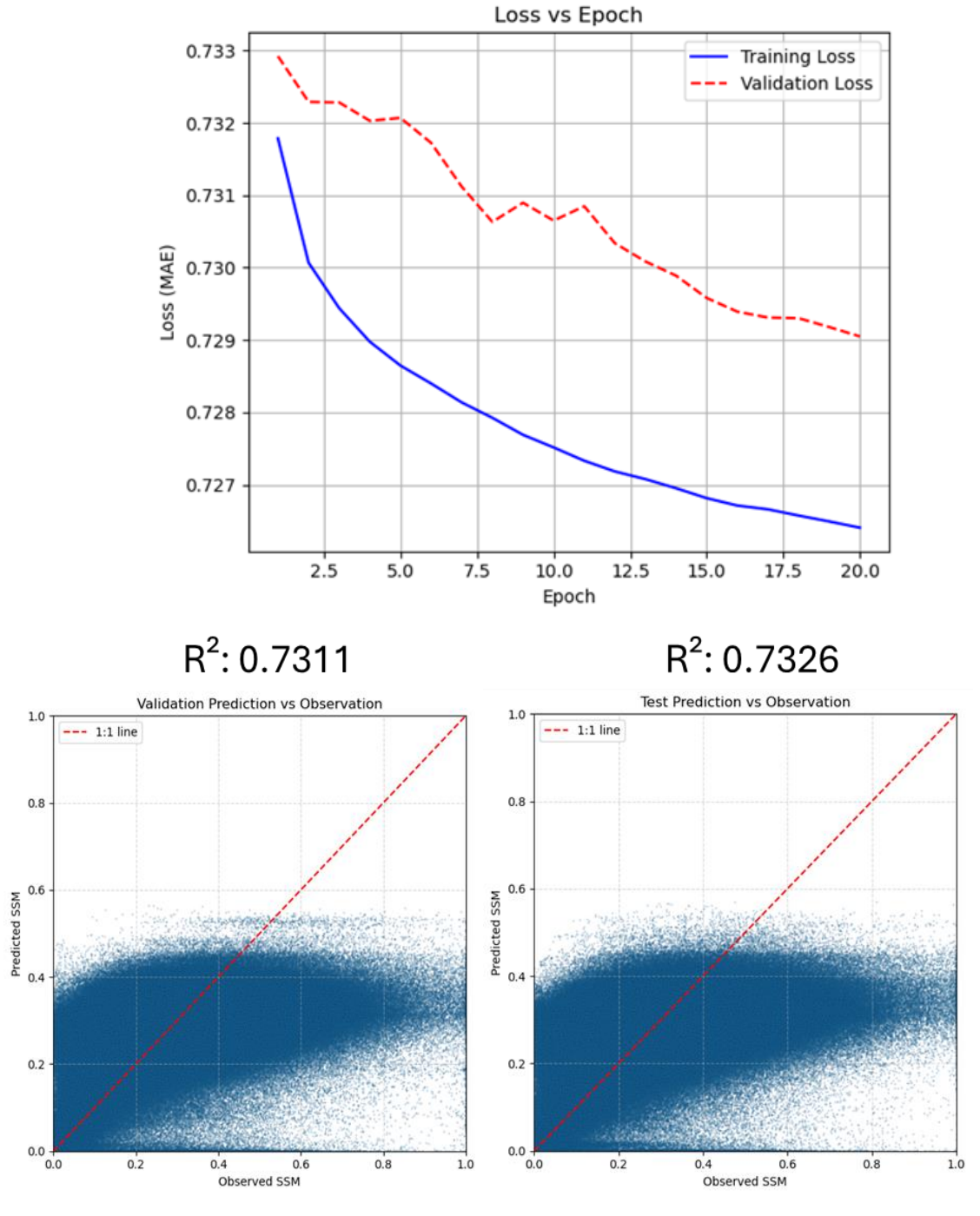


Figure 5.8: Predicted SSM values using ML-SSM model (2Day, 20 epochs, 32 filters) versus observed SSM.

Figure 5.9 shows the best model performance achieved so far using the 2-day configuration with 32 filters and 40 epochs. The improvement in model accuracy can also be attributed to

proper preprocessing, as in earlier configurations, negative and missing SSM values were not masked correctly, leading to errors in loss computation.

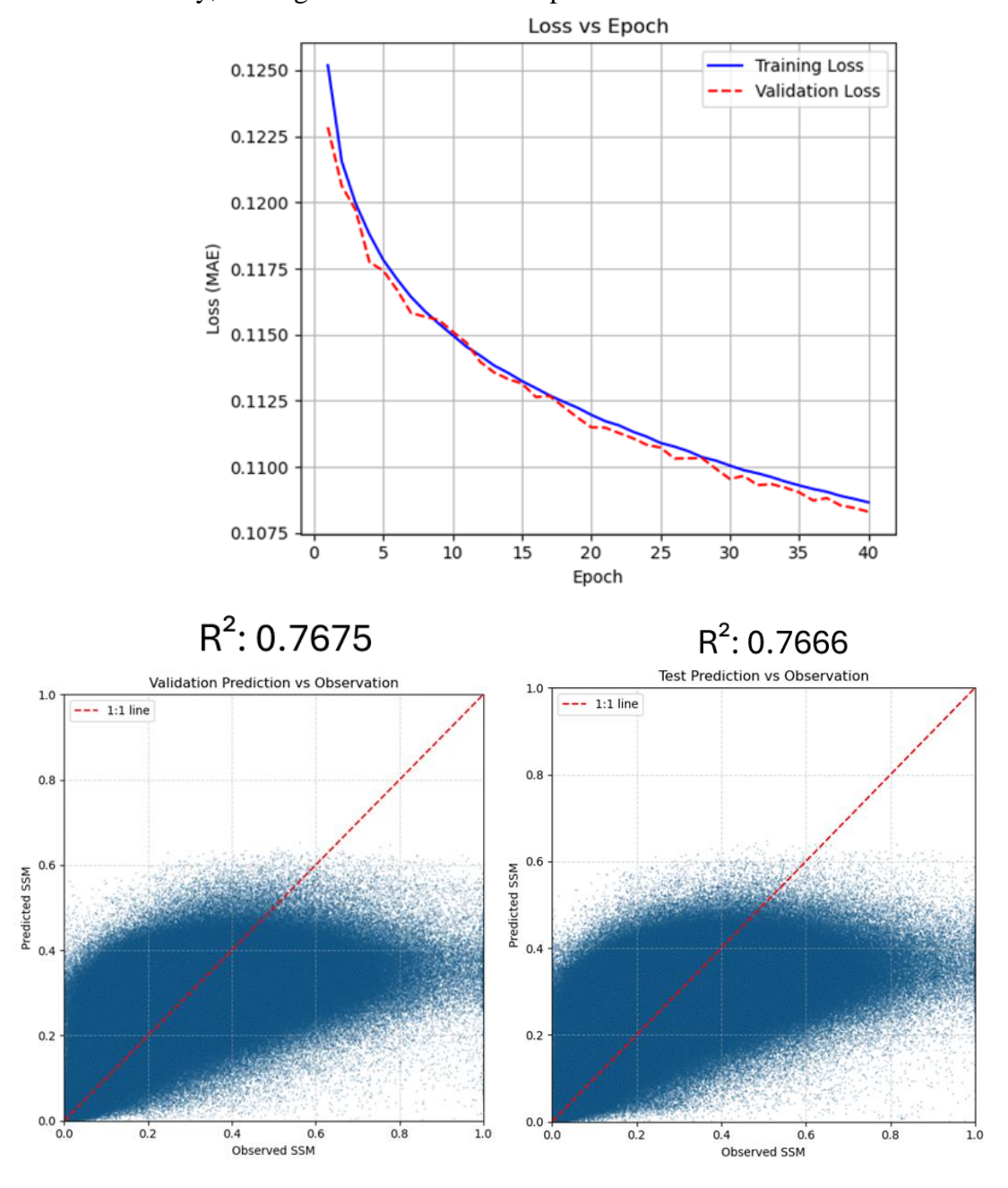


Figure 5.9: Predicted SSM values using ML-SSM model (2Day, 40 epochs, 32 filters) versus observed SSM.

Despite the improvements, the model consistently underestimates SSM values above 0.6. To understand the cause of this, a histogram analysis of the training data was conducted (Figure 5.10). The results show that more than 97% of SSM values are below 0.6, indicating a strong class imbalance. As a result, the model primarily learns from the majority of data in the lower SSM range and fails to accurately predict higher values.

To address this issue, a rebalancing strategy was introduced in the patch generation process.

By ensuring that more samples with higher SSM values are included in the training data, the model is expected to better learn the full distribution and improve prediction accuracy for underrepresented high SSM values.

M Value Distribution (excluding masked values):

0-0.2 : 2,161,907 pixels (56.89%) 0.2-0.4: 1,354,086 pixels (35.63%) 0.4-0.6: 251,954 pixels (6.63%) 0.6-0.8: 28,446 pixels (0.75%) 0.8-1.0: 3,779 pixels (0.10%)

#### SSM Distribution in Value Ranges

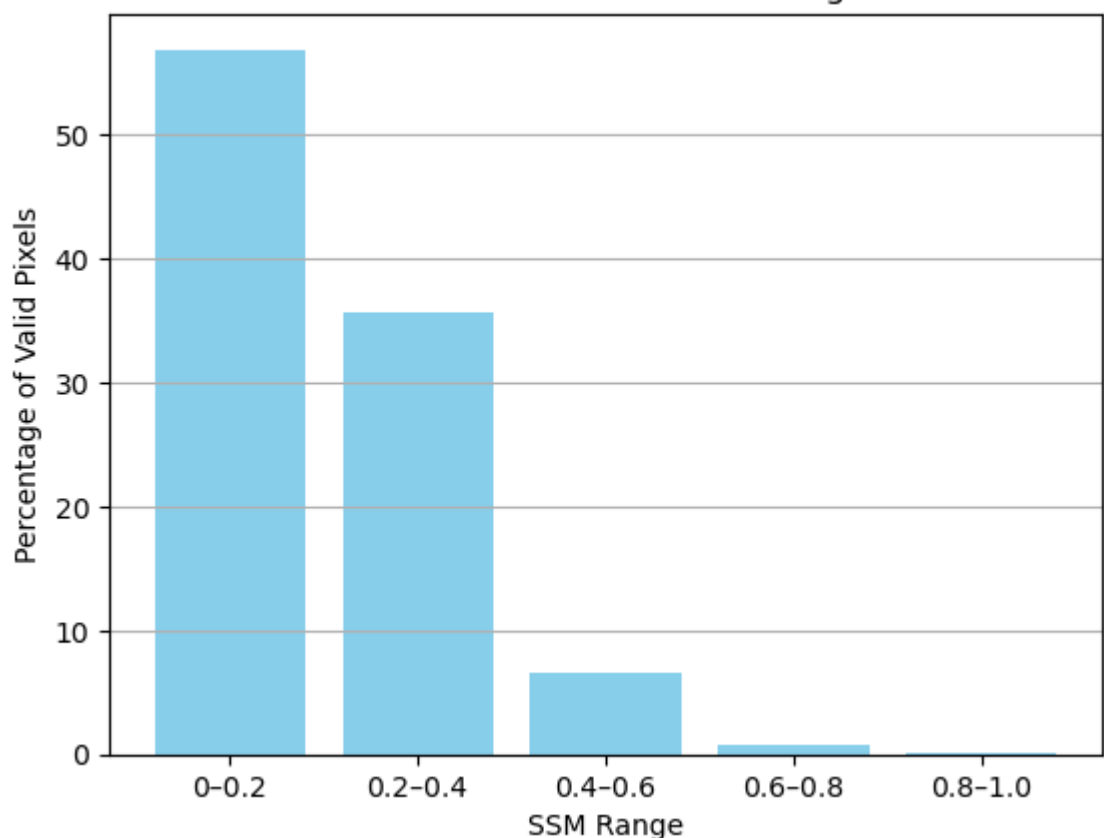


Figure 5.10: SSM data histogram and distribution

# **5.5.** Conclusion and Future Works

This study presents a novel deep learning framework for high-resolution, spatiotemporal SSM mapping using a ConvLSTM architecture. By integrating static terrain and soil parameters with multi-temporal meteorological and vegetation data, the model successfully captures both spatial and temporal dependencies influencing soil moisture dynamics. The use of Sentinel-1-derived SSM maps as training targets, produced through a self-calibrated change detection approach, eliminates the dependence on sparse in-situ measurements and ensures consistent,

fine-scale labeling. The results demonstrate the potential of this model to generate accurate and continuous SSM predictions across diverse landscapes. Performance evaluations indicate strong generalization capabilities, although prediction accuracy for high soil moisture values remains a challenge due to class imbalance in the training data. Addressing this issue through targeted rebalancing strategies has shown promising improvements. Importantly, the framework supports downstream applications such as infiltration estimation and landslide susceptibility assessment by enabling the conversion of SSM predictions into infiltration maps using the Green-Ampt model. This capability is particularly valuable in topographically complex and data-scarce regions where traditional physically based models are computationally intensive and hard to generalize.

Overall, the proposed ML-SSM approach offers a scalable, adaptable, and physically meaningful solution for modeling soil moisture at the landscape scale. It lays the groundwork for more accurate hydrological forecasting and geohazard risk assessment, particularly for rainfall-induced landslides.

Future work will focus on enhancing model performance through systematic use of rebalanced patches to improve the prediction of both low and high SSM values. Following the SSM prediction, the next step involves converting the SSM maps into infiltration estimates using the Green-Ampt equation to support physically meaningful hydrological modeling. In the final phase of this research, a hybrid physical—machine learning approach will be developed to produce landslide susceptibility maps, bridging the gap between data-driven predictions and physically based slope stability assessments.

# 6 Numerical model development for quantitative landslide risk assessment

Seok Jun Kang, Samuel Fadipe, Sunil Lamsal, Yi Liu, Zhuping Sheng, Oludare Owolabi

#### 6.1 Introduction

Landslides are among the most destructive natural hazards, resulting in significant human casualties and substantial economic losses worldwide. Regions characterized by mountainous topography and steep slopes are particularly susceptible due to the complex interplay of geological, geomorphological, and climatic factors. In such regions, precise risk assessment and the establishment of proactive prevention and mitigation strategies are regarded as essential components of disaster management.

Existing methodologies for landslide risk assessment can be broadly classified into four categories considering their approaches for data processing and interpretation: (1) GIS-Based Qualitative Approaches for Large-Scale Assessment, (2) Physically Based, Site-Specific Quantitative Analysis, (3) Simplified Models for Quantitative Slope Stability Assessment, and (4) Integrating Physics and Data: Physics-Guided Machine Learning.

#### (1) GIS-Based Qualitative Approaches for Large-Scale Assessment

Many large-scale studies rely heavily on Geographic Information Systems (GIS) to collect, manage, and analyze spatial data for identifying areas susceptible to landslides. These approaches involve quantifying various terrain-conditioning factors—including topography, soil types, land use, rainfall patterns, and vegetation—and analyzing their correlation with known landslide occurrences to generate Landslide Susceptibility Maps (LSMs) [86, 87].

While early models employed statistical methods such as frequency ratio and logistic regression [88], recent advancements have introduced machine learning (ML) and deep learning (DL) techniques to enhance predictive accuracy [89, 90]. Algorithms such as Random Forest, Support Vector Machines (SVMs), Artificial Neural Networks (ANNs), and Gradient Boosting Machines have shown high performance in susceptibility classification tasks. In addition, Convolutional Neural Networks (CNNs) are increasingly used for learning complex spatial patterns from geospatial data [91].

These models offer scalability and automation, enabling the rapid generation of susceptibility maps across large areas. However, they are fundamentally limited by

their dependence on statistical associations rather than physical mechanisms. In particular, the accuracy of these models tends to deteriorate in regions with limited landslide inventories or uncommon terrain configurations [88, 90]. Moreover, most GIS-based approaches focus primarily on spatial features, often neglecting temporal dynamics such as seasonal rainfall, antecedent moisture conditions, and climate variability—factors that critically influence landslide triggering [87].

#### (2) Physically Based, Site-Specific Quantitative Analysis

For areas with historical landslide activity or identified geotechnical vulnerability, detailed site-specific quantitative analyses are commonly employed. These analyses use field investigations and in-situ measurements to build numerical or theoretical models that simulate the underlying physical processes driving slope instability. Such models provide quantitative estimates of slope stability, failure probability, and potential run-out distances [92-94].

For instance, the TRIGRS (Transient Rainfall Infiltration and Grid-based Regional Slope-Stability) model simulates the time-dependent increase in pore-water pressure due to rainfall infiltration, enabling real-time assessment of rainfall-induced landslide risk [95]. Additionally, finite element and finite difference software such as GeoStudio and PLAXIS allow for advanced stress-strain analysis and failure scenario modeling under realistic ground conditions [94].

Physically based models have the advantage of explicitly representing key triggering mechanisms, such as pore pressure buildup, hydraulic conductivity contrasts, and soil mass mobilization [94]. However, they require extensive site-specific data, high-resolution parameterization, and substantial computational effort, limiting their scalability and generalizability to broader contexts [96].

#### (3) Simplified Models for Quantitative Slope Stability Assessment

To bridge the gap between complex numerical simulations and purely statistical models, simplified analytical models such as the Infinite Slope Model and Limit Equilibrium Methods (LEM) have been widely adopted [96]. These models assume simplified geometries—typically planar or circular slip surfaces—and calculate the Factor of Safety (FoS) as the ratio of resisting to driving forces, based on parameters such as slope angle, shear strength, unit weight, and groundwater position.

The Infinite Slope Model is particularly suited for analyzing shallow slope failures, while LEM includes methods such as Bishop's, Janbu's, and Morgenstern—Price formulations, which can handle more complex geometries and loading conditions [97]. These methods are grounded in classical geotechnical theory and are widely used in engineering practice due to their simplicity and computational efficiency.

However, simplified models may oversimplify nonlinear soil behavior, heterogeneous layering, and soil—water interactions, potentially leading to discrepancies between modeled and actual failure behavior [98]. Additionally, their ability to incorporate temporal factors such as rainfall infiltration is limited and often

requires additional assumptions or external coupling [99].

#### (4) Integrating Physics and Data: Physics-Guided Machine Learning

To address the limitations of purely data-driven and purely physics-based models, hybrid approaches, particularly Physics-Guided Machine Learning (PGML), have gained increasing attention. This emerging methodology combines the flexibility of ML algorithms with the interpretability of physics-based models by incorporating physically meaningful variables—such as FoS, slope geometry, and shear strength—as constraints or features in ML models [86].

For example, temporal changes in slope stability simulated through numerical models can be used to train ML models, enabling the latter to learn from physical insights while improving generalizability across diverse terrain conditions. This approach allows for the enhancement of sparse observational datasets and supports the development of robust, scalable models for landslide risk assessment [100].

In summary, GIS-based qualitative models are effective for rapid, large-scale assessments but are limited in representing the actual physical mechanisms behind landslides. In contrast, site-specific quantitative models provide high-fidelity physical interpretations but lack general applicability and require significant resources. Simplified analytical models offer a practical middle ground but struggle with complex or dynamic conditions.

To overcome these challenges, there is a growing need for the development and application of quantitative, physics-informed methodologies that integrate numerical modeling and data-driven techniques. Such approaches are essential for enabling accurate, scalable, and dynamic landslide risk assessments in both data-rich and data-scarce environments.

# 6.2 Objectives

#### 6.2.1 Overall Research Objectives

The overarching goal of this study is to establish a robust, interpretable, and quantitatively grounded framework for Landslide Risk Assessment (LRA) by integrating physics-based numerical modeling with machine learning. The research aims to overcome the limitations of conventional qualitative or empirical methods by introducing a novel approach that ensures both physical validity and spatial generalizability.

Conventional LRA methodologies often suffer from structural limitations, including poor interpretability, limited applicability across varying terrain conditions, and inadequate treatment of temporal factors. To address these issues, this study seeks to develop a dynamic, generalizable, and mechanistically interpretable LRA system. The research includes the following objectives:

- (1) Evaluation of physics-based, quantitative assessment methods that reflect the underlying mechanisms of slope failure;
- (2) Development of a simplified, generalizable numerical model capable of simulating typical slope instability scenarios;

- (3) Construction of a numerical simulation-based dataset capturing the relationship between key input variables (geometry, material properties, water head) and slope stability metrics (e.g., Factor of Safety);
- (4) Training and evaluation of ML models using the constructed dataset to identify optimal predictive frameworks;
- (5) Extension to a GIS-integrated risk mapping system and eventual incorporation of real-time rainfall data for spatio-temporal LRA.

#### 6.2.2 Objectives of the Current Stage (Stage 2)

In this second stage of the research project, efforts were focused primarily on the following key objectives from the long-term plan:

- (1) Establishment of a physics-based slope stability analysis framework: A simplified numerical model was developed to represent typical slope failure mechanisms, enabling the computation of the FoS under various conditions. Three numerical approaches—Infinite Slope, PLAXIS 2D LE, and FLAC3D—were examined to evaluate their relative accuracy, applicability, and computational characteristics.
- (2) Development and validation of a generalized slope model: The numerical model was designed to reflect representative slope conditions rather than site-specific cases, with the aim of building a generalizable analysis framework. Model assumptions, boundary conditions, and saturation behavior were carefully structured to support extensibility.
- (3) Preliminary construction of an input—output mapping dataset: A parametric analysis was partially conducted using combinations of slope geometry, soil properties, and water head. Although not fully completed at this stage, the initial simulations enabled the identification of key trends in FoS responses and laid the groundwork for a more comprehensive dataset in future stages.

This stage of the project primarily focused on building the core numerical infrastructure and verifying the feasibility of a generalized, physics-informed LRA model. These foundational efforts will support subsequent development of a full-scale simulation-based dataset and the integration of ML-based predictive modeling in later phases.

# 6.3 Methodology

# **6.3.1** Overview of Methodology

This study aims to evaluate and compare three representative quantitative approaches for assessing slope stability in the context of Landslide Risk Assessment. The selected methods reflect increasing levels of analytical complexity and modeling fidelity:

(1) Infinite Slope Model – A classical analytical model based on limit equilibrium theory, assuming infinite slope geometry.

- (2) PLAXIS 2D LE A commercial geotechnical software implementing two-dimensional Limit Equilibrium Methods, offering various slip surface algorithms (e.g., Bishop Simplified).
- (3) FLAC3D A three-dimensional numerical tool based on the Finite Difference Method (FDM), capable of simulating nonlinear and stress-path-dependent behavior.

All three methods were used to compute the FoS under consistent input conditions. In this stage, five key parameters affecting slope stability were varied across simulations: Slope angle (°), Soil friction angle (°), Soil Cohesion (kPa), Soil unit weight (kN/m³), and Groundwater level (m). In all simulations, the slope geometry was kept consistent across cases, with the exception of the slope angle. The height of the slope varied depending on the angle, while the slope width was uniformly maintained at 10 meters.

#### 6.3.2 Modeling details for each methodology

#### (1) Infinite Slope Model

The Infinite Slope model assumes a shallow failure surface that runs parallel to the ground surface. This method is suited for simplified, planar slopes under drained conditions and is commonly used for preliminary or GIS-based risk screening.

The FoS is calculated using the following equation [97]:

$$FoS = \frac{c + \gamma z \cos^{2}(\beta) \tan(\emptyset)}{\gamma z \cos\beta \sin\beta}$$
(6.1)

where c: cohesion,  $\phi$ : friction angle,  $\gamma$ : unit weight of soil,  $\gamma' = \gamma - \gamma_{\text{water}}$ : effective unit weight of soil, z: depth to failure surface, and  $\beta$ : slope angle. The water table is assumed to coincide with the failure surface, and the ground under the water table is assumed to be fully saturated.

# (2) Limit Equilibrium Model (PLAXIS 2D LE)

PLAXIS 2D LE employs the Limit Equilibrium Method, offering several analytical techniques. In this study, the Bishop, Swedish Circle, Janbu, and Lowe models were applied for assuming the slip surface under plane strain conditions [101]. The boundary conditions were defined such that the bottom boundary was fixed in the vertical direction, while the side boundaries were allowed to deform vertically but were laterally constrained using roller supports. To mitigate boundary effects, continuous ground regions were modeled beneath and alongside the slope, each with the same length as the slope itself. Soil behavior was modeled using the Mohr–Coulomb failure criterion under effective stress conditions. Once the slope geometry, geotechnical properties, and groundwater level were specified, the software automatically identified the critical slip surface and calculated the Factor of Safety using the selected Limit Equilibrium formulation [101].

#### (3) Finite Difference Model (FLAC3D)

FLAC3D offers advanced 3D continuum modeling capabilities based on explicit FDM. It can account for nonlinear behavior, post-failure deformation, and pore pressure-stress interactions. In this study, the slope was modeled with a very narrow width to ensure a two-dimensional geometry, thereby facilitating a consistent comparison between the two 2D-based analytical approaches. The simplified slope geometry consists of the slope itself along with continuous ground extensions at the bottom and lateral boundaries, designed to eliminate boundary effects in the numerical analysis.

In the numerical simulations, boundary conditions were defined to realistically represent slope behavior. The bottom boundary was fully fixed in the vertical direction, while the side boundaries were constrained only in the horizontal direction, allowing for vertical displacement. The top surface was modeled as a free surface to account for potential infiltration and changes in matric suction. The Mohr-Coulomb failure criterion was adopted as the constitutive model, and the FoS was computed using the Strength Reduction Method (SRM) under effective stress conditions. For meshing, 8-node hexahedral elements were employed, with local mesh refinement applied near anticipated slip surfaces to enhance accuracy. A mesh sensitivity analysis was also performed to determine the minimum mesh resolution required for stable FoS estimates, while coarser meshes were applied to peripheral zones to reduce computational demands [102] as shown in Fig. 6.1. The results of the sensitivity analysis based on the fixed slope geometry scale are presented in Figure 6.2. As the mesh becomes finer and the number of elements increases, the FoS shows a gradual decrease and eventually converges to a stable value. This indicates that a mesh size yielding more than 2,000 elements is required to obtain reliable FoS estimates for this model. To ensure both accuracy and computational efficiency, the optimal mesh size was determined to produce approximately 2,200 elements.

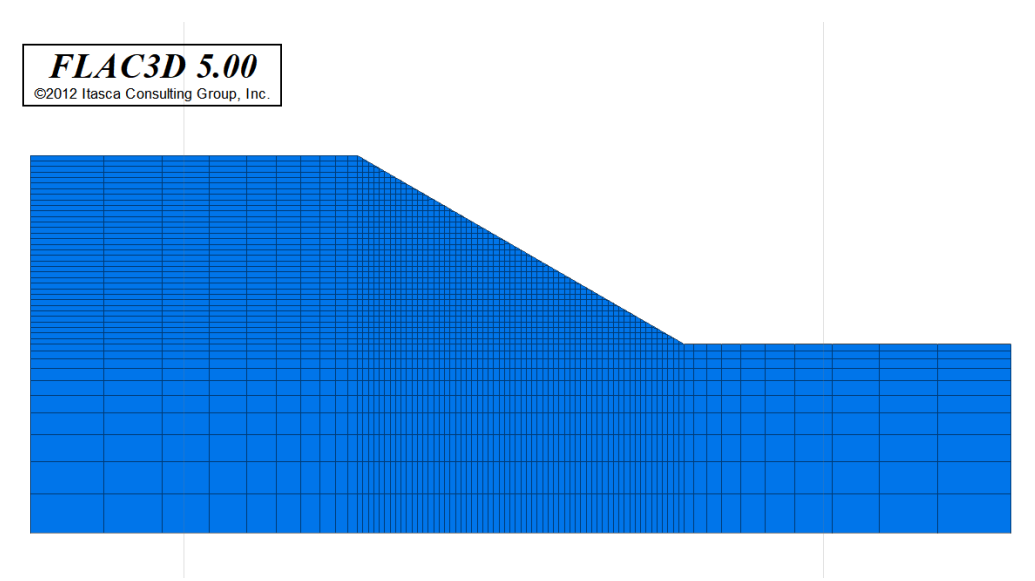


Figure 6.1: Finite difference model with the optimal mesh configuration.

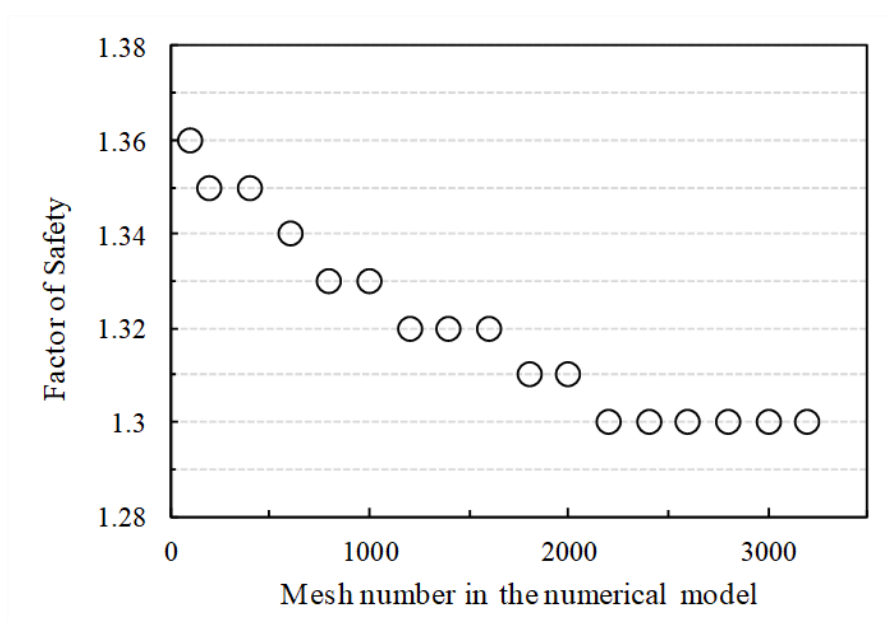


Figure 6.2: Sensitivity analysis for the FoS according to the mesh number.

#### 6.3.3 Groundwater Modeling and Pore Pressure Simulation

Proper modeling of groundwater conditions is critical in landslide risk assessment, as pore water pressure significantly influences slope stability by reducing effective stress and shear strength. Each numerical method employed in this study incorporates groundwater modeling differently, based on its dimensionality, governing equations, and degree of physical realism.

#### (1) Infinite Slope Model

In the Infinite Slope model, groundwater influence is simplified through the water table height (h), where the water table aligns parallel to the slip surface. The factor of safety is calculated using the classical formula:

$$FoS = \frac{c' + z(\beta) \left[ (1 - m)\gamma_{soil} - m\gamma' \right] tan(\phi')}{zcos\beta sin\beta \left[ (1 - m)\gamma_{soil} - m\gamma' \right]}$$
(6.2)

where c': effective cohesion,  $\phi'$ : effective friction angle,  $\gamma$ : unit weight of soil or water, z: depth to failure surface, h: water level, m=h/z (slope is not fully saturated), and  $\theta$ : slope angle.

This approach assumes hydrostatic pore pressure and uniform infiltration, and does not account for lateral flow or transient effects.

#### (2) Numerical Methods

Numerical modeling approaches allow for the water table (phreatic surface) to be defined independently of the slope geometry. To reflect a more realistic groundwater profile, the Dupuit-Forchheimer model [103] was applied. Under the assumptions of homogeneous and isotropic soil, steady-state conditions, and horizontal flow only, the water table follows a parabolic distribution (Figure 6.3), which can be expressed by the following equation:

$$h(x) = \sqrt{H_1^2 + (H_2^2 - H_1^2) \cdot \frac{x}{L_p}}$$
 (6.3)

where H<sub>1</sub>: higher water head at one end of the slope, H<sub>2</sub>: lower water head at the opposite end, x: horizontal distance from the left boundary of the slope, and L<sub>p</sub>: horizontal length of the phreatic surface.

According to the Dupuit-Forchheimer model, the shape of the phreatic surface is governed by the hydraulic head difference between the upper and lower ends of the slope and the length of the slope. The head difference, in turn, is affected by the soil's permeability and the steady-state flow rate, which follows Darcy's Law:

$$H_2 = H_1 - \frac{q}{K}x \tag{6.4}$$

where g: Darcy's velocity (flow rate in unit area) and K: permeability.

To define the phreatic surface in the numerical model, three parameters were determined: the higher head value, hydraulic conductivity, and unit discharge. In some cases, this formulation can lead to an unrealistic situation where the phreatic surface is computed to be higher than the actual slope surface. To prevent this, the initial phreatic surface was checked, and if any portion exceeded the slope surface, the water table was adjusted to follow the slope surface instead (Figure 6.4).

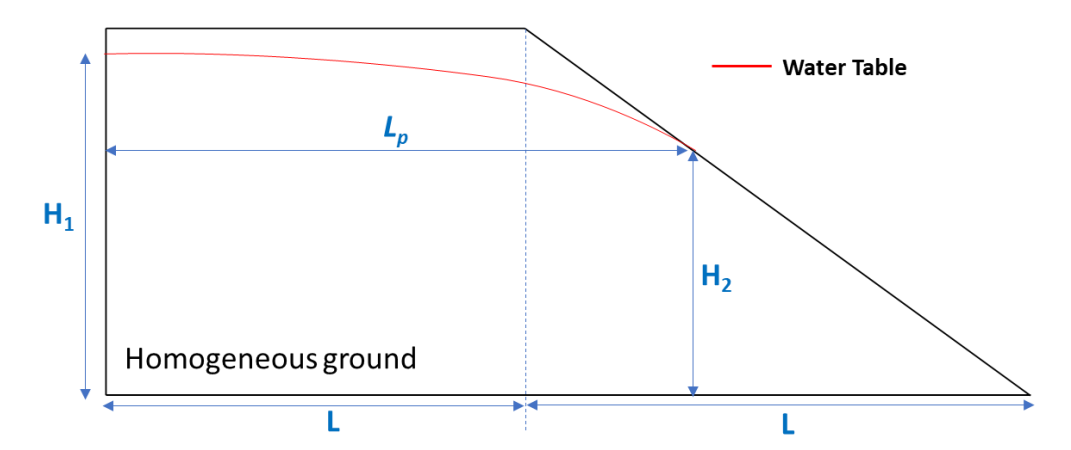


Figure 6.3: Phreatic surface assumption on the simplified slope geometry.

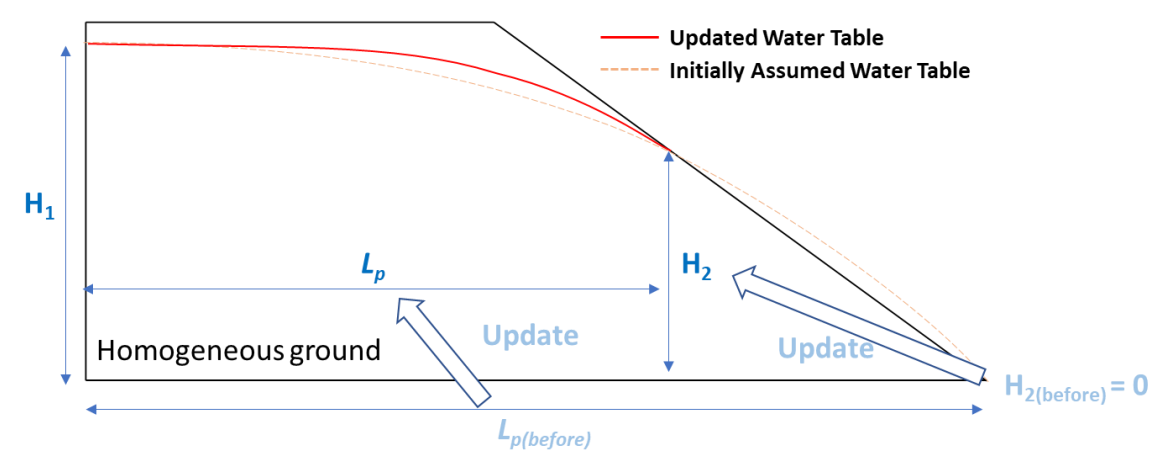


Figure 6.4: Phreatic surface adjustment considering outlet through slope surface.

Once the phreatic surface was defined, it was assumed that the soil below it was fully saturated. Based on this assumption, the pore water pressure and effective stress at different depths were computed, using the following effective strength equation:

$$\tau = c' + (\sigma_v - u)tan(\phi')$$
 (6.5)

where  $\tau$  is the shear strength,  $\sigma_v$  is the total vertical stress, u is the pore water pressure, c' is the effective cohesion, and  $\phi'$  is the effective friction angle.

This approach enables the slope stability analysis to reflect the reduced strength of saturated soil, thereby enhancing the accuracy of the FoS calculation.

#### 6.3.4 Parametric Case Design

To systematically investigate the influence of individual geotechnical parameters on slope stability, a parametric study was conducted using a defined control case, with each key parameter varied independently while keeping the others constant.

The control slope geometry and soil properties were set as:

• Slope angle (β): 30°

• Friction angle (φ): 30°

• Cohesion (c): 3 kPa

• Unit weight ( $\gamma$ ): 19.6 kN/m<sup>3</sup>

• Phreatic surface: Bottom boundary (no water)

This baseline scenario was considered representative of a typical shallow failure-prone slope under moderate soil strength and hydrological conditions. Each parameter was independently varied across representative values to evaluate its influence on the computed Factor of Safety. The variations were designed to cover realistic field conditions while maintaining numerical stability, as summarized in Table 6.1.

Table 6.1: Input parameters variation

Parameter	Range of Values Simulated
Slope angle (β)	10 – 50 °
Friction angle (φ)	2 – 45 °
Cohesion (c)	0 – 180 kPa
Unit weight (γ)	17.6 – 21.4 kN/m³
Water level	Bottom – Toe of Slope

Variations in groundwater level were simulated by first assuming the lower water head (H<sub>2</sub>) to be located at the slope toe, and then systematically varying the unit discharge (q) to derive corresponding higher water head (H<sub>1</sub>) values. This approach allowed for the generation of 11 representative phreatic surface scenarios that commonly occur in natural slopes.

In each simulation, only one parameter was changed at a time, and the others were fixed at the control case values. This allowed for isolated sensitivity analysis and consistent dataset generation for ML model training.

### 6.4 Preliminary Results and Discussion

#### **6.4.1 Slope Failure Surface**

The Infinite Slope Method, which assumes a planar failure surface parallel to the slope, has limitations in realistically simulating actual slope failures. In contrast, the two numerical methods employed in this study allow for relatively reliable predictions of failure surface geometry.

In the control case—characterized by a slope angle equal to the friction angle and a low cohesion value, representing a highly failure-prone condition—both the Limit Equilibrium Method and the Finite Difference Method produced similar results. The calculated FoS was 1.4 for LEM and 1.5 for FDM, and the predicted failure surfaces appeared as circular slip surfaces of comparable shape (Fig. 6.5).

However, when cohesion was reduced to near-zero under the same slope condition, notable discrepancies between the two methods emerged. The FoS values dropped to 1.0 in LEM and 1.2 in FDM, and the predicted failure surfaces diverged significantly in shape and location (Fig. 6.6), indicating increased sensitivity of the models to changes in shear strength parameters.

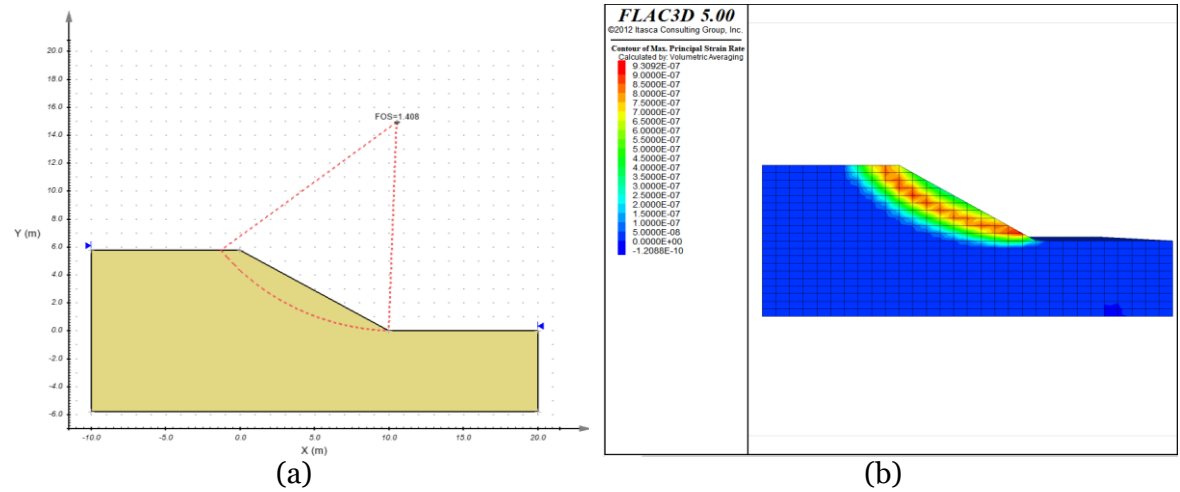


**Figure 6.5** Slope failure shape derived from (a) Limit Equilibrium and (b) Finite Difference models in the control case (c=3kPa,  $\gamma=19.6kN/m3$ , friction angle= $30^{\circ}$ , and slope angle= $30^{\circ}$ )

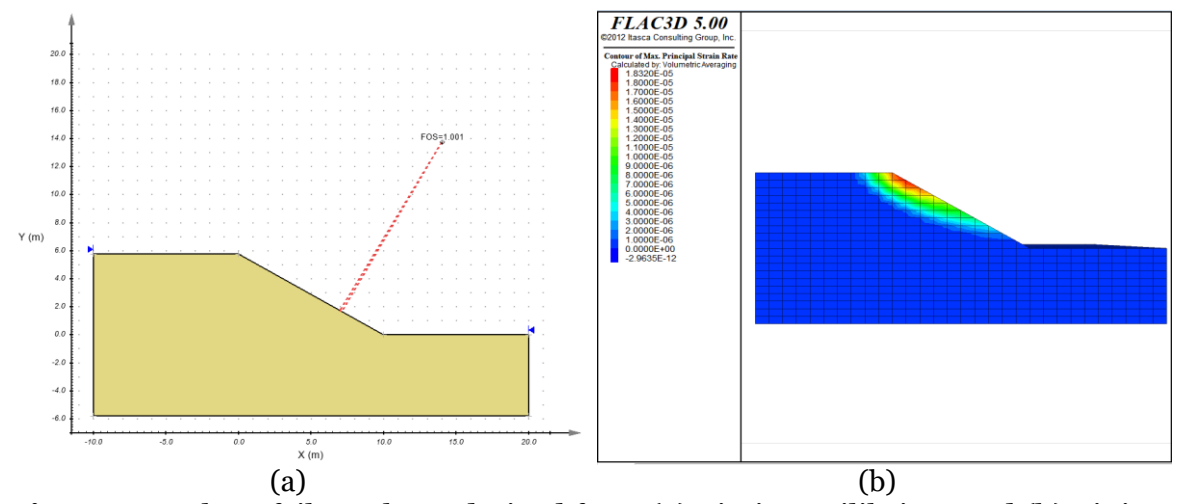


**Figure 6.6** Slope failure shape derived from (a) Limit Equilibrium and (b) Finite Difference models in the cohesionless condition (c=0.001kPa,  $\gamma$ =19.6kN/m³, friction angle=30°, and slope angle=30°)

The failure surface predicted by the LE method under cohesionless conditions appeared highly unrealistic. This is likely due to the inherent nature of LE methods, which search through numerous potential circular or elliptical slip surfaces and select the one that yields the lowest FoS. In cases where the slope angle is equal to the friction angle and the soil exhibits very low cohesion, any considered failure surface would tend to produce similar FoS values. As a result, under near-critical conditions (i.e., FoS  $\approx$  1), there is a high likelihood of selecting an implausible failure geometry. As shown in Fig. 6.6(a), the LE method predicted an extremely small circular failure surface, which is physically unrealistic.

In contrast, the failure surface derived from the FDM indicated local failure occurring near the upper part of the slope, where the vertical stress is lower and thus the frictional shear strength is reduced due to the absence of cohesion. This result is

mechanically reasonable and aligns with expected failure mechanisms in weak, cohesionless soils.

This comparison highlights fundamental differences in performance between LE and FDM approaches. Importantly, incorrect assumptions regarding the failure surface in LE can also lead to erroneous FoS calculations. Therefore, when conducting large-scale parametric analyses using LE methods across a range of slope conditions, it is essential to carefully inspect the predicted failure geometries. If the results show unrealistic failure surfaces, those specific cases should be re-evaluated or excluded from interpretation.

#### 6.4.2 Parametric analysis for FoS Calculation

The results of the parametric analysis using soil unit weight, cohesion, friction angle, and slope angle as variables are summarized in Figure 6.7. The influence of each parameter on the FoS showed consistent trends across all three methods employed in this study. Despite the wide range of input values considered, unit weight exhibited minimal impact on the FoS. This observation aligns with theoretical expectations, as unit weight contributes to both the driving and resisting forces in slope stability analysis, effectively offsetting its net influence.

Cohesion, a key factor in determining shear strength, showed varying degrees of influence on FoS depending on the method used. The Infinite Slope model exhibited a linear relationship between cohesion and FoS due to its simplified assumptions and decoupled input variables. In contrast, both numerical methods displayed nonlinear behavior, as changes in cohesion affected the failure surface geometry, leading to more complex interactions within the model.

For slope angle and friction angle, all three methods exhibited similar trends. This consistency is attributed to the control case settings, where either the slope angle or the friction angle was held constant while the other was varied, leading to a proportional change in their relative magnitudes. However, it is expected that the influence of these angles on FoS would vary significantly if cohesion values were altered, given their interplay with the overall shear strength.

To further investigate key input variables prior to conducting a more extensive parametric study, a focused preliminary analysis was conducted using both the theoretical Infinite Slope model and the FDM, specifically examining the influence of slope angle and cohesion. The results revealed that while the Infinite Slope model exhibited predictable, directly proportional behavior in response to parameter changes—consistent with its analytical formulation—FDM results showed abrupt trend shifts under certain conditions. These shifts occurred when slope angles became excessively gentle or when cohesion values became overly large.

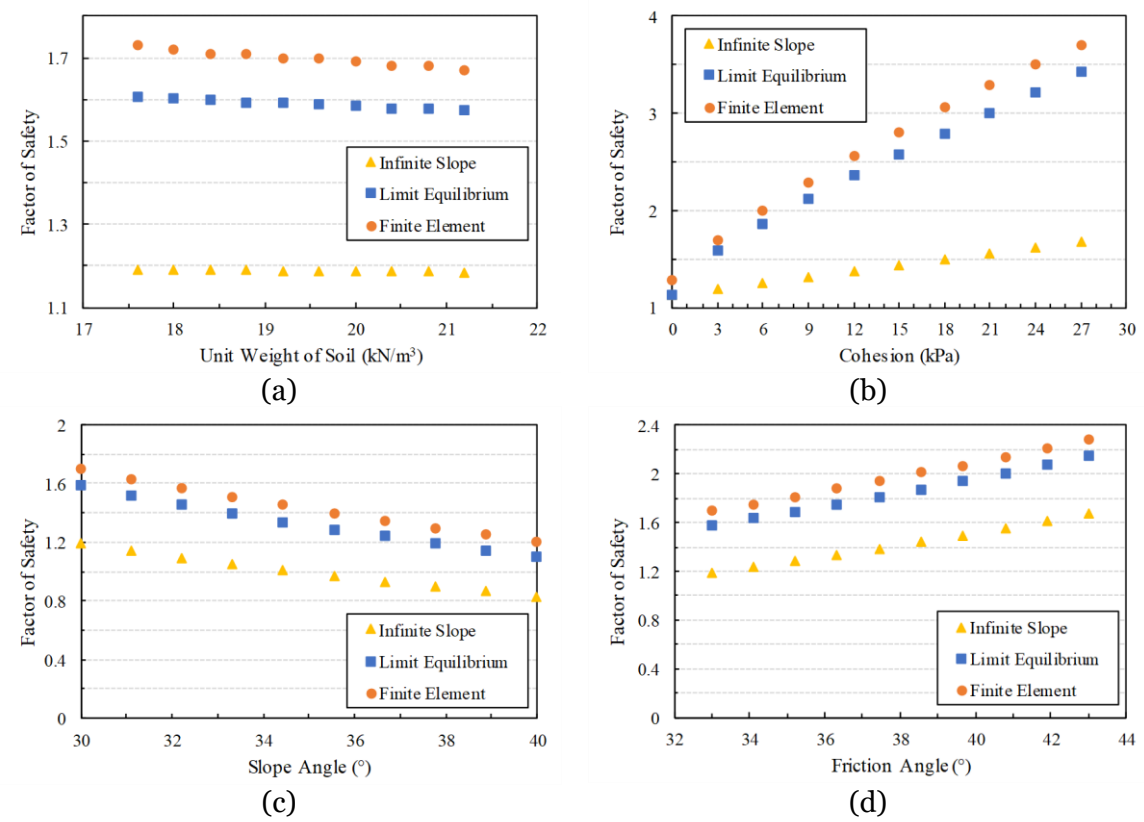


Figure 6.7: Parametric analysis on the FoS with varying (a) Soil unit weight, (b) Cohesion, (c) Slope angle, and (d) Friction angle.

Upon inspecting the failure surfaces in such cases, it was observed that very shallow slopes or high-cohesion conditions prevented the simulation of slope failure under the strength reduction method. Instead, local instability within the model—unrelated to typical slope failure mechanisms—was reflected in the calculated FoS. These cases produced FoS values exceeding 1.8, which fall well outside the range of concern for landslide risk assessments, even when considering safety margins and model uncertainty.

Therefore, for the purposes of reliable dataset generation, scenarios with overly stable slopes—specifically those with very low slope angles or extremely high cohesion leading to FoS values above 1.8—should be excluded. This consideration can be practically addressed during the definition of parameter ranges, by avoiding input values that represent unrealistically stable slope conditions.

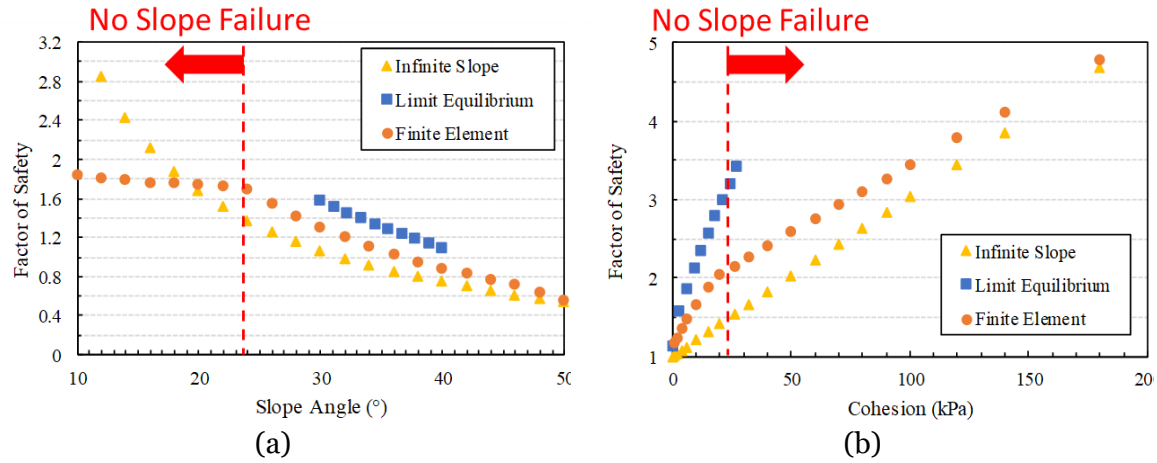


Figure 6.8: Parametric analysis with varying (a) Slope angle and (b) Cohesion, including unrealistic ranges

#### 6.4.3 Effect of Groundwater Table Distribution

Using two numerical methods, a variety of realistic water table distributions were modeled by assuming a water outlet at the slope toe and varying the flow rate (refer to Section 6.3.4). Increasing the flow rate (Darcy's velocity) resulted in higher hydraulic heads, which indirectly simulate rising groundwater levels due to rainfall. Figure 6.9 presents the resulting changes in the Factor of Safety (FoS) in response to elevated groundwater conditions. As the water level rises, pore water pressure increases in accordance with hydrostatic pressure, leading to a reduction in effective stress and, consequently, shear strength.

This shift affects both the location and size of the slip surfaces predicted by LE methods, while in the FDM, the distribution of failure zones—captured via strain localization—changes more significantly. As a result, the relationship between FoS and increasing groundwater level appeared nonlinear, exhibiting two local extrema. When applying different LE models, significant variations in FoS were observed due to differing failure surface assumptions and calculation schemes. To reduce model-specific bias, the arithmetic mean of FoS values calculated by four different LE models was used as a representative value for comparison with FDM results.

At lower Darcy velocities—i.e., when water levels were low—LE and FDM produced similar FoS estimates. However, as groundwater levels rose, FDM began to yield lower FoS values. This discrepancy indicates that the LE method, which assumes circular slip surfaces, fails to adequately capture the spatial variation in shear strength resulting from pore pressure increases, particularly in the lateral direction.

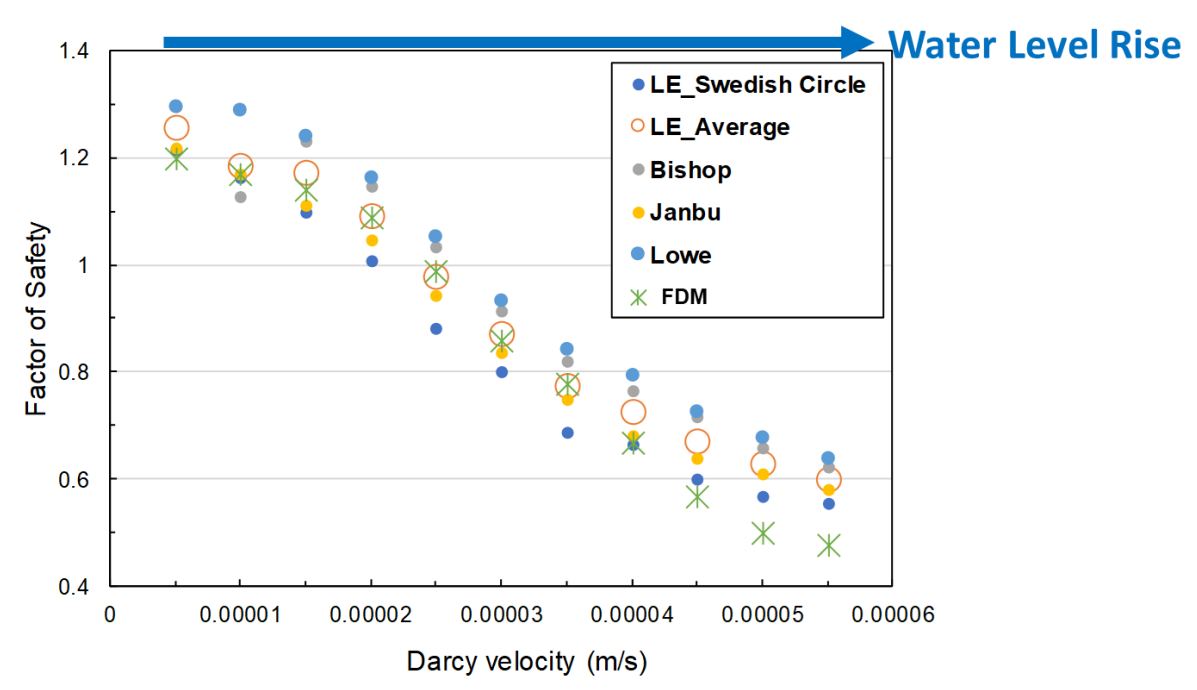


Figure 6.9: Effect of Darcy velocity (flow rate) on the FoS.

To more clearly evaluate the evolving failure surface under rising water levels, six numerical models were selected at equal intervals along the range of increasing Darcy velocities. These numerical models follow the conditions of the control case (slope length =  $10\,$  m, slope angle =  $30^{\circ}$ , soil density =  $18\,$  kN/m³, soil cohesion = 3kPa, soil friction angle =  $30^{\circ}$ ), but the variations in the water table were applied differently to each model depending on the flow rate. These were used to conduct a sequential analysis simulating prolonged rainfall leading to eventual slope failure. This six-stage simulation began with an initial condition (Stage 0) where the water table reached only the slope toe, and progressed toward a scenario in which the entire slope became saturated due to continuous infiltration (Figure 6.10).

In the early stages (Stages 0–2), with FoS greater than 1.0, no visible shear strain or failure was observed. Initial failure was captured at Stage 3, where FoS dropped below 1.0. As the simulation progressed through Stages 4 and 5, both the magnitude of shear strain and the extent of the failure surface increased. Since the simulation was conducted sequentially, rather than as independent static cases, it effectively captured the accumulation of shear deformation under prolonged rainfall. The failure initiated at the slope toe and gradually extended toward the upper part of the slope. While this analysis does not simulate material detachment or debris flow (due to the continuum assumption in FDM), it nonetheless offers valuable insight for landslide risk assessment by indicating how failure zones may evolve in response to groundwater rise.

Compared to LE, which produced less realistic changes in FoS and failure surface geometry under varying water tables, the FDM approach provided more reliable and plausible results.

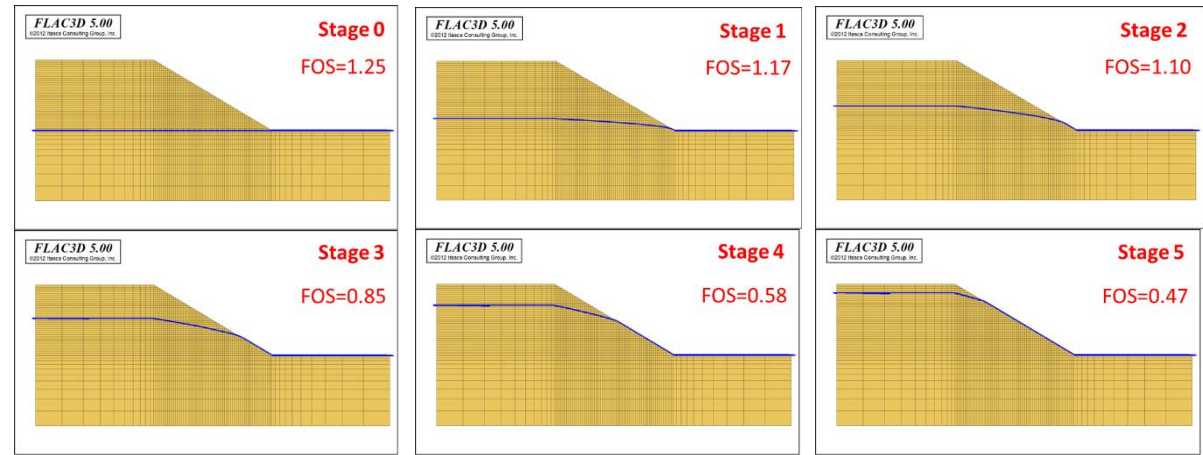


Figure 6.10: Sequential slope failure simulation cases according to water table rise.

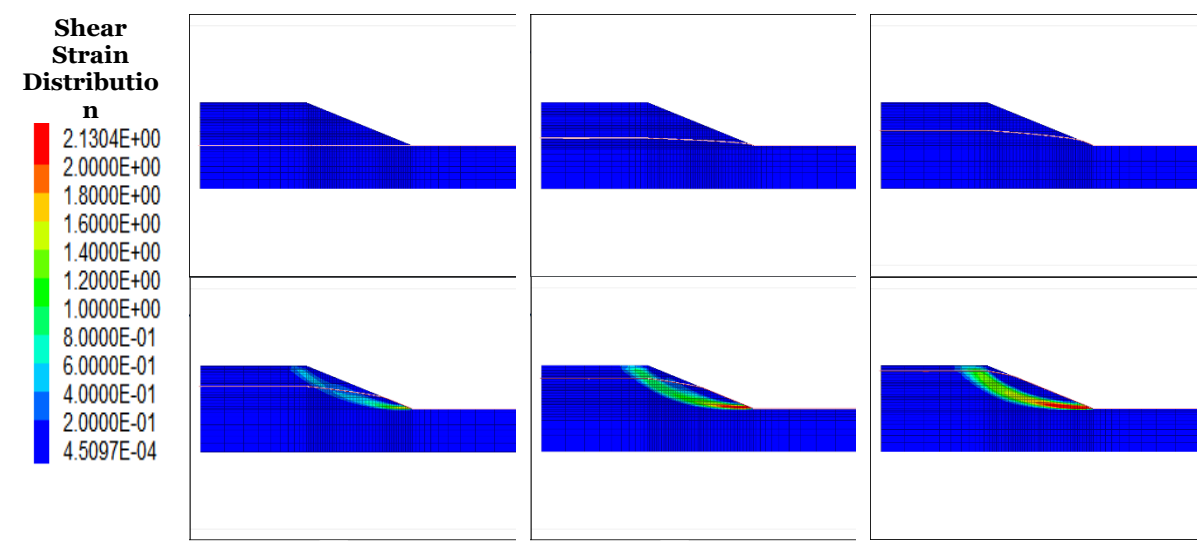


Figure 6.11: Slope failure according to increased water tables.

# **6.5 Conclusions and Future Works**

This study investigated slope stability under varying geotechnical and hydrological conditions using three methods: the infinite slope model, LEM, and FDM. A series of numerical simulations and parametric analyses were conducted to evaluate each method's capacity to estimate the Factor of Safety (FoS) and predict failure surface geometry under realistic slope conditions.

Numerical modeling has been proven to be an effective approach for visualizing failure mechanisms and quantifying slope stability. The use of the Dupuit model enabled the simulation of phreatic surface changes induced by infiltration and allowed for realistic water table distributions across a range of scenarios. Sequential simulations further captured the progression of failure surfaces due to rising water tables, providing insight into rainfall-induced landslide behavior.

Among the three methods, the infinite slope model consistently produced

conservative and overly simplified results, while LEM, despite its widespread use, showed clear limitations under cohesionless or near-critical conditions—often predicting unrealistic slip surfaces due to its reliance on circular failure assumptions and minimum FoS search algorithms. These shortcomings highlight the importance of validating LEM results, especially for marginally stable slopes.

In contrast, FDM demonstrated the highest level of reliability and physical realism. It effectively captured nonlinear responses in FoS due to variations in cohesion, slope angle, and groundwater level, while also representing internal failure mechanisms and strain localization. Importantly, FDM was the only method that consistently responded to changing hydrological conditions with credible shifts in both FoS values and failure geometries.

Based on these findings, FDM was identified as the most robust and trustworthy method for slope stability analysis among those evaluated. It aligns closely with the objectives of this research, particularly the need to simulate realistic failure behavior for a broad range of input conditions. As such, FDM will be used as the foundation for future synthetic dataset generation and the training of machine learning models for landslide prediction and risk assessment. This approach holds strong potential for extending slope stability research into data-driven domains, enabling more reliable and scalable hazard evaluations in geotechnical practice.

#### 6.5.2 Future Works

Building upon the validated performance of the FDM for slope stability analysis, future research will focus on leveraging this method for large-scale data-driven modeling and landslide risk prediction. The proposed workflow (Fig. 6.12) is structured to systematically integrate numerical modeling with deep learning-based predictive systems and culminate in a real-time early warning application. The following key tasks are planned:

#### (1) Synthetic Dataset Generation via FDM

Using FDM, a wide range of slope stability scenarios will be simulated by systematically varying soil properties, slope geometry, and groundwater conditions. This process will generate a robust synthetic dataset that reflects both realistic and extreme conditions under which slope failure may occur.

#### (2) Training and Evaluation of Deep Learning Models

The generated dataset will be used to train various deep learning models. The performance of these models will be evaluated not only based on predictive accuracy but also on computational efficiency, to ensure scalability for real-time applications. Through this comparative analysis, the most suitable DL model will be identified.

#### (3) Application of the Optimal Model to Real-World Data

The selected DL model will be applied to perform a large-scale Landslide Risk Assessment across the Maryland region, using spatially distributed geotechnical and geomorphological data. The model's robustness will be further evaluated through regional sensitivity analysis and parameter contribution techniques (e.g., SHAP).

#### (4) Development of a Real-Time Early Warning System

The optimal DL model will be integrated with real-time rainfall data to establish an automated landslide Early Warning System (EWS). This system aims to provide timely alerts based on forecasted slope stability conditions under changing hydrological scenarios.

#### (5) Model Feedback Loop and Enhancement

As part of a long-term vision, insights from real-world performance and domain expert feedback will be used to continually refine both the numerical and ML models. This includes improving the FEM-based simulation framework used in dataset generation, resulting in an enhanced end-to-end modeling loop.

This structured future direction enables the transition from reliable numerical analysis to scalable, intelligent prediction systems capable of supporting proactive landslide hazard management.

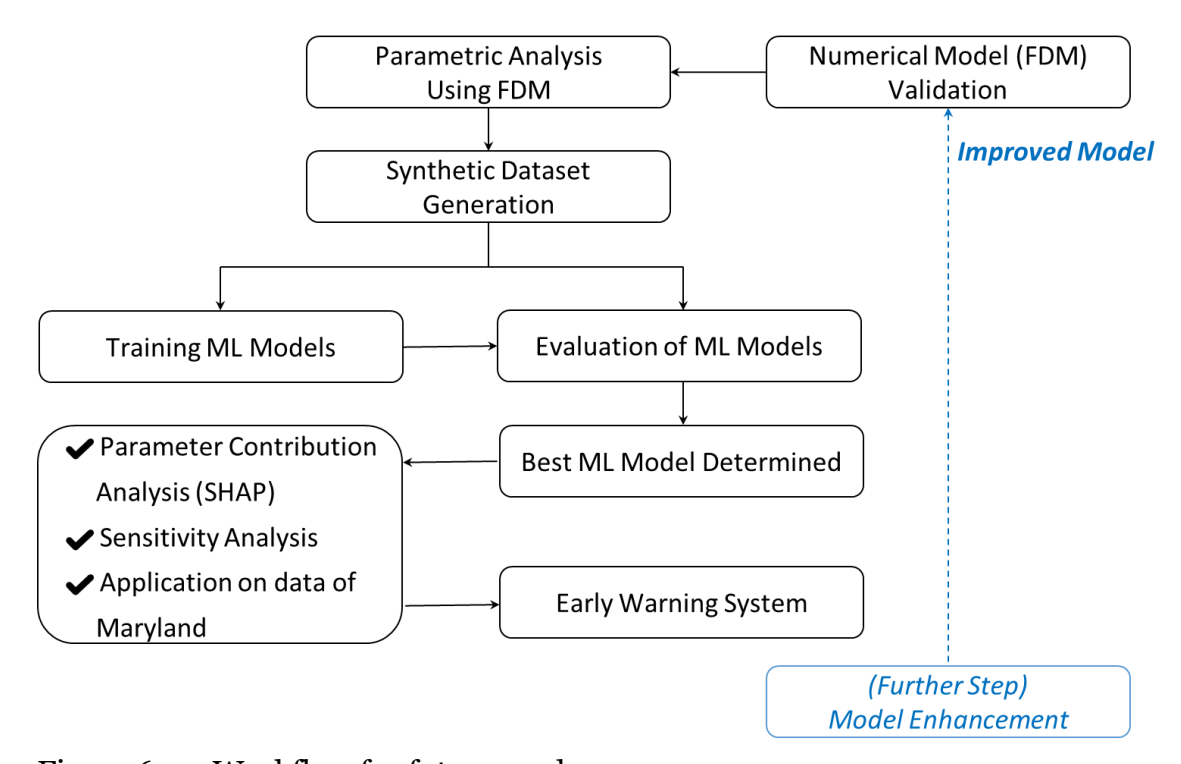


Figure 6.12: Workflow for future works.

#### Chapter 7

# 7 Integrating GIS-Based Susceptibility Mapping and Machine Learning for Landslide Prediction and Early Warning in in Baltimore County, Maryland

Oyinkansola Aladeokin, Ollie Hare, Zhuping Sheng, Yi Liu, Oludare Owolabi

#### 7.1 Introduction

Landslides remain one of the most devastating natural hazards, causing extensive economic damage, disruption, loss of life, and economic degradation in highly susceptible areas worldwide. Its occurrence is closely associated with complex interactions among geological, hydrological, morphological, and anthropogenic elements, frequently intensified by extreme weather events and unpredictable changes to the climate [104-106]. As the rapid expansion of urban communities gradually changes into hazard-prone areas, it is crucial to mitigate this occurrence with the generation of a comprehensive landslide susceptibility mapping (LSM). LSM offers geographical assessments of landslide occurrence probability, functioning as an essential instrument for risk mitigation, urban planning, and infrastructure resilience [107, 108].

Various conventional landslide susceptibility mapping approaches have been used by researchers, some of which include heuristic, statistical, and physically based models. These approaches have limitations in accurately capturing the complex nonlinear relationships between landslide occurrence and the causative factors [109, 110]. However, the recent advancements in artificial intelligence (AI) and machine learning (ML) techniques have provided significant improvements in LSM. Machine learning algorithms, such as Support Vector Machines (SVM), Random Forest (RF), Logistic Regression (LR), and Gradient Boosting Machines (GBM), have demonstrated superior performance due to their ability to handle large datasets, model complex relationships, and produce highly accurate predictive results [111, 112].

Despite the breakthrough in technological advancement, there still remain challenges such as model interpretability, generalization across diverse geographic locations, and the effective management of data imbalances that is characterized in landslide datasets [113]. Addressing these challenges is crucial for developing robust and reliable susceptibility maps that can be effectively integrated into various decision-making processes. This study focuses on the application and assessment of various modern machine learning methods (SVM, RF, LR, GBM) to develop an effective and reliable landslide susceptibility map for Baltimore County, Maryland. The study seeks

to enhance the precision and applicability of susceptibility maps by utilizing diverse geographic and environmental parameters, thereby improving landslide risk management and facilitating informed planning and development initiatives.

#### 7.1.1 Research goals and objectives

The primary goals of this project are to (1) develop and validate a machine learning framework for predicting landslide susceptibility in Baltimore County, Maryland, and (2) integrate the predictive model into an early warning system to support proactive geohazard mitigation and transportation infrastructure safety.

The objectives include:

- **Identify and map high-risk areas** by analyzing contributing and triggering factors such as slope, aspect, soil content, curvatures, and vegetation cover etc. using historical data.
- **Develop and test an early warning system** that leverages susceptibility outputs and real-time monitoring protocols for hazard detection and risk communication.

#### 7.2 Related Works

While physical models provide an extensive understanding of slope dynamics, they are resource-demanding and necessitate considerable data, hence limiting their application in regions with limited data availability [114, 115] conducted a comprehensive analysis of conventional landslide hazard assessment methods, analyzing statistical, heuristic, and deterministic models. Their research highlighted the imperative for probabilistic and data-driven approaches capable of addressing intricate geological, topographical, and climatic factors. While their assessment established a solid basis for further research, it was lacking in extensive real-world applications of machine learning implementations. Statistical methods, like the Frequency Ratio Method (FRM), have been widely employed due to their simplicity and effectiveness in quantifying the relationship between landslide events and the various causative factors [110]. These models often inadequately capture the nonlinear relationships and spatial variability characteristic of landslide processes [116]. The frequency ratio method (FRM) and logistic regression were utilized to conduct landslide susceptibility mapping in Malaysia [110]. Their research includes categorizing many environmental variables affecting landslides and assessing the probability of landslide events using historical data. The findings indicated that logistic regression offered a solid framework for anticipating landslide vulnerability; however, it presented limitations related to the assumptions of linearity and independence of variables.

With the emergence of machine learning (ML), LSM evolved into a more data-driven, scalable, and adaptive framework capable of processing high-dimensional, nonlinear datasets. Machine learning models have been successfully employed in LSM, exhibiting superior classification performance relative to traditional approaches [117-119]. Numerous studies have assessed machine learning performance in various geographic applications; for example, Support Vector Machines (SVM) was employed for identifying landslide vulnerability in northern Italy [118]. Their methodology entailed the application of kernel functions to limited datasets, resulting in elevated accuracy and generalization proficiency. However, they observed challenges with the

model's interpretability due to its dense character. A comparative investigation of various machine-learning approaches, including Random Forest (RF), Support Vector Machines (SVM), and Decision Trees (DT), was performed for susceptibility mapping in Vietnam [112]. Their findings demonstrated that RF offered enhanced accuracy and stability owing to its ensemble learning features; however, the interpretability of results continued to pose challenges, requiring subsequent explanatory methods. Additionally, Support vector machines were successfully employed with radial basis function kernels for susceptibility mapping in Hong Kong, efficiently navigating complex terrain conditions [120]. Nevertheless, the authors highlighted challenges with model calibration and susceptibility to outliers. While LSTM networks were implemented for predicting rainfall-induced landslides in southwestern China [121], demonstrating enhanced prediction accuracy relative to ANN and linear regression models, it was attributed to the temporal memory characteristic of LSTM. Studies by Goetz et al. [122] integrated physical and empirical modeling techniques, discovering that ensemble-based methods, especially Gradient Boost Machine and Random Forests, outperformed simpler statistical models in effectively representing complexities' spatial dependencies in landslide susceptibility mapping due to their resilience to overfitting and ability to capture complex interactions. Similar comparison by utilizing Frequency Ratio, Support Vector Machine, Logistic Regression, and Random Forest, also confirmed that the ensemble-based models exhibited enhanced predictive accuracy and resilience [123].

In summary, the integration of machine learning with the Frequency Ratio Method presents a promising hybrid framework that merges the interpretability of statistical techniques with the predictive capabilities of machine learning [124]. This research employs a dual approach for landslide susceptibility mapping (LSM) in Baltimore County, Maryland, utilizing frequency ratio modeling (FRM) to create an initial landslide susceptibility index (LSI) and applying four machine learning classifiers—logistic regression (LR), support vector machine (SVM), random forest gradient boosting machine (GBM)—to enhance temporal predictions. A dataset consisting of 12 parameters contributing to landslides (e.g., elevation, slope, NDVI, SPI, TWI, soil texture, and aspect) along with balanced landslide and non-landslide points was utilized. The models were assessed using such as using Accuracy, Precision, Recall, F1 Score, and Area performance metrics Under the Curve (AUC), with SVM and RF attaining the maximum classification accuracy. These results offer significant insights for incorporating predictive modeling into early warning systems, disaster management, and sustainable land-use planning.

# 7.3 Materials and Methods

#### 7.3.1 Study Area

This study focuses on Baltimore County, Maryland, as the selected area for landslide susceptibility mapping. Located in the north-central part of the state, Baltimore County was chosen because of its varied landscape, diverse environmental conditions, and past occurrences of landslides linked to heavy rainfall. The county spans about 682 square miles and includes a mix of urban, suburban, agricultural, and forested areas. This variety makes it a suitable location for developing a machine learning model that can account for different physical and land use conditions. Although there have been no recorded landslides in the county since 2014, the natural terrain and

weather patterns suggest that certain areas remain at risk. As a result, Baltimore County offers a valuable opportunity to test and improve prediction tools that can later be applied in other parts of Maryland and similar regions with transportation systems exposed to slope instability. Geologically, the county lies at the boundary between the Piedmont Plateau and the Atlantic Coastal Plain, creating a mix of hills, slopes, and flatlands. This setting results in a wide range of soil types, rock formations, and slope angles, all of which affect how water moves through the ground and how stable the slopes are. The county has a humid subtropical climate, with steady rainfall throughout the year and occasional storms. While recent landslide activity has been limited, the combination of rainfall and complex terrain still creates conditions where slope failures could occur, especially during extreme weather. This makes Baltimore County an important area for improving early-warning systems and supporting safer transportation planning.

#### 7.3.2 Data sources

This research employed landslide data from three principal sources in Maryland: the Maryland State Highway Administration (SHA), the U.S. Geological Survey (USGS), and the National Aeronautics and Space Administration (NASA). These datasets collectively recorded 129 landslides in Maryland from 2008 to 2019 (Fig. 7.1). The datasets offer spatial and spatiotemporal information used for spatial and temporal analysis, respectively.

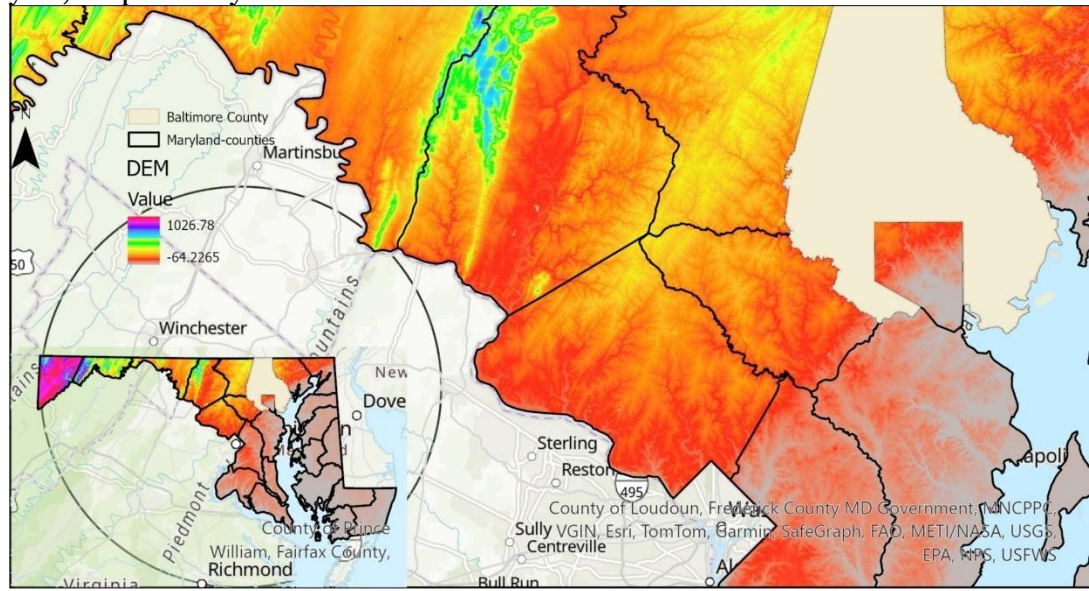


Figure 7.1: Recorded landslide location across Maryland and the selected case study area, Baltimore County.

According to the dataset, Baltimore County has the second highest number of landslide events in Maryland, with 23 out of 129, accounting for approximately 18.37 percent of all occurrences shown in Fig. 7.2. Due to the county's large population and extensive built environment, careful evaluation and proactive management of landslide hazards are critical to minimize potential impacts on public safety and critical infrastructure.

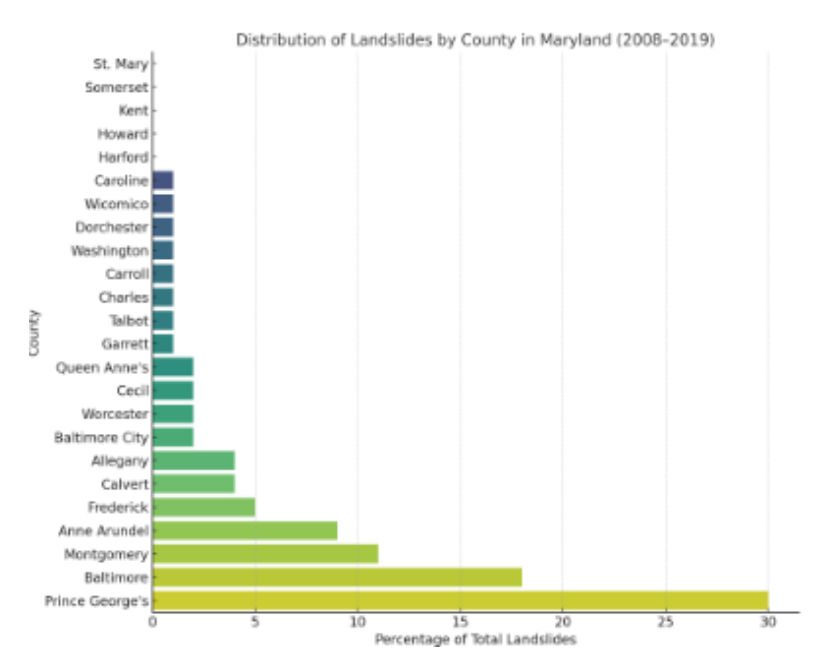


Figure 7.2: Distribution of Landslides by County in Maryland.

#### 7.3.3 Methodology

The conceptual architecture of the intelligent landslide detection and early warning system is shown in Figure 7.3. This framework outlines the essential components and processes that drive this research. The steps in this framework consist of the following: (1) gathering the landslide inventory for the study area, (2) selecting landslide causative environmental factors, and reclassifying the generated input; (3) Frequency Ratio Analysis: analyzing each factor using the frequency ratio (FR) method to determine its FR values, which are then used to calculate the Landslide Susceptibility Index (LSI). An initial susceptibility map is created based on this index, designating non-landslide areas as 0 and potential landslide areas as 1; (4) creation of the output dataset, which is used to develop prediction models using four machine learning algorithms: Support Vector Machine (SVM), Random Forest (RF), Logistic Regression (LR), and Gradient Boosting Machine (GBM); and (5) integration of the best-performing predictive model into an early warning signal system.

#### 7.3.3.1 Data Preparation

Spatial factors provided in a polygon shapefile format were extracted from geospatial databases, with the Digital Elevation Model (DEM) serving as the foundational dataset. The DEM captures the Earth's bare terrain. Causative factors, such as slope, aspect, plan curvature, etc., were derived from calculations from the elevation data. All DEM-based variables used in this study maintain a spatial resolution of 10 meters.

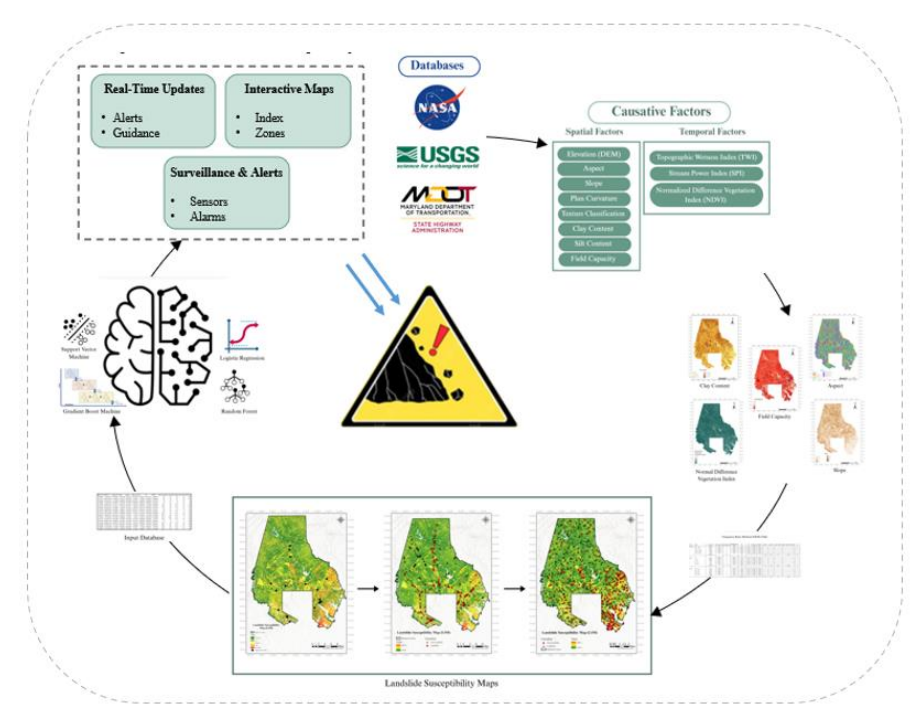


Figure 7.3: Design Architecture of an Intelligent Landslide Detection and Alert System.

Twelve causative factors were chosen for Landslide Susceptibility Mapping, shown in Table 1. These selected causative factors are related to geology, hydrology, and land cover [108, 125]. Additionally, a comprehensive soil map was obtained from the Maryland Soil Survey Geographic Database (SSURGO) for the extraction of soil content variables. The highway polygon was devoid of soil data; thus, an estimate was derived using the average values from adjacent soil polygons.

Table 7.1: Landslide Causative Factors

Table	Table 7.1. Landshue Causative Lactors			
Type of factors	Causative factors			
Topography	Slope, aspect, elevation, plan curvature, soil content (sand, clay, and silt), and field capacity			
Hydrology	Stream power index (SPI), topographic wetness index (TWI)			
Land use/cover	Normalized Difference Vegetation Index (NDVI)			

#### 7.3.3.2 Landslide Susceptibility Computation

Landslide susceptibility indicates the likelihood of landslides occurring under certain environmental and geological factors. It is an essential tool for identifying high-risk locations and mitigating landslide hazards. In previous investigations, various assessment methodologies such as physics-based, knowledge-based, and data-driven techniques were examined. Based on the several benefits of data-driven approach from previous literature, a hybrid approach is adopted in this study. The Frequency Ratio (FR) approach, known for its simplicity and demonstrated efficacy in prior

research, is integrated with machine learning (ML) methods to enhance accuracy forecasting and identify nonlinear correlations. The model included twelve causal factors, comprising topographic (e.g., slope, elevation), hydrological (e.g., stream power index), and land cover (e.g., NDVI) variables. The landslide susceptibility map, created with ArcGIS Pro, is a high-resolution resource for hazard evaluation and infrastructure design in Baltimore County. Figure 7.4 illustrates the spatial and temporal raster layers of all input parameters. These parameters were extracted and included in the FR modeling framework to facilitate accurate landslide prediction.

#### 7.3.3.3 Frequency Ratio Method

The Frequency Ratio Method (FRM) is a widely used bivariate statistical technique in landslide susceptibility modeling, valued for its simplicity, interpretability, and efficiency in determining the influence of causative environmental factors. It evaluates the spatial correlation between landslide occurrences and the attribute classes associated with various geo-environmental factors by analyzing their spatial frequency distributions.

Landslide occurrences are generally affected by nonlinear and intricate interactions with topography and environmental variables; thus, the FRM provides a quantitative method to quantify the contribution of each factor class to landslide susceptibility. To use the approach, each causal factor is initially segmented into classes to effectively capture internal data variance. These intervals serve as the foundation for developing grid-based factor layers, whereupon spatial overlays with landslide inventory data facilitate pixel-level frequency analysis. The frequency ratio (FR) for each class *i* of a factor is calculated using the following equation:

$$FRi = \frac{Xi / X}{Yi / Y}$$
(7.1)

where:

 $X_i$  is the number of landslide pixels within the *i-th* class of the factor,

X is the total number of landslide pixels in the study area,

Yi is the number of pixels in the i-th class of the factor,

Y is the total number of pixels in the study area.

Equation 7.1 defines the ratio of the percentage of landslide occurrences within a particular class to the percentage of area that the class occupies in the overall study area. When the value of FR*i* exceeds 1, this signifies that a landslide is likely in that class, indicating a positive correlation. An FR*i* value below 1 indicates that the factor class is unfavorable for landslide occurrence and adversely affects susceptibility. Upon computing the frequency ratios for all classes across all causative factors, the Landslide Susceptibility Index (LSI) can be determined for each pixel by aggregating the corresponding FR values using equation 7.2.

$$LSI = \sum_{j=1}^{m} FR^{(j)} \tag{7.2}$$

 $FR^{(j)}$  represents the frequency ratio for the j-th factor at a given pixel, while m signifies the total number of causative factors. Higher LSI value indicates an increased likelihood of landslide occurrence, and a lower value indicates a reduced likelihood of

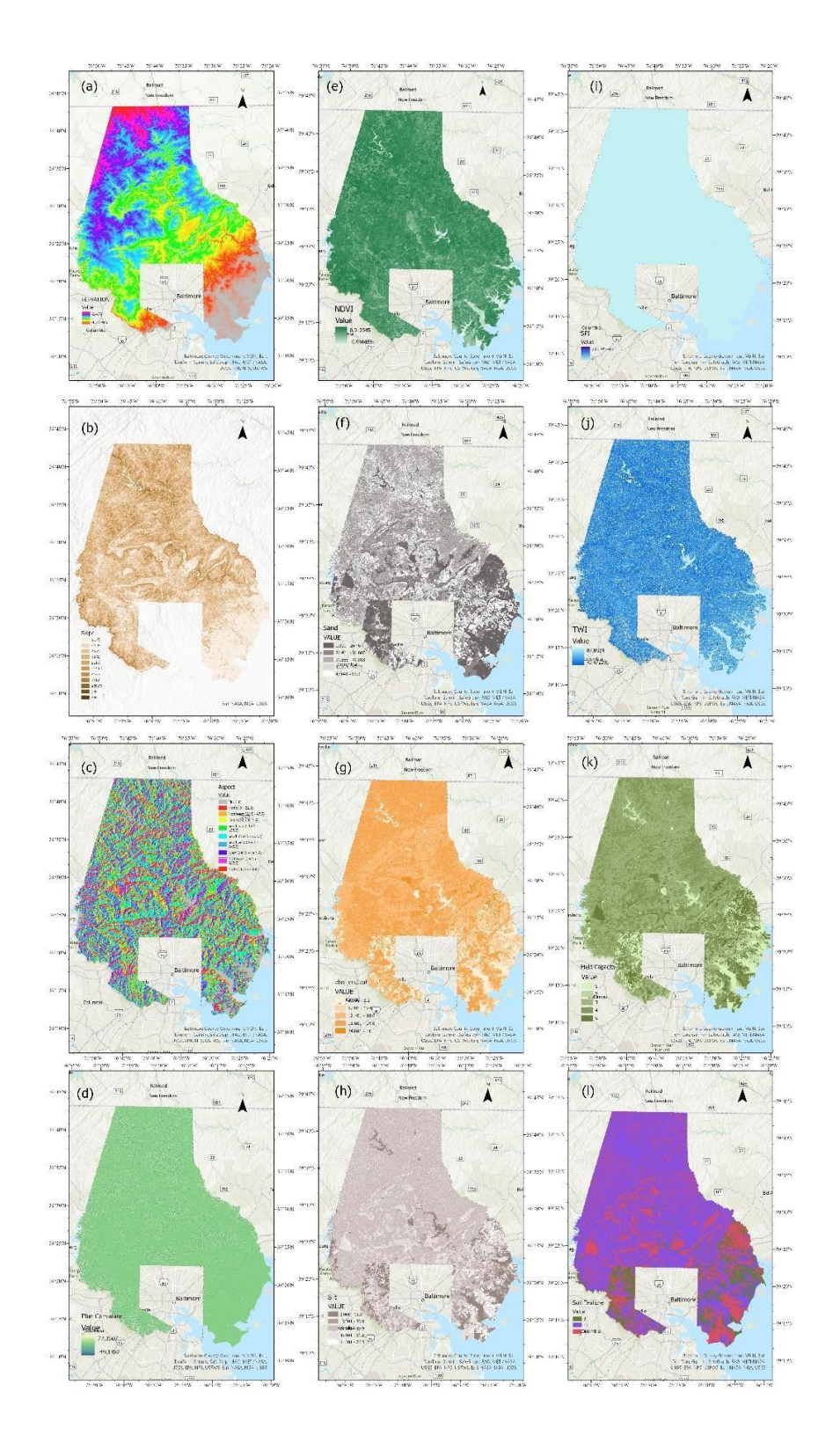


Figure 7.4: Causative factors of Landslides (a) Elevation; (b) Slope; (c) Aspect; (d) Plan profile; (e) NDVI; (f) Sand content; (g) Clay content; (h) Silt content; (i) SPI; (j) TWI; (k) Field Capacity; (l) Soil texture.

landslide occurrence. A landslide susceptibility map is then generated by classifying the LSI values into susceptibility zones ranging from very low to very high.

Table 7.2: Frequency ratios of causative factors.

Factor	Class	Class pixels	Class pixels (%)	Landslide pixels	Landslide pixels (%)	FR
Elevation	-0.77 ~ 58.15	3168245	19.73	13	56.52	2.87
	58.15 ~ 117.07	2842506	17.70	4	17.39	0.98
	117.07 ~ 175.99	5780526	35.99	6	26.09	0.72
	175.99 ~ 234.91	3758498	23.40	0	0.00	0.00
	234.91 ~ 294.79	510624	3.18	0	0.00	0.00
		16060399		23		4.57
Slope	o ~5°	9763489	60.89	14	60.87	1.00
Бюрс	5 ~ 15°	5629879	35.11	9	39.13	1.11
	15 ~ 25°	584349	3.64	0	0.00	0.00
	25 ~ 35°	52459	0.33	0	0.00	0.00
	35 ~ 90.0°	3629	0.02	0	0.00	0.00
		16033805				2.11
Aspect	135 ~ 225°	4526207	29.05	7	30.43	1.05
	112.5 ~ 135°	1121622	7.20	1	4.35	0.60
	225 ~ 292.5°	4643679	29.80	5	21.74	0.73
	22.5 ~ 67.5°	3500251	22.47	8	34.78	1.55
	337.5 ~ 22.5°	1788668	11.48	2	8.70	0.76
		15580427				4.69
Plan	30 ~ -72.35	21	0.0	0	0.00	0.0
Timi	10 ~ -30	430	0.00	0	0.00	0.0
	-10 ~ -10	16059021	99.994	23	100.00	1.0
	-30 ~ -10	554	0.0034	0	0.00	0.0
	-49.14 ~ -30	9	0.00006	0	0.00	0.0
		16060035				1.0

Table 7.2: Frequency ratios of causative factors (cont.).

Factor	Class	Class pixels	Class pixels (%)	Landslide pixels	Landslide pixels (%)	FR
Sand content	0 ~ 18.51%	118810	1.84	0	0.00	0.00
	18.51 ~ 37.02%	922153	14.31	0	0.00	0.00
	37.02 ~ 55.53%	6443451	99.99	3	75.00	0.75
	55.53 ~ 74.04%	6953264	107.90	16	400.00	3.71
	74.05 ~ 83.33%	1622334	25.18	4	100.00	3.97
		16060012				8.43
Clay content	0 ~ 6.89%	1603496	9.98	2	8.70	0.87
	6.89 ~ 13.78%	1426899	8.88	5	21.74	2.45
	13.78 ~ 20.67%	10408680	64.81	16	69.57	1.07
	20.67 ~ 24.11%	550014	3.42	0	0.00	0.00
	24.11 ~ 31%	2070923	12.89	0	0.00	0.00
		16060012				4.39
Silt content	O ~ 17%	1475080	9.18	2	8.70	0.95
	17 ~ 34%	710334	4.42	0	0.00	0.00
	34 ~ 51%	8643837	53.82	3	13.04	0.24
	51 ~ 68%	5042793	31.40	16	69.57	2.22
	68 ~ 76.5%	187968	1.17	2	8.70	7.43
		16060012				10.83
NDVI	0.6 ~ 1.0	4298448	26.76	0	0.00	0.00
	0.4 ~ 0.6	7233883	45.04	3	13.04	0.29
	0.2 ~ 0.4	2933074	18.26	7	30.43	1.67
	0.0 ~ -0.2	1059594	6.60	13	56.52	8.57
	-1.0 ~ -0.0	536208	3.34	0	0.00	0.00
		16061207				10.52
Texture	1	760808	4.74	0	0.00	0.00
	2	10214131	63.60	6	26.09	0.41
	3	4509018	28.08	17	73.91	2.63
	4	24378	0.15	0	0.00	0.00
	5	551677	3.44	0	0.00	0.00
		16060012				3.04
FC	0.26 ~ 0.33%	1356270	8.45	2	8.70	1.03
	0.34 ~ 0.41%	829108	5.16	0	0.00	0.00
	0.42 ~ 0.48%	6443920	40.12	3	13.04	0.33
	0.49 ~ 0.55%	5970541	37.18	13	56.52	1.52
	0.56 ~ 0.63%	1460173	9.09	5	21.74	2.39
		16060012			0.00	5.27

Table 7.2: Frequency ratios of causative factors (cont.).

Factor	Class	Class pixels	Class pixels (%)	Landslide pixels	Landslide pixels (%)	FR
SPI	o ~ 4.0e5	16033786	100.00	23	100.00	1.00
	4.0 ~ 8.0e5	324	0.00	0	0.00	0.00
	8.0 ~ 1.2e6	39	0.00	0	0.00	0.00
	1.2 ~ 1.6e6	4	0.00	0	0.00	0.00
	1.6 ~ 2.0e6	5	0.00	0	0.00	0.00
		16034158				1
TWI	-0.47 ~ 17.06	13365903	99.89	23	100.00	1.00
	17.06 ~ 35.17	14901	0.11	0	0.00	0.00
	35.17 ~ 53.29	28	0.00	0	0.00	0.00
	53.29 ~ 71.41	1	0.00	0	0.00	0.00
	71.41 ~ 87.88	3	0.00	0	0.00	0.00
		13380836				1.00

Table 7.2 presents the frequency ratio (FR) values that quantify the correlation between various causative factors and landslide occurrences in Baltimore County. An FR value greater than 1 indicates a strong positive correlation between a specific class of a factor and the likelihood of landslides, while an FR below 1 implies a weak or negligible association. For instance, certain aspect classes—particularly between 22.5° and 67.5°—showed a notably high FR of 1.55, indicating a strong susceptibility to landslides in that directional range. Similarly, for soil-related parameters, sand content ranging from 55.53% to 74.04% had an FR of 1.61, and silt content between 51% and 68% had an FR of 2.22, both suggesting a significant contribution to landslide potential.

Upon calculation of the Frequency Ratio (FR) values for each causative factors classes, the Landslide Susceptibility Index (LSI) was computed by using the expression in Equation (7.2). The resulting LSI values were classified into five susceptibility levels ranging from very low, low, moderate, high, and very high, using equal interval classification in ArcGIS. The final Landslide Susceptibility Map (LSM), presented in Figure 7.5, highlights areas with varying degrees of landslide risk across Baltimore County. To strengthen the robustness of the training dataset, potential landslide points were generated from regions classified within the high and very high susceptibility zones of the LSM, while non-landslide points were generated within the very low and low susceptibility zones. These synthesized samples enhance the initial landslide inventory, facilitating a more proportionate dataset for model training. This practice is comparable with emerging trends in literature [126, 127].

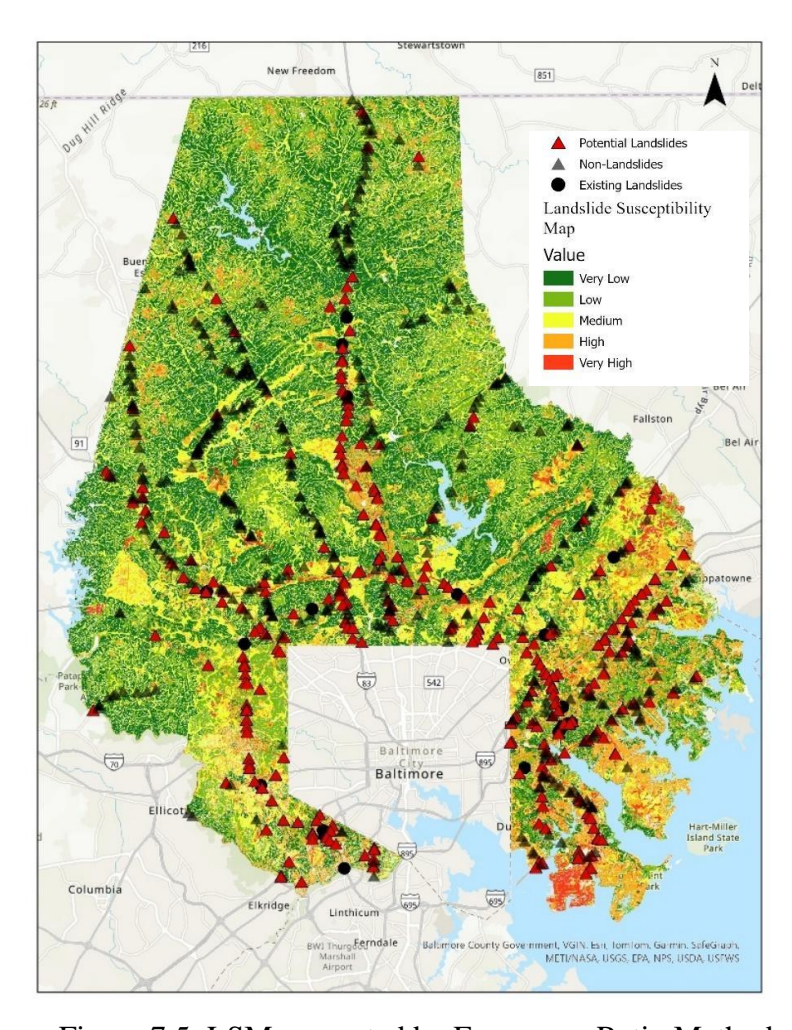


Figure 7.5: LSM generated by Frequency Ratio Method.

Table 7.3 highlights the relationship of susceptibility zones with their associated landslide probabilities, serving as an essential input for further machine learning-based landslide prediction.

Table 7.3. Relationship between susceptibility classes and landslide probability.

Susceptibility Class	Probability of Landslide		
Very Low	0-20%		
Low	20-40%		
Medium	40-60%		
High	60-80%		
Very High	80-100%		

#### 7.3.4.4 Machine Learning Method

Recent years have seen a significant increase in the adaptation of machine learning (ML) algorithms in landslide susceptibility modeling, largely due to its superiority in accurately analyzing vast amounts of temporal and spatial data, accuracy over conventional techniques in intricate modeling, and nonlinear relationships. Additionally, its ability to automatically identify patterns in high-dimensional datasets and enhance prediction accuracy in contrast to deterministic or knowledge-driven systems. Machine learning models such as Random Forest, Support Vector Machine, and Gradient Boosting Machine, which identify subtle interdependence between landslide occurrence and causative causes, have been used to make informed data-driven decision-making for hazard risk mitigation. In this research, a high-resolution Landslide Susceptibility Map for Baltimore County was created by integrating machine learning models with FR-based LSI values.

This landslide prediction research is approached as a binary classification model. The study area was categorized as either a potential landslide zone or a nonlandslide-prone zone based on the correlation between landslide susceptibility and the selected causative factors. To provide accurate predictions, four different machine learning (ML) methods were used: logistic regression (LR), support vector machine (SVM), random forest (RF), and gradient boosting machine (GBM). Logistic Regression is a linear model that uses a logistic function to predict the likelihood of class membership, making it appropriate for datasets with linear input-output relationships. In scenarios with well-separated classes, the Support Vector Machine creates a hyperplane that maximizes the margin between classes in a highdimensional feature space, resulting in excellent performance. Random Forest, an ensemble of decision trees trained on random subsets of data and characteristics, enhances classification accuracy and robustness by aggregating predictions from numerous trees. Gradient Boosting Machine, another ensemble method, constructs models progressively, with each iteration attempting to rectify the flaws of the preceding one, resulting in excellent predicted accuracy, particularly on complex datasets. These models were chosen due to their demonstrated reliability and ease of interpretation in extensive prior geohazard research.

#### Step 1 Data preparation

A total of 292 landslides were used in the database created as input for ML models. The model for LSM considers twelve landslides causative factors shown in Table 7.1. To train a ML model to recognize the pattern of features for various classes in a binary classification task, positive and negative sample features are required. As a result, the study area is sampled with 146 non-landslides labeled as 0 and 146 existing and potential landslides labeled as 1 respectively. A section of the input database used is as shown in Figure 7.6.

POINT_X	POINT_Y	dem_balt	Slope	Aspect	plan_curve	twi	spi	NDVI	Sand_content	clay_content	Silt_content	soil_texture	Field_Capa	Labels
1407738.34989	679028.300003	127.3236	13.54292	345.7658	0.763748	2.618896	1.134684	0.355897	26.5	20	53.5	12	0.55	1
1453438.22568	623769.317673	68.09829	14.53599	166.381	0.443817	3.765716	1.635022	0.564156	26.5	20	53.5	12	0.55	1
358008.416979	14390154.2198	158.1958	6.026412	161.235	0.23201	4.775163	1.210761	0.19962	42.1	20	37.9	1	0.48	1
345568.416979	14389334.2198	215.9347	7.467983	353.5851	-0.376236	2.664991	0.276622	0.455204	42.1	20	37.9	1	0.48	0
345988.416979	14387924.2198	207.5311	4.072436	264.2286	0.044556	4.247251	0.35698	0.438549	42.1	20	37.9	1	0.48	0
356938.416979	14389554.2198	138.8548	5.044843	5.011919	0.00441	4.819543	0.973974	0.461089	50	15	35	4	0.45	0
357748.416979	14389274.2198	128.5694	9.175709	290.2042	-0.259674	5.988427	7.537953	0.438746	45	19	36	1	0.47	0
357458.416979	14388254.2198	158.872	14.32095	14.11263	0.294037	4.447819	4.157518	0.456456	45	19	36	1	0.47	0
357528.416979	14388174.2198	170.9222	9.621971	18.47543	-0.247345	3.945232	1.911062	0.633297	45	19	36	1	0.47	0
359178.416979	14395154.2198	230.5737	2.316536	168.8081	-0.057922	4.58638	0.162945	0.161685	31.79	24.79	43.4	4	0.52	1
359088.416979	14394854.2198	234.3861	4.710535	5.037613	-0.1884	3.902236	0.322447	0.053391	31.79	24.79	43.4	4	0.52	1
358418.416979	14391924.2198	193.1942	3.975666	112.8478	0.343552	4.660241	0.463068	0.19716	42.1	20	37.9	1	0.48	1

Figure 7.6: Machine Learning Input database.

## Step 2: Data Preprocessing

The first step to training a machine learning (ML) model is training of a predetermined dataset. After this first training phase, data not used during training is used to evaluate the model's predictive capabilities. To thoroughly assess the ML model's generalizability, common practice is to separate the original dataset into separate training and testing subsets. A 70%/30% split was used in this study, with 70% of the data used for training the model and the remaining 30% used for testing and evaluating the predicted accuracy of the model.

### Step 3: Model Evaluation

Evaluating the performance of machine learning (ML) models is essential for determining how well a model adapts to new data and makes predictions. These assessment matrices help to determine overall accuracy and how well the model recognizes positive cases and reduces false alarms.

Five evaluation metrics: Accuracy, Precision, Recall, F1 Score, and AUC Score, were used to evaluate the effectiveness of machine learning models for landslide susceptibility classification. The metrics obtained from the confusion matrix offer a thorough insight into how successful the model accurately predicts potential landslide areas and non-landslide areas [128]. Accuracy provides a comprehensive performance assessment, whereas Precision and Recall emphasize the correctness and completeness of positive predictions. The F1 Score establishes a balance between these two, particularly when decisions are required. The AUC Score assesses model efficacy across all potential categorization levels utilizing the ROC curve. Table 7.4 summarizes the evaluation metrics, and their corresponding formulas used for this study.

Table 7.4: Performance Metrics for Binary Classification Models.

Metric	Definition	Formula		
Accuracy	Overall correct predictions	$\frac{TP + TN}{TP + TN + FP + FN}$		
Precision	Correct positive predictions	$\frac{TP}{TP+FP}$		
Recall	Correctly identified actual positives	$\frac{TP}{TP+FN}$		
F1 Score	Balance between precision and recall	$\frac{2 \cdot \operatorname{Precision} \cdot \operatorname{Recall}}{\operatorname{Precision} + \operatorname{Recall}}$		
AUC Score	Area under ROC curve	Area under TPR vs. FPR curve		

#### Where:

- TP (True Positive): Model correctly predicts the potential landslide (positive) class.
- TN (True Negative): Model correctly predicts the non-landslide (negative) class.
- FP (False Positive): Model incorrectly predicts the potential landslide (positive) class.
- FN (False Negative): Model incorrectly predicts the non-landslide (negative) class.
- TPR: True Positive RateFPR: False Positive Rate

## 7.4 Preliminary Results

To evaluate the prediction performance of the machine learning models, each method was trained and tested on a standardized dataset with a five-fold cross-validation strategy. The preliminary findings show how well each model distinguishes between potential landslide and non-landslide areas using the given environmental factors. Key performance measures including accuracy, precision, recall, F1 score, and AUC were calculated to provide a thorough evaluation. The results of these measures provide insights into each model's strengths and limitations, as well as a basis for comparison when determining the best technique for predicting landslide vulnerability.

Table 7.5 compares the model performance of the four algorithms and finds that SVM outperforms the other three algorithms in terms of classification performance. The SVM technique has the highest AUC value of the four models, at 0.99, indicating excellent accuracy in categorizing landslides and non-landslides at various probability thresholds. As a result, the trained SVM model will be used to forecast the likelihood of landslides occurring across the entire study area. Specifically, twelve landslide causative factors are assigned to each pixel in the study area, and the trained model is used to estimate the likelihood of a landslide for each one.

Table 7.5: Model classification across ML models

Model	Accuracy	Precision	Recall	F1	AUC
LR	0.94	0.95	0.94	0.94	0.99
SVM	0.98	0.98	0.98	0.98	0.99
RF	0.98	0.98	0.98	0.98	0.98
GBM	0.95	0.95	0.95	0.95	0.98
Avg.	0.95	0.96	0.95	0.96	0.98

Figure 7.6 displays confusion matrices for all four models, illustrating the distribution of true positives, true negatives, false positives, and false negatives. As observed, SVM and RF produced higher true positive rates with fewer incorrect classifications.

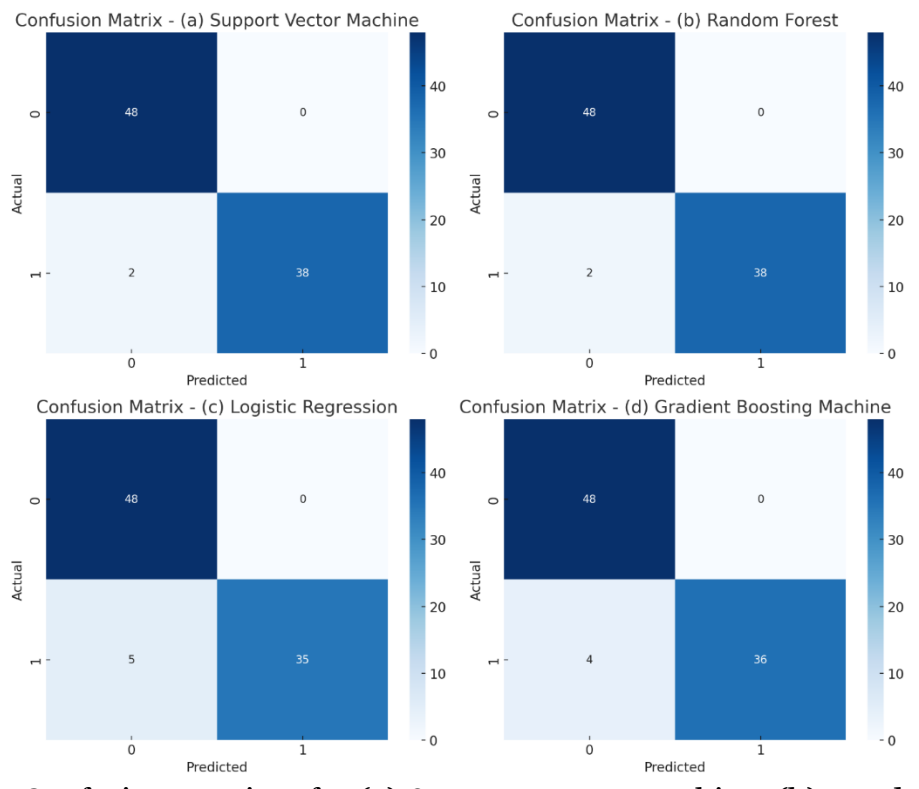
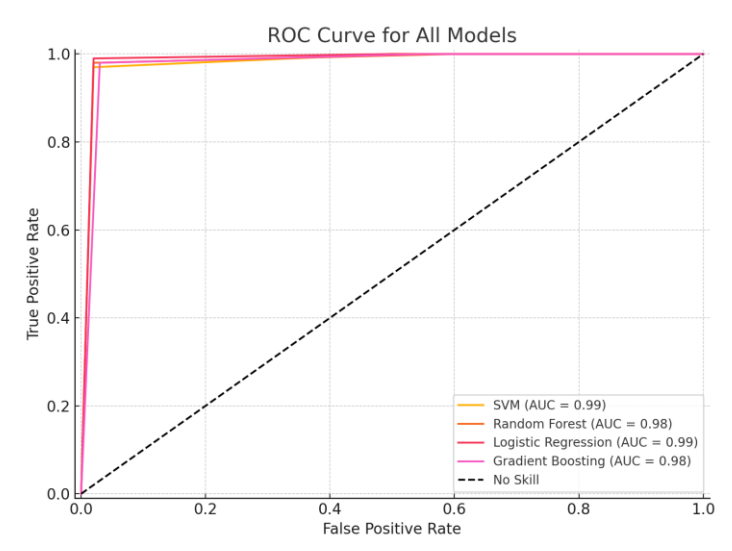


Figure 7.6: Confusion matrices for (a) Support Vector Machine, (b) Random Forest, (c) Logistic Regression, and (d) Gradient Boosting Machine showing model predictions versus actual class labels.

The Receiver Operating Characteristic (ROC) curves for the four models are illustrated in Figure 7.7. These plots clearly show that all models perform well above the diagonal baseline, with SVM and LR exhibiting near-perfect classification behavior, as indicated by their AUC scores (0.99).



**Figure 7.7**: ROC curves of the four ML models with AUC scores. SVM and LR show the best performance (AUC = 0.99).

Figure 7.8 shows feature importance plots to help understand how each causative element affects model outcomes. These plots show that, across all four machine learning models, sand content and NDVI were consistently the most influential parameters influencing landslide susceptibility. Both characteristics had high significance scores in Gradient Boosting and Random Forest models, demonstrating significant predictive value in ensemble-based learning. Similarly, the SVM and Logistic Regression models awarded significant coefficients (positive or negative) to these variables, emphasizing their importance. While sand content was positively related to landslide risk across models, implying that places with high sand content are more prone to landslides, NDVI was generally negative, showing that vegetated areas are less susceptible. Other features such as Field Capacity, Silt content, and Clay content were moderately important in tree-based models (RF, GBM), while their influence was less obvious in linear models (SVM, LR). Topographic variables such as slope, aspect, and TWI exhibited relatively low relevance across all models, indicating a restricted role in this dataset and location.

## 7.5 Conclusions

This study demonstrates the feasibility of employing machine learning models for landslide susceptibility mapping by providing an effective framework for binary classification based on environmental variables. Among the four models examined, SVM demonstrated exceptionally excellent prediction capability. The comparison of important performance indicators such as accuracy, precision, recall, F1 score, and AUC reveals each model's strengths and limitations. The study adds to the increasing body of geospatial predictive analytics and establishes the framework for incorporating advanced machine learning algorithms into operational early warning systems. With additional improvements such as ground-truth validation and an alert system, the suggested methodology has the potential to improve disaster preparedness and reduce landslide risks.

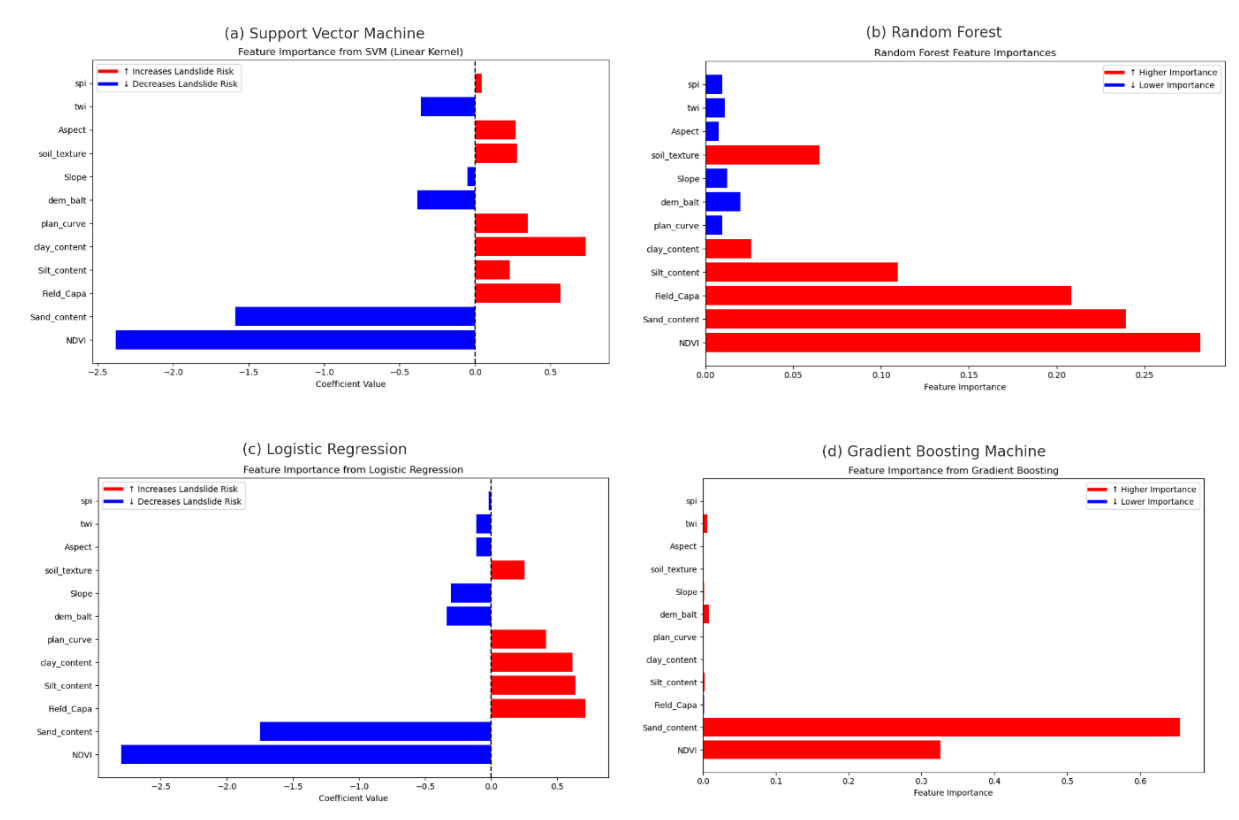


Figure 7.8. Feature importance across ML models.

#### 7.6 Future Work

Future work will focus on creating a thorough Landslide Susceptibility Map (LSM) with the Support Vector Machine (SVM) model, which was found as one of the best-performing classifiers in this study. The LSM will be integrated into a real-time landslide early warning system that uses spatial and temporal analytics to anticipate the chance of landslides occurring at specific locations and times. This technology will help with proactive risk mitigation by sending timely notifications to individuals. Furthermore, the model's predictive capabilities will be evaluated by ground-truthing activities, which will involve checking predicted landslide-prone locations with field observations and existing records in order to increase reliability and operational readiness. These improvements are intended to bridge the gap between susceptibility modeling and actionable geohazard management systems.

## **Chapter 8**

## 8 Summaries

### 8.1 Conclusions

This report summarizes work completed for the phase 2 of the project. They include:

- Review of geotechnical asset management (GAM) framework. current status and recommendations for implementing in Maryland.
- Updates on field and lab investigation with geotechnical test results.
- Applications of LiDAR data in detection and characterization of landslides in Prince George's County.
- Test soil moisture mapping procedures using Sentinel I data with ML approaches with a case study in Prince George's County Maryland.
- Numerical model development for quantitative landslide risk assessment, aiming at establishing a robust, interpretable, and quantitatively grounded framework for Landslide Risk Assessment (LRA) by integrating physicsbased numerical modeling with machine learning approaches
- Integrating GIS-Based Susceptibility Mapping and Machine Learning framework for Landslide Prediction and Early Warning with a case study in in Baltimore County, Maryland.

They are parts of the multi-phase project, aiming development of landslides risk assessment and early warning smart system. The Phases 1 and 2 work provides a strong foundation for next phase.

#### 8.2 Future Work

The phase 3 will expand site investigation with additional survey and soil sampling as well as inventory of landslides along railroad. Additional laboratory tests will be carried out. LiDAR and InSAR images processing and interpretation will be further enhanced by integrating with other photo imaging approaches and site image acquisition. Integrated soil moisture mapping and physics based slope instability risk assessment will be further developed. Multiple scenarios will be simulated to gain a better understanding controlling and triggering factors, which will be feed into the machine learning model to assess risk assessment of slope failure. Protocols for real time monitoring network will be developed and tested at selected sites in consultation with agencies and organizations (such as DOT SHA, Federal Railroad Administration) and in cooperation with MSU AI/ML program, CMU and other partners within UTC Safety 21 program and beyond.

## Chapter 9

## 9. Appendices

## Appendix A

# A: Research Products for this Project

#### A.1 Conference Publications

- 1. Hosseinizadeh, A., Z. Sheng, Y. Liu. The Impact of Climate Change on Soil Water Content with Considering Machine-Learning Methods as a Downscaling Tool, EWRI World Environmental and Water Congress, Anchorage Alaska, May 18-21, 2025 [Abstract, Presentation].
- 2. Hosseinizadeh, A., A. Olude, K. Nieto, S. Qian, B. Gui, Y. Liu, J. Li, Z. Sheng, O. Owolabi, Samuel Fedipe. Enhancing Rainfall-Induced Landslide Risk Mapping & determining the landslide location using LiDAR data for improving transportation safety. The USDOT National Safety Summit of University Transportation Centers. March 27, 2025 [Poster presentation].
- 3. Sheng Z. Improve Highway Safety by Reducing the Risks of Landslides with Smart Alert & Warning Systems. NSF CyberTraining in Disaster Management Webinar, March 19, 2025.
- 4. Sheng, Z., Liu, Y., Owolabi, O. Research Highlights: Integrated hydrological model and GIS-based model to map rainfall-induced landslide risk, UTC Safety 21, CMU, Faculty Seminar, February 27, 2025.
- 5. Hosseinizadeh, A., Isola, F., Sheng, Z. Liu, Y., Owolabi, O., Lamsal, S., Olude. A., Walrath, B.J., Nur, N.N. Integrated Hydrological Model and GIS-based Model to Map Landslides Risks within the Anacostia Watershed of Maryland, the 104th Transportation Research Board annual meeting, Washington DC, January 5-9, 2025 [Paper, oral presentation].
- 6. Hosseinizadeh, A., Z. Sheng, 2024. Machine Learning-Based Downscaling of GCM Precipitation Data: A Case Study of the Anacostia Watershed, Maryland, AGU Fall Meeting 2024, Washington DC, December 9-13 [Poster Presentation].
- 7. Atieh Hosseinizadeh, Adebayo Olude, Sean Qian, Bin Gui, Yi Liu, Jiang Li, Zhuping Sheng, Oludare Owolabi, Samuel Fadipe. Integrated Hydrological Model and GIS based Model to Map Landslides Risks within the Anacostia Watershed of Maryland for improvement of transportation safety, National University Transportation Center –Safety 21 Deployment Partners Consortium Symposium, November 14, 2024, Pittsburgh, PA [Poster presentation].
- 8. Samuel Fadipe, Adebayo Olude, Sunil Lamsal, Atieh Hosseinizadeh, Yi Liu, Zhuping Sheng, Oludare Owolabi, Sean Qian, Benjamin Walrath. Prediction of Landslides

Risks to Improve Highway Safety Using TRIGRS Approach, National University Transportation Center –Safety 21 Deployment Partners Consortium Symposium, November 14, 2024, Pittsburgh, PA [Poster presentation].

9. Adebayo Olude, Katherine Nieto, Ahmir Muley, Oludare Owolabi, Atieh Hosseinizadeh, Yi Liu, Zhuping Sheng, Sunil Lamsal, Samuel Fadipe. Identifying and Comparing Potential Slope Failures Using Remote Sensing Techniques: LiDAR and InSAR, National University Transportation Center –Safety 21 Deployment Partners Consortium Symposium, November 14, 2024, Pittsburgh, PA [Poster presentation]. 10. Hosseinizadeh, A., A. Olude, K. Nieto, S. Qian, B. Gui, Y. Liu, J. Li, Z. Sheng, O. Owolabi, S. Fadipe. Precipitation threshold for triggering landslides & detecting landslides using LiDAR and InSAR data for enhancement of transportation system safety, The Inaugural USDOT Future of Transportation Summit, Washington, DC, August 13-15, 2024 [Poster Presentation].

## A.2 Datasets

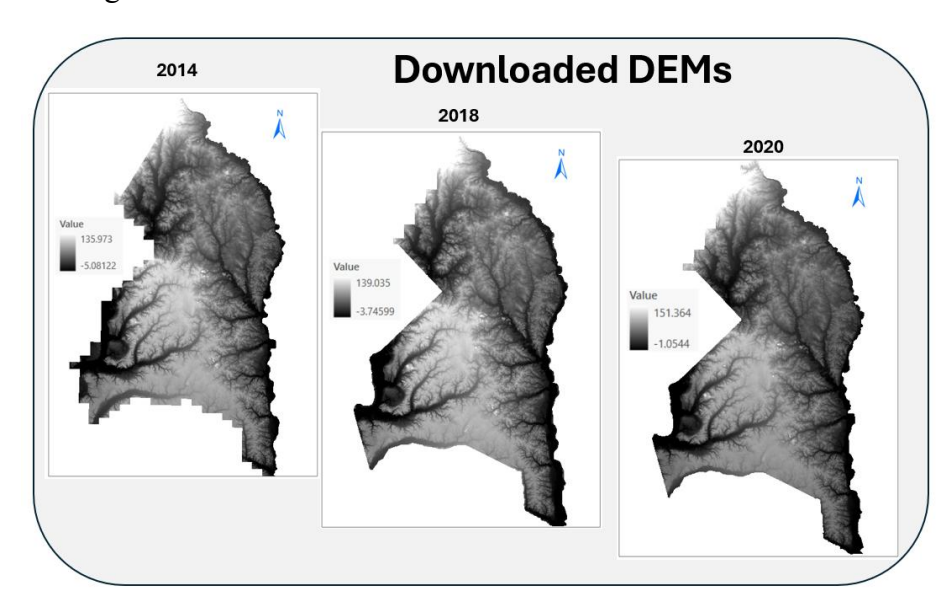
## A.2.1 Appendices for Chapter 4

**Appendix 4A**: Data and Data Source

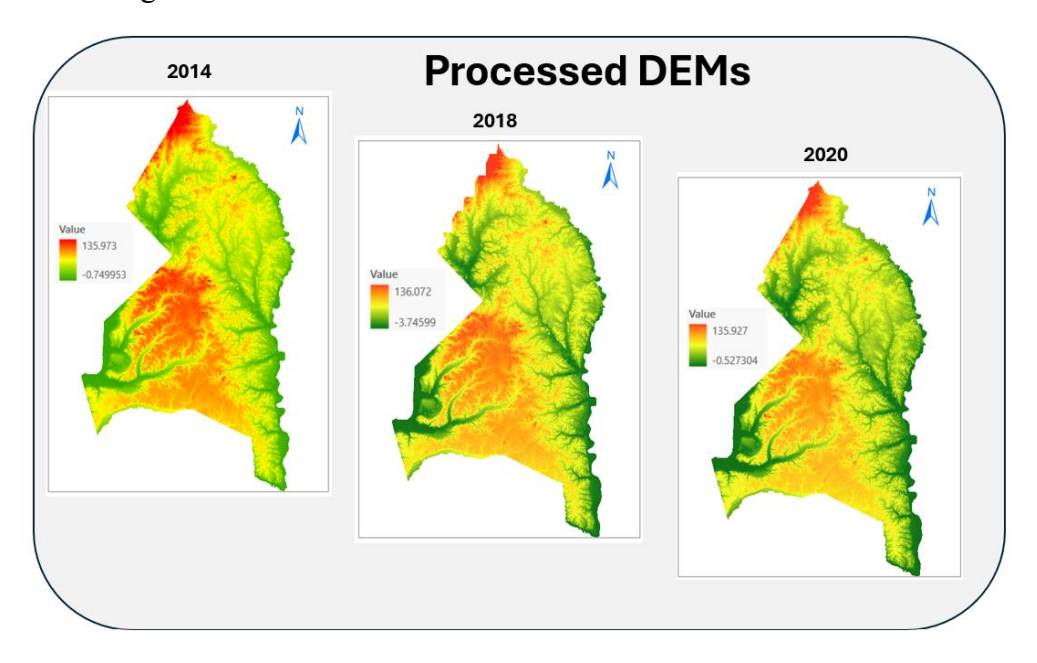
S/No	Item	Data Source/Download Link			
1.	DEM Data Download	https://doitdataservices.maryland.gov/s/N9xGBYPKq4QSZNq			

#### Appendix 4B: Prince George's LiDAR Maps

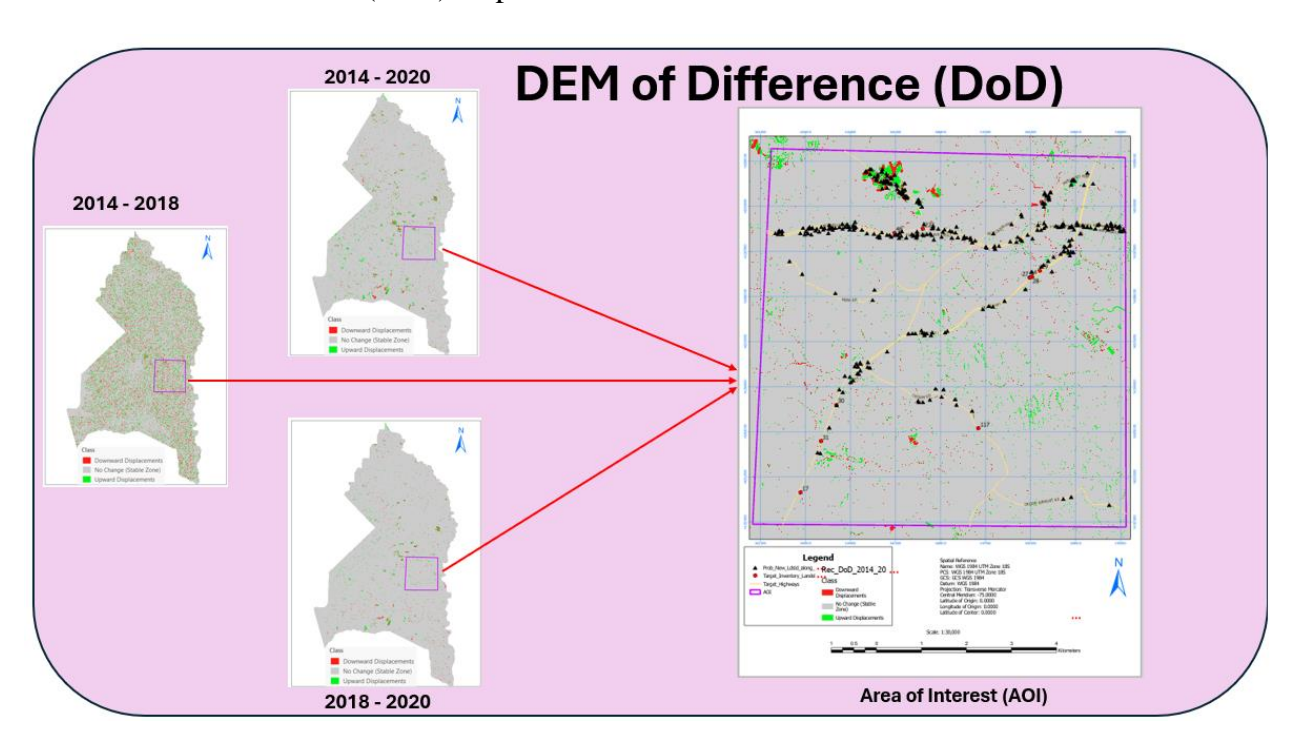
#### 4B1: Prince George's DEM



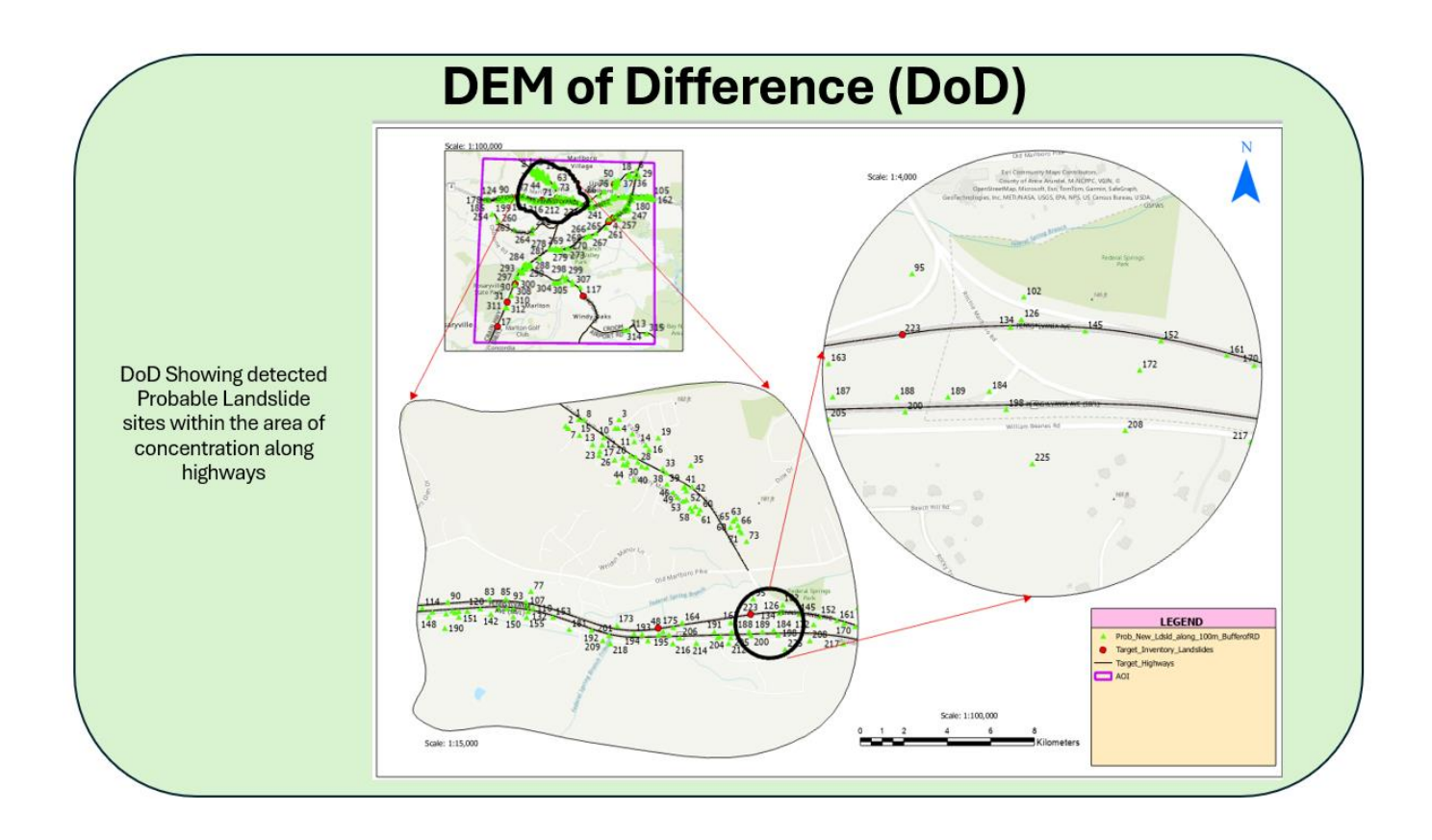
**4B2**: Prince George's Processed DEM



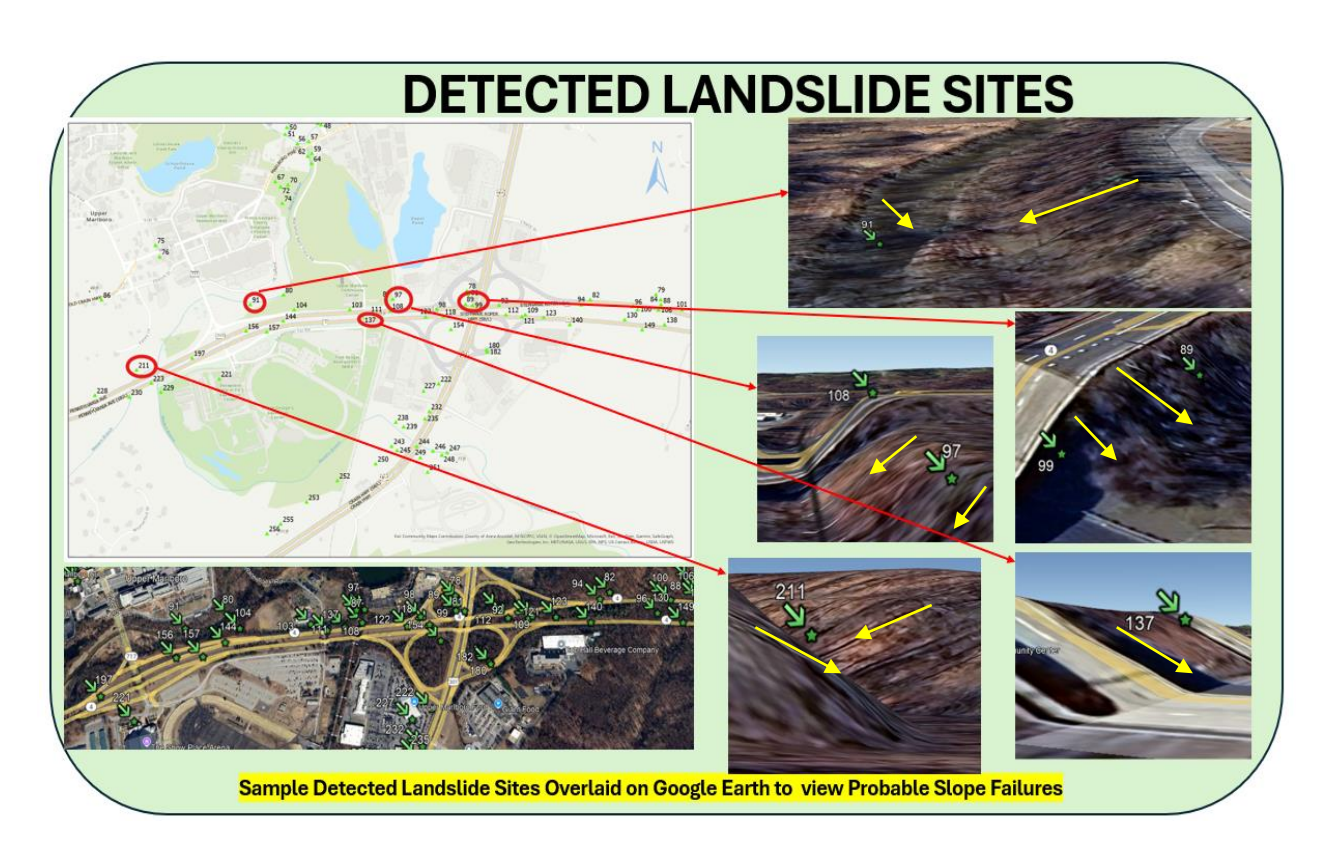
4B3: DEMs of Difference (DoD) maps



Appendix 4C: Generated Risk Map



**Appendix 4D**: Result validation: Detected sample probable landslide sites overlaid on Google earth for visualization



## **A.2.2 GIS coverages for Historical Landslides**

Table C2.2: Merged landslides (updated)

1 4516 6=1=1 11161664 14114611465 (up 44664)							
File Name	Detail	Format	Link				
Merge_landslides	Including landslide inventories collected from SHA, USGS website, and NASA website	.Shp	merged data from SHA information, USGS, and NASA				

## A.3 Research Symposium

1. 2025 Summer Research Symposium: Improve Highway Safety by Reducing the Risks of Landslides with Smart Warning Systems, July 23, 2025.

# **Bibliography**

- 1. Sheng, Zhuping, Owolabi, Oludare, & Liu, Yi. Improve Highway Safety by Reducing the Risks of Landslides (Phase 1). Carnegie Mellon University. Traffic21 Institute. Safety21 University Transportation Center (UTC). July 2024. https://rosap.ntl.bts.gov/view/dot/78031
- 2. Schuster, R. L., Highland, L. M., & Survey, U. S. G. Socioeconomic and environmental impacts of landslides in the western hemisphere. U.S. Geological Survey Editorial. August, 2001.
- 3. Petley, D. Global patterns of loss of life from landslides. Geology, 40, 927–930. 2012. https://doi.org/10.1130/G33217.1
- 4. Froude, M. J., & Petley, D. N. Global fatal landslide occurrence from 2004 to 2016. Natural Hazards and Earth System Sciences, 18, 2161–2181. 2020. https://doi.org/10.5194/nhess-18-2161-2018
- 5. Petley, D. N., Dunning, S., & Rosser, N. The analysis of global landslide risk through the creation of a database of worldwide landslide fatalities. In Landslide risk management, 367–374. 2005. Balkema. https://doi.org/10.1201/9781439833711-18
- 6. Kirschbaum, D. B., Stanley, T., & Zhou, Y. Spatial and temporal analysis of a global landslide catalog. Geomorphology, 249, 4–15. 2015. https://doi.org/10.1016/j.geomorph.2015.03.016
- 7. Sidle, R. C., & Ochiai, H. Natural factors influencing landslides. In Landslides: Processes, prediction, and land use. Water Resources, 41–119. 2006. American Geophysical Union.
- 8. Terzaghi, K. Mechanism of landslides. In S. Paige (Ed.), Application of geology to engineering practice. 1950, Geological Society of America.
- 9. Huang, J., Wu, X., Ling, S. et al. A bibliometric and content analysis of research trends on GIS-based landslide susceptibility from 2001 to 2020. Environ Sci Pollut Res., 29, 86954–86993. 2022. https://doi.org/10.1007/s11356-022-23732-z.
- 10. Maryland Department of Transportation/State Highway Administration. MDOT SHA Geotechnical Asset Management Plan. 2022.
- 11. U.S. Department of Transportation. Strategic Plan, FY 2022-2026. 2022. https://www.transportation.gov/mission/dot-strategic-plan-fy2022-2026
- 12. National Academies of Sciences, Engineering, and Medicine. 2019. Geotechnical Asset Management for Transportation Agencies, Volume 1: Research Overview. Washington, DC: The National Academies Press. https://doi.org/10.17226/25363.
- 13. R. E. Wolf, W. Thomas, and B. Oommen. Sustainable Geotechnical Asset Management along the Transportation Infrastructure Environment Using Remote Sensing, Final Report. https://rosap.ntl.bts.gov/view/dot/38809/dot\_38809\_DS1.pdf. 2020.
- 14. E. Loomis and E. Plasencia. Strategic Asset Management Plan: Message from the Transportation Secretary, MDOT. https://blog.mdot.maryland.gov/heres-what-you-should-know-about-mdots-

 $new-strategic-asset-management-plan.\ 2025.$ 

- 15. P. D. Thompson. Geotechnical Asset Management Plan Report STP000S(802)(B). 2017.
- 16. K. M. Tappenden and R. K. Skirrow. Vision for Geotechnical Asset Management at Alberta Transportation. Alberta Transportation. 2018.
- 17. A. E. Mines, D. L. Beckstrand, and M. D. Bunn. Development of a Geotechnical Asset Management Collection and Rating Program for Missouri Department of Transportation. MoDOT Research Report CMR 23-004. https://www.modot.org/research-publications. 2023.
- 18. FHWA and AASHTO. Transportation Asset Management Webinar Series: Webinar 43. Geotechnical Assets. 2019.
- 19. B. A. Leshchinsky, M. J. Olsen, and M. D. Bunn. Enhancing Landslide Inventorying, Lidar Hazard Assessment and Asset Management, Final Report SPR 786. 2018.
- 20. Washington State Department of Transportation (WSDOT). Chapter 20: Unstable Slope Management. Geotechnical Design Manual M 46-03. 2013.
- 21. Colorado Department of Transportation (CDOT). CDOT Geotechnical Design Manual. 2025.
- 22. M. Vessely. CDOT Geohazard Management Plan Evolution: A Leap Forward with Open Source Lidar and New Algorithms. CDOT. 2024.
- 23. Vermont Agency of Transportation (VTrans). Transportation Asset Management Plan: Right Investment, Right Asset, Right Time. 2019.
- 24. Y. Suk. Towards the Implementation of a Geotechnical Asset Management Program in the State of Georgia. Office of Performance-Based Management and Research. https://orcid.org/0000-0002-0457-4824. 2023.
- 25. Louisiana Department of Transportation and Development (LA DOTD). DOTD Geotechnical Asset Management (GAM) Guide. http://www.tamptemplate.org/wp-content/uploads/tamps/036 louisianadotd.pdf. 2019.
- 26. Ohio Department of Transportation (ODOT). Ohio Rock Slope Dashboard. https://gis.dot.state.oh.us/tims\_classic/Map/Geotechnical. 2025.
- 27. WSDOT. Geotechnical Design Manual, Environmental and Regional Operations Construction Division Geotechnical Office. 2021.
- 28.K. Tappenden and R. K. Skirrow. Alberta Transportation Geotechnical Asset Management (GAM) Framework Development, GAM Planner Application and Pilot Study. https://www.researchgate.net/publication/365201878. 2022.
- 29. Y. Li, S. Rangarajan, Y. Cheng, H. Rahardjo, and A. Satyanaga. Random forest-based prediction of shallow slope stability considering spatiotemporal variations in unsaturated soil moisture. Scientific Reports, 15(1). 2025. doi: 10.1038/s41598-025-92739-6.
- 30. Aminpour, M., Alaie, R., Kardani, N., Moridpour, S., & Nazem, M. Slope stability predictions on spatially variable random fields using machine learning surrogate models. Engineering Geology, 2021.
- 31. D. A. Stanley. Asset Management in a World of Dirt Emergence of an Underdeveloped Sector of Transportation Asset Management. TR News, 275, 30–33. 2011.

- 32. National Academies of Sciences, Engineering, and Medicine. 2019. Geotechnical Asset Management for Transportation Agencies, Volume 2: Implementation Manual. Washington, DC: The National Academies Press. https://doi.org/10.17226/25364.
- 33. Cambridge Systematics Inc., PB Consult, and System Metrics Group Inc. Analytical Tools for Asset Management, NCHRP Report 545, Transportation Research Board. https://onlinepubs.trb.org/onlinepubs/nchrp/nchrp\_rpt\_545.pdf. 2025.
- 34. M. Kinde, E. Getahun, and M. Jothimani, "Geotechnical and slope stability analysis in the landslide-prone area: A case study in Sawla Laska road sector, Southern Ethiopia," Sci. African, vol. 23, p. e02071, 2024.
- 35. X. Zhao, S. Qaisar, M. Rauf, and M. H. Shafqat, "Landslide Development Characteristics and Risk Zoning along the Dir Road in North Pakistan," South. J. Eng. Technol., vol. 1, no. 1, pp. 328–339, 2024.
- 36. L. Chen et al., "Deformation monitoring and failure mode research of mining-induced Jianshanying landslide in karst mountain area, China with ALOS/PALSAR-2 images," Landslides, vol. 18, no. 8, pp. 2739–2750, 2021.
- 37. Virginia Energy. Virginia Energy Geology and Mineral Resources Landslide Hazard Mapping.
  https://energy.virginia.gov/geology/FEMA\_landslide.shtml. [Online; accessed July 07, 2025]
- 38. World Health Organization. Landslides. <a href="https://www.who.int/health-topics/landslides">https://www.who.int/health-topics/landslides</a> [Online; accessed July 17, 2025].
- 39.O. Petrucci. Landslide Fatality Occurrence: A Systematic Review of Research Published between January 2010 and March 2022. *Sustainability*, 14(15), 9346. 2022. doi: 10.3390/su14159346.
- 40.C. J. Van Westen, T. W. J. Van Asch, and R. Soeters. Landslide hazard and risk zonation—why is it still so difficult?. *Bull. Eng. Geol. Environ.*, 65(2), 167–184, 2006. doi: 10.1007/s10064-005-0023-0.
- 41. F. Guzzetti, P. Reichenbach, M. Cardinali, M. Galli, and F. Ardizzone, Probabilistic landslide hazard assessment at the basin scale. *Geomorphology*, 72(1–4), 272–299. 2005. doi: 10.1016/j.geomorph.2005.06.002.
- 42. S. Scudero and G. De Guidi. Landslide Processes and Susceptibility Mapping in NE Sicily, Italy. in Landslide Science and Practice: Volume 1: Landslide Inventory and Susceptibility and Hazard Zoning. Berlin, Heidelberg: Springer Berlin Heidelberg, 493–498. 2013. doi: 10.1007/978-3-642-31325-7\_64.
- 43. K. J. Beven and M. J. Kirkby. A physically based, variable contributing area model of basin hydrology. *Hydrol. Sci. Bull.*, 24(1), 43–69. 1979. doi: 10.1080/02626667909491834.
- 44. L. Ayalew and H. Yamagishi. The application of GIS-based logistic regression for landslide susceptibility mapping in the Kakuda-Yahiko Mountains, Central

- Japan. *Geomorphology*, 65(1–2), 15–31. 2005. doi: 10.1016/j.geomorph.2004.06.010.
- 45. A. Akgun. A comparison of landslide susceptibility maps produced by logistic regression, multi-criteria decision, and likelihood ratio methods: a case study at İzmir, Turkey. *Landslides*, 9(1), 93–106. 2012. doi: 10.1007/s10346-011-0283-7.
- 46.S. Lee and B. Pradhan. Landslide hazard mapping at Selangor, Malaysia using frequency ratio and logistic regression models. *Landslides*, 4(1), 33–41. 2007. doi: 10.1007/s10346-006-0047-y.
- 47. H. R. Pourghasemi, B. Pradhan, and C. Gokceoglu. Application of fuzzy logic and analytical hierarchy process (AHP) to landslide susceptibility mapping at Haraz watershed, Iran. *Nat. Hazards*, 63(2), 965–996. 2012. doi: 10.1007/s11069-012-0217-2.
- 48.Zêzere, J. L., Reis, E., Garcia, R., Oliveira, S., Rodrigues, M. L., Vieira, G., and Ferreira, A. B. Integration of spatial and temporal data for the definition of different landslide hazard scenarios in the area north of Lisbon (Portugal). *Nat. Hazards Earth Syst. Sci.*, 4(1), 133–146. 2004. doi: 10.5194/nhess-4-133-2004.
- 49.B. Pradhan. Landslide susceptibility mapping of a catchment area using frequency ratio, fuzzy logic and multivariate logistic regression approaches. *J. Indian Soc. Remote Sens.*, 38(2), 301–320. 2010. doi: 10.1007/s12524-010-0020-z.
- 50.O. Petrucci. Review article: Factors leading to the occurrence of flood fatalities: a systematic review of research papers published between 2010 and 2020. *Nat. Hazards Earth Syst. Sci.*, 22(1), 71–83. 2022, doi: 10.5194/nhess-22-71-2022.
- 51. Mirco Galli, Francesca Ardizzone, Mauro Cardinali, Fausto Guzzetti, Paola Reichenbach. Comparing landslide inventory maps. Geomorphology, 94, 268–289. 2008. doi:10.1016/j.geomorph.2006.09.023
- 52. T. R. Martha, N. Kerle, V. Jetten, C. J. Van Westen, and K. V. Kumar, Characterising spectral, spatial and morphometric properties of landslides for semi-automatic detection using object-oriented methods. *Geomorphology*, 116(1–2), 24–36. 2010. doi: 10.1016/j.geomorph.2009.10.004.
- 53. J. N. Goetz, R. H. Guthrie, and A. Brenning. Integrating physical and empirical landslide susceptibility models using generalized additive models. *Geomorphology*, 129(3–4), 376–386. 2011. doi: 10.1016/j.geomorph.2011.03.001.
- 54. A. Bhardwaj and L. Sam. Reconstruction and Characterisation of Past and the Most Recent Slope Failure Events at the 2021 Rock-Ice Avalanche Site in Chamoli, Indian Himalaya. *Remote Sens.*, 14(4), 4. 2022. doi: 10.3390/rs14040949.

- 55. Corominas, J., van Westen, C., Frattini, P., Cascini, L., Malet, J. P., Fotopoulou, S., ... & Smith, J. T. Recommendations for the quantitative analysis of landslide risk. *Bull. Eng. Geol. Environ.* 2013. doi: 10.1007/s10064-013-0538-8.
- 56. I. Yilmaz. Landslide susceptibility mapping using frequency ratio, logistic regression, artificial neural networks and their comparison: A case study from Kat landslides (Tokat—Turkey). *Comput. Geosci.*, 35(6), 1125–1138. 2009. doi: 10.1016/j.cageo.2008.08.007.
- 57. L. Chen, P. Ma, C. Yu, Y. Zheng, Q. Zhu, and Y. Ding. Landslide susceptibility assessment in multiple urban slope settings with a landslide inventory augmented by InSAR techniques. *Eng. Geol.*, 327, 107342. 2023. doi: 10.1016/j.enggeo.2023.107342.
- 58. Vereecken, H., Huisman, J. A., Bogena, H., Vanderborght, J., Vrugt, J. A., and Hopmans, J. W. On the value of soil moisture measurements in vadose zone hydrology: A review. *Water resources research*, 44(4). 2008.
- 59. Orth, R. Global soil moisture from in-situ measurements using machine learning--SoMo. ml. arXiv preprint arXiv:2010.02374. 2020.
- 60. Batchu, V., Nearing, G., and Gulshan, V. A machine learning data fusion model for soil moisture retrieval. arXiv preprint arXiv:2206.09649. 2022.
- 61. Liu, Y., Jing, W., Wang, Q., & Xia, X. Generating high-resolution daily soil moisture by using spatial downscaling techniques: A comparison of six machine learning algorithms. *Advances in Water Resources*, 141, 103601. 2020.
- 62. Li, Q., Zhu, Y., Shangguan, W., Wang, X., Li, L., and Yu, F. An attention-aware LSTM model for soil moisture and soil temperature prediction. *Geoderma*, 409, 115651. 2022.
- 63. Wang, Y., Shi, L., Hu, Y., Hu, X., Song, W., and Wang, L. A comprehensive study of deep learning for soil moisture prediction. *Hydrology and Earth System Sciences Discussions*, 2023, 1-38. 2023.
- 64. Koné, B. A. T., Grati, R., Bouaziz, B., and Boukadi, K. A new long short-term memory based approach for soil moisture prediction. *Journal of Ambient Intelligence and Smart Environments*, 15(3), 255-268. 2023.
- 65. Jiang, P., Niu, G., and Li, G. Soil moisture prediction based on long short-term memory networks and meteorological data, 1–15. 2024.
- 66. Ahmad, S., Kalra, A., and Stephen, H. Estimating soil moisture using remote sensing data: A machine learning approach. *Advances in water resources*, 33(1), 69-80. 2010.

- 67. Halter, T., Lehmann, P., Wicki, A., Aaron, J., and Stähli, M. Optimising landslide initiation modelling with high-resolution saturation prediction based on soil moisture monitoring data. *Landslides*, 1-18. 2024.
- 68. Bindlish, R., Jackson, T. J., Gasiewski, A. J., Klein, M., and Njoku, E. G. Soil moisture mapping and AMSR-E validation using the PSR in SMEXO2. *Remote Sensing of Environment*, 103(2), 127-139. 2006.
- 69. Masters, D., Axelrad, P., and Katzberg, S. Initial results of land-reflected GPS bistatic radar measurements in SMEXo2. *Remote sensing of environment*, 92(4), 507-520. 2004.
- 70. Paloscia, S., Macelloni, G., Santi, E., and Koike, T. A multifrequency algorithm for the retrieval of soil moisture on a large scale using microwave data from SMMR and SSM/I satellites. *IEEE Transactions on Geoscience and Remote Sensing*, 39(8), 1655-1661. 2002.
- 71. Senyurek, V., Lei, F., Boyd, D., Kurum, M., Gurbuz, A. C., and Moorhead, R. Machine learning-based CYGNSS soil moisture estimates over ISMN sites in CONUS. *Remote Sensing*, 12(7), 1168. 2020.
- 72. Persson, M., and Haridy, S. Estimating water content from electrical conductivity measurements with short time-domain reflectometry probes. *Soil Science Society of America Journal*, 67(2), 478-482. 2003.
- 73. Torres, R., Snoeij, P., Geudtner, D., Bibby, D., Davidson, M., Attema, E., ... and Rostan, F. GMES Sentinel-1 mission. *Remote sensing of environment*, 120, 9-24. 2012. https://doi.org/10.1016/j.rse.2011.05.028.
- 74. Miranda, N., Torres, R., Geudtner, D., Pinheiro, M., Potin, P., Gratadour, J. B., ... and Cossu, M. Sentinel-1 First Generation Status, Past and Future. In *IGARSS 2023-2023 IEEE International Geoscience and Remote Sensing Symposium*, 4560-4563. 2023.
- 75. Massart, S., Vreugdenhil, M., Bauer-Marschallinger, B., Navacchi, C., Raml, B., and Wagner, W. Mitigating the impact of dense vegetation on the Sentinel-1 surface soil moisture retrievals over Europe. *European Journal of Remote Sensing*, 57(1), 2300985. 2024.
- 76. Li, J., and Heap, A. D. A review of spatial interpolation methods for environmental scientists. Geoscience Australia, Canberra, Australia. 2008.
- 77. Drusch, M., Del Bello, U., Carlier, S., Colin, O., Fernandez, V., Gascon, F., ... and Bargellini, P. Sentinel-2: ESA's optical high-resolution mission for GMES operational services. *Remote sensing of Environment*, 120, 25-36. 2012.
- 78. Pettorelli, N., Vik, J. O., Mysterud, A., Gaillard, J. M., Tucker, C. J., and Stenseth, N. C. Using the satellite-derived NDVI to assess ecological responses to environmental change. *Trends in ecology & evolution*, 20(9), 503-510. 2005.

- 79. Wagner, W., Lemoine, G., and Rott, H. A method for estimating soil moisture from ERS scatterometer and soil data. *Remote sensing of environment*, 70(2), 191-207. 1999.
- 80.Shi, X., Chen, Z., Wang, H., Yeung, D. Y., Wong, W. K., and Woo, W. C. Convolutional LSTM network: A machine learning approach for precipitation nowcasting. *Advances in neural information processing systems*, 28. 2015.
- 81. Ulloa, N. I., Yun, S. H., Chiang, S. H., and Furuta, R. Sentinel-1 spatiotemporal simulation using convolutional LSTM for flood mapping. *Remote sensing*, 14(2), 246. 2022.
- 82. ElSaadani, M., Habib, E., Abdelhameed, A. M., and Bayoumi, M. Assessment of a spatiotemporal deep learning approach for soil moisture prediction and filling the gaps in between soil moisture observations. *Frontiers in artificial intelligence*, 4, 636234. 2021.
- 83. Green, W. H., & Ampt, G. A. Studies on Soil Phyics. *The Journal of Agricultural Science*, 4(1), 1-24. 1911.
- 84. Gowdish, L., & Muñoz-Carpena, R. An improved Green–Ampt infiltration and redistribution method for uneven multistorm series. *Vadose Zone Journal*, 8(2), 470-479. 2009.
- 85. Rawls, W. J., Brakensiek, D. L., and Saxtonn, K. E. Estimation of soil water properties. *Transactions of the ASAE*, 25(5), 1316-1320. 1982.
- 86.T. Pei and T. Qiu, Landslide susceptibility mapping using physics-guided machine learning: a case study of a debris flow event in Colorado Front Range. *Acta Geotech*, 19(10), 6617–6641. 2024.
- 87. C. J. Van Westen, E. Castellanos, and S. L. Kuriakose. Spatial data for landslide susceptibility, hazard, and vulnerability assessment: An overview. *Eng Geol*, 102(3–4), 112–131. 2008.
- 88.P. Reichenbach, M. Rossi, B. D. Malamud, M. Mihir, and F. Guzzetti. A review of statistically-based landslide susceptibility models. *Earth Sci Rev*, 180, 60–91. 2018.
- 89.J. N. Goetz, A. Brenning, H. Petschko, and P. Leopold. Evaluating machine learning and statistical prediction techniques for landslide susceptibility modeling. *Comput Geosci*, 81, 1–11. 2015.
- 90.I. Chowdhuri, S. C. Pal, R. Chakrabortty, S. Malik, B. Das, and P. Roy. Torrential rainfall-induced landslide susceptibility assessment using machine learning and statistical methods of eastern Himalaya. *Natural Hazards*, 107(1), 697–722. 2021.
- 91. P. Kainthura and N. Sharma. Hybrid machine learning approach for landslide prediction, Uttarakhand, India. *Sci Rep*, 12(1), 20101. 2022.

- 92. W. Haneberg. Computational geosciences with Mathematica. *Springer Science & Business Media*. 2004.
- 93. F. Guzzetti, M. Galli, P. Reichenbach, F. Ardizzone, and M. Cardinali. Landslide hazard assessment in the Collazzone area, Umbria, Central Italy. *Natural hazards and earth system sciences*, 6(1), 115–131. 2006.
- 94.D. V Griffiths and P. A. Lane. Slope stability analysis by finite elements. *Geotechnique*, 49(3), 387–403. 1999.
- 95. R. L. Baum, W. Z. Savage, and J. W. Godt. TRIGRS: a Fortran program for transient rainfall infiltration and grid-based regional slope-stability analysis, version 2.0. US Geological Survey Reston, VA, USA. 2008.
- 96. D. P. Salunkhe, R. N. Bartakke, G. Chvan, P. R. Kothavale, and P. Digvijay. An overview on methods for slope stability analysis. *International Journal of Engineering Research & Technology (IJERT)*, 6(3), 2181–2278. 2017.
- 97. J. M. Duncan, S. G. Wright, and T. L. Brandon. Soil strength and slope stability. John Wiley & Sons. 2014.
- 98.N. Kumar, A. K. Verma, S. Sardana, K. Sarkar, and T. N. Singh. Comparative analysis of limit equilibrium and numerical methods for prediction of a landslide. *Bulletin of Engineering Geology and the Environment*, 77(2), 595–608. 2018.
- 99. R. M. Iverson. Landslide triggering by rain infiltration. *Water Resour Res*, 36(7), 1897–1910. 2000.
- 100. Y. Wang, L. Q. Wang, W. G. Zhang, S. L. Liu, W. X. Sun, L. Hong, and Z. W. Zhu. A physics-informed machine learning solution for landslide susceptibility mapping based on three-dimensional slope stability evaluation. *J Cent South Univ*, 31(11), 3838–3853. 2024.
- 101. Bentley Systems International Limited. *PLAXIS 2D Reference Manual*. Dublin, Ireland. 2019.
- 102. Inc. Itasca Consulting Group. *FLAC3D User Manual: Version 5.0.* USA. 2004.
- 103. P. K. Mishra and K. L. Kuhlman. Unconfined aquifer flow theory: from Dupuit to present. in *Advances in hydrogeology*, Springer, 2013, 185–202. 2013.
- Dai, F. C., Lee, C. F., and Ngai, Y. Y. Landslide risk assessment and management: an overview. *Engineering Geology*, 64(1), 65-87. 2002.
- 105. Petley, D. N. Global patterns of loss of life from landslides. *Geology*, 40(10), 927–930. 2012.

- 106. Guzzetti, F., Reichenbach, P., Cardinali, M., et al. Probabilistic landslide hazard assessment. *Earth and Planetary Science Letters*, 195(3-4), 289–303. 2005.
- 107. Fell, R., Corominas, J., Bonnard, C., Cascini, L., Leroi, E., Savage, W. Z., and JTC-1 Joint Technical Committee on Landslides and Engineered Slopes. Guidelines for landslide susceptibility, hazard and risk zoning for land use planning. *Engineering Geology*, 102(3-4), 85–98. 2008.
- 108. Van Westen, C. J., Castellanos, E., and Kuriakose, S. L. Spatial data for landslide susceptibility, hazard, and vulnerability assessment: An overview. *Engineering Geology*, 102(3-4), 112–131. 2008.
- 109. Chung, C. J., and Fabbri, A. G. Validation of spatial prediction models for landslide hazard mapping. *Natural Hazards*, 30(3), 451–472. 2003.
- 110. Lee, S., & Pradhan, B. Landslide hazard mapping at Selangor, Malaysia using frequency ratio and logistic regression models. *Landslides*, 4(1), 33–41. 2007.
- 111. Hong, H., Naghibi, S. A., Pourghasemi, H. R., and Pradhan, B. GIS-based landslide spatial modeling in Ganzhou City, China. Arabian Journal of *Geosciences*, 10(3), 53. 2017.
- 112. Pham, B. T., et al. Hybrid models for landslide prediction. *Sustainability*, 11(7), 1866. 2019.
- 113. Merghadi, A., Yunus, A. P., Dou, J., Whiteley, J., ThaiPham, B., Bui, D. T., ... and Abderrahmane, B. Machine learning methods for landslide susceptibility studies. *Earth-Science Reviews*, 207, 103225. 2020.
- 114. Iverson, R. M. Landslide triggering by rain infiltration. *Water Resources Research*, 36(7), 1897–1910. 2000.
- 115. Guzzetti, F., Reichenbach, P., Ardizzone, F., Cardinali, M., and Galli, M. Estimating the quality of landslide susceptibility models. *Geomorphology*, 81(1-2), 166–184. 2006.
- 116. Süzen, M. L., and Doyuran, V. A comparison of the GIS based landslide susceptibility assessment methods. *Environmental Geology*, 45(5), 665–679. 2004.
- 117. Pradhan, B., and Lee, S. Delineation of landslide hazard areas using frequency ratio, logistic regression, and artificial neural network models. *Environmental Earth Sciences*, 59(1), 227–238. 2010.
- 118. Ballabio, C., and Sterlacchini, S. Support vector machines for landslide susceptibility mapping: the Staffora River basin case study, Italy. *Mathematical Geosciences*, 44(1), 47–70. 2012.

- 119. Youssef, A. M., & Pourghasemi, H. R. (2021). Landslide susceptibility mapping using machine learning. Geosciences, 11(1), 14.
- 120. Yao, X., Tham, L.G., Dai, F.C., Li, Y.Y., and Xu, C. Landslide susceptibility mapping based on Support Vector Machine: A case study on natural terrain landslide in Hong Kong, China. *Bulletin of Engineering Geology and the Environment*, 67(2), 209–223. 2008.
- 121. Liu, Z., Huang, F., Wang, Y., and Xie, M. Rainfall-induced landslide prediction using long short-term memory neural network in southwestern China. *Engineering Geology*, 298, 106521. 2022. https://doi.org/10.1016/j.enggeo.2021.106521
- 122. Goetz, J. N., Guthrie, R. H., and Brenning, A. Integrating physical and empirical landslide susceptibility models using generalized additive models. *Geomorphology*, 249, 508–524. 2015. https://doi.org/10.1016/j.geomorph.2015.03.001
- 123. Bai, S., Wang, J., Lü, G., Zhou, P., Hou, S., Xu, S., and Liu, X. Application of hybrid frequency ratio, support vector machine and logistic regression methods for landslide susceptibility mapping in the Dongchuan area, Yunnan, China. *Environmental Earth Sciences*, 80(11), 1–16. 2021. https://doi.org/10.1007/s12665-021-09735-4
- 124. Pourghasemi, H. R., and Rahmati, O. Hybrid spatial models for landslide susceptibility assessment. *CATENA*, 160, 1–16. 2018.
- 125. Hadji, R., Limani, Y., Baghem, M., el Madjid Chouabi, A., and Demdoum, A. Geologic, topographic and climatic controls in landslide hazard assessment using GIS modeling: a case study of Souk Ahras region, NE Algeria. *Quaternary International*, 302(2013): 224-237. 2013.
- 126. Liu, B., Ma, X., Wang, Y., and Xu, C. Generation and validation of synthetic landslide samples using Markov Chain Monte Carlo and SVM for susceptibility mapping in data-scarce regions. *Scientific Reports*, 15, 10651. 2025. https://doi.org/10.1038/s41598-025-10651-5
- 127. Ge, Y., Zhu, D., Deng, W., Liu, J., and Hu, L. Data-augmented landslide displacement prediction using generative adversarial network. *Engineering Geology*, 330, 107304. 2024. https://doi.org/10.1016/j.enggeo.2023.107304
- 128. Qiu, Tong, and Jun Xiong. Artificial Intelligence (AI) for Building a Landslide Inventory & Advanced Landslide Warning System in PA. No. FHWA-PA-2024-003-CIAMTIS WO 02. Pennsylvania. Department of Transportation. Bureau of Planning and Research. 2023.